Doctor of Environmental Management

A quantitative approach on understanding emission and removal of trace gases and atmospheric oxidation chemistry in remote and suburban forest

Kyoto University Graduate School of Global Environmental Studies

Sathiyamurthi Ramasamy

Academic Supervisor: Prof. Yoshizumi Kajii

August 2016

Abstract

The continuous increasing trend in photochemical oxidants (surface O_3) has been observed for a long time in Japan, even though the precursors volatile organic compounds (VOCs) and nitrogen oxides (NO_X = NO + NO_2) have decreased from 1990-2010 after several strict regulations for anthropogenic emission. Although anthropogenic VOCs can be controlled, a vast amount of biogenic VOCs from plants is still continuously emitted in Japan, because of 67 % forest coverage. Despite, BVOCs are important; there is substantial uncertainty in their contribution to the oxidant formation. OH reactivity is an efficient tool to understand the local air quality because it predicts the total reactivity of an air mass comprised of reactive species. Also, OH reactivity calculated from simultaneous measurements of sinks such as VOCs, NO_X, O_3 are compared with direct OH reactivity to get the relative ratio of each species and examine whether all the main sinks being measured. Due to the higher reactivity and rapid destruction of BVOCs in oxidant rich polluted atmosphere, comprehensive measurements of atmospheric OH loss rate and trace gases were conducted in remote (Wakayama Research Forest Station- WFRS) forest during summer-2014, to understand the distribution of BVOCs and how they respond to the meteorological conditions. During the cleaner period of this campaign 89 % species present in the forest were identified and quantified. BVOCs accounted for 44 % especially larger fraction (30-40 %) of monoterpenes in the night-time, due to temperature dependency and shallow boundary layer. Despite strong biogenic emission in the remote forest, photochemical product O_3 was observed in a small amount due to less anthropogenic sources. In another study, OH reactivity and trace gas measurement conducted in the suburban site (Field Museum Tama) during early-2012 and summer-2013 were compared to understand the biogenic and anthropogenic species distribution, and their involvement in photochemical O_3 formation. In autumn, even though NOx (22%) and VOCs (44%) distribution was substantial, relatively weaker solar strength resulted in less photochemical O_3 formation. However, in the summer season, strong light dependent biogenic emission and also significant anthropogenic sources in the presence of stronger solar strength led to subsequent high photochemical O_3 production. This work highlights BVOCs play a major role in O_3 formation if anthropogenic sources interact and meteorological conditions favoured.

Contents

1. Introduction …1

1.1. Air pollution issues and countermeasures in Japan …1

1.2. Importance of Biogenic VOCs emission and photochemical O_3 formation …3

1.3. Nature of BVOCs emission …5

1.4. Photochemical oxidation and trace gas removal in the atmosphere …6

1.5. Scope of this research work …9

2. Identification and characterisation of VOCs in Wakayama forest …11

2.1. Observation …11

2.1.1 Field site description …11

2.1.2. Measurement VOCs …13

2. 2. Results and discussion …17

2.2.1. Anthropogenic VOCs and Carbonyl species …17

2.2.2. Monoterpenes, sesquiterpenes, and OBVOCs diurnal profile …17

2.2.3. Isoprene and OVOCs diurnal profile …30

2.2.4. Correlations of O_3 with VOCs …33

2.2.5. Comparison of BVOCs in WFRS with that in boreal forest …34

2.3. Summary …38

3. Total OH reactivity measurements in Wakayama forest …40

3.1 Ambient OH reactivity measurements …40

3.2. Observation …41

3.2.1. Details of OH reactivity measurement …41

3.2.2. Simultaneous measurements of trace species, aerosol particles and meteorological conditions …43

3.3. Results and discussion …43

3.3.1. Classification of measurement campaign …43

3.3.2. Total OH reactivity …46

3.3.3. Contribution to the total OH reactivity …49

3.3.4. Missing OH reactivity …52

3.3.5. Less photochemical O_3 formation …54

3.3.6. Average diurnal variation in the relative fraction of trace species …54

3.3.7. Average diurnal variation in the relative fraction of calculated monoterpenes OH reactivity …56

3.3.8. OH steady state concentration ([OH]s.s molec cm^{-3}) …57

3.3.8.1. Derivation of $J(O^1D)$ …57

3.3.8.2. $[H_2O]$ concentration calculation …59

3.3.8.3. Calculation of [OH]s.s concentration …59

3.4. Summary …63

4. OH reactivity and trace species measurement in a suburban forest near Tokyo during AQUAS-TAMA campaign …64

4.1. Observation …64

4.1.1. Description of field site …64

4.1.2. OH reactivity measurement details …64

4.1.3. VOCs measurement …66

4.1.4. NO_X, O_3, and CO measurement …69

4.2. Results and discussion …70

4.2.1. Overview of VOCs and inorganic pollutants …70

4.2.2. Total OH reactivity …73

4.2.3. Contribution to the OH reactivity …74

4.2.4. O_3 formation potential calculation …80

4.3. Summary …83

5. Conclusions …84

6. Acknowledgement …87

7. References …88

List of figures

Fig. 1-1. Annual average concentrations of NO_2 (1970-2012). (Adopted from Wakamatsu et al., 2013). …2

Fig. 1-2. Annual average of daily maximum concentrations of Ox (1976-2012) and annual average concentrations of NMHC between 6 am and 9 am (1976-2012). (Adopted from Wakamatsu et al., 2013). …3

Fig. 1-3. Spatial distribution of monthly mean emissions of (a) isoprene, (b) monoterpenes, (mg m^{-2} day^{-1}) for January (top) and July (bottom) averaged over the modelled period 1980–2010 calculated by the MEGAN model. (Adopted from Sindelarova et al., 2014). ….4

Fig. 1-4. Primary biogenic and anthropogenic emissions and atmospheric photochemical process. (Controls of BVOC emission, Ref.: Laothawornkitkul et al., 2009). …7

Fig.2-1. Measurement site located at Wakayama forest research station (WFRS) …12

Fig. 2-2. Schematic diagram of BVOC-GCFID. …13

Fig. 2-3. Molecular structure of monoterpenes, sesquiterpene and oxygenated biogenic volatile organic compounds (OBVOCs). …18

Fig. 2-4. Time series of mixing ratio (ppt) of monoterpenes (α-pinene, camphene, β-pinene, myrcene) measured using BVOC GC-FID. …20

Fig. 2-5. Time series of mixing ratio (ppt) of monoterpenes α-phellandrene, Δ-3-carene, α-terpinene, ρ-cymene) measured using BVOC GC-FID. …21

Fig. 2-6. Time series of mixing ratio (ppt) of monoterpenes limonene, ocimene, γ-terpinene, terpinolene measured using the BVOC-GCFID. …22

Fig. 2-7. Time series of mixing ratio (ppt) of OBVOCs (linalool, limonene oxide) and sesquiterpene (β-caryophyllene), measured using the Fast-GC. …23

Fig. 2-8. Seasonal ratio of leaves calculated as, V [quantity of leaves]/[maximum quantity of leaves in summer] (Adopted from Bao et al., 2008). …24

Fig. 2-9. Leaf oil contents and the amounts of terpene emission from Cryptomeria japonica and Chamaecyparis obtusa (Adopted from Yatagai et al., 1995). …24

Fig. 2-10. Average diurnal profile of mixing ratio (ppt) of monoterpenes (α-pinene, camphene, β-pinene). Error bars indicate standard deviation (1σ). …26

Fig. 2-11. Average diurnal profile of mixing ratio (ppt) of monoterpenes ρ-cymene, limonene, Δ-3-carene. Error bars indicate standard deviation (1σ). …27

Fig. 2-12. Average diurnal profile of mixing ratio (ppt) of monoterpenes myrcene, α-phellandrene, ocimene. Error bars indicate standard deviation (1σ). …28

Fig. 2-13. Average diurnal profile of mixing ratio (ppt) of monoterpene (terpinolene), OBVOC (linalool) and sesquiterpene (β-caryophyllene). Error bars indicate standard deviation (1σ). …29

Fig.2-14. Time series of average (1 hour) meteorological parameters (temperature, relative humidity), J(NO_2), and mixing ratios of isoprene and (MVK+MACR) (*m*/*z* 71). …31

Fig.2-15. Time series of average (1 hour) mixing ratio (ppb) of acetaldehyde, acetone, MEK (*m*/*z* 73), EVK (*m*/*z* 85) and acetic acid (*m*/*z* 61). …32

Fig. 2-16. Station for Measuring Ecosystem–Atmosphere Relations (SMEAR). …35

Fig. 2-17. Diurnal profiles of BVOCs measured in WFRS (left side) and SMEAR-II (right side). …36

Fig. 3-1. OH reactivity measurement system diagram …42

Fig. 3-2. Time series of average (1 hour) mixing ratio of NO, NO_2, and O_3. …44

Fig. 3-3. Backward trajectory analysis (noon-time [UTC+9]) at 500 m height. Black lines (Period 1a- July 28th and 29th, 2014), red lines (Period 1b- July 30th to August 1st, 2014), green lines (Period 2- August 5th to the 8th, 2014) and blue lines (continuous rainy days- August 2nd to 4th). …45

Fig. 3-4. Linear regression analysis coefficient (r^2) for OH reactivity with temperature. …46

Fig. 3-5. Linear regression analysis coefficient (r^2) for OH reactivity with J(NO_2). …47

Fig. 3-6. Diel cycle of OH reactivity during the campaign. Dots, open squares, the boxes and the whiskers indicate medians, averages, 25-75 % and 10-90 % of the data respectively. …48

Fig. 3-7. Measured (lines) and calculated (stacked area) OH reactivity. Measured total OH reactivity 2-minute data (grey line) and 1 hour average (red line). Rainy days measurements (August 2nd to 4th, 2014) was not available due to instrument failure. …49

Fig. 3-8. Contribution of trace species to the total OH reactivity for the whole campaign and different periods. …50

Fig. 3-9. Average diurnal variation in the calculated OH reactivity of each species and missing OH reactivity. …51

Fig. 3-10. Average diurnal variation in the fraction of trace species and missing sinks to the total OH reactivity. …55

Fig. 3-11. Average diurnal variation in the fraction of monoterpenes which contribute to the OH reactivity. …56

Fig. 3-12. Time series of J(O^1D) and electromagnetic radiation (mW m^{-2}). …57

Fig. 3-13. Linear correlation between J(O^1D) and electromagnetic radiation (mW m^{-2}) during second half of the campaign (August 5th to 8th). …58

Fig. 3-14. Derived J(O^1D) using the relationship between J(O1D) and mW m^{-2}. …58

Fig. 3-15. Time series of calculated [OH]s.s. concentration. …60

Fig. 3-16. Calculation of linear correlation between [OH]s.s concentration and P(OH) during 29th July 11:30 to 16:30 and August 5th to 8th . …61

Fig. 3-17. Derived [OH]s.s concentration for missed hours. …61

Fig. 3-18. Calculated and derived [OH]s.s concentration. …62

Fig. 4-1. AQUAS-TAMA campaign suburban forest measurement site. …65

Fig. 4-2. Comparison of mixing ratio of VOCs measured at FM TAMA and TMU …70

Fig.4-3. Time series of mixing ratio of CO, O_3, NO and NO_2 during autumn and summer season. …71

Fig 4-4. Regression analysis of NO (ppb) vs. O_3 (ppb). …72

Fig. 4-5. Measured OH reactivity during autumn – 2012, AQUAS-TAMA campaign. …73

Fig. 4-6. Measured OH reactivity during summer – 2013, AQUAS-TAMA campaign. …73

Fig. 4-7. Average contribution of trace species to the total OH reactivity during autumn and summer campaign. …74

Fig. 4-8. Average contribution of trace species to the measured OH reactivity during morning (09:30), noon (12:30), afternoon (15:30) and evening (18:30). …75

Fig. 4-9. Average fraction of trace species to the measured OH reactivity during morning (09:30), noon (12:30), afternoon (15:30) and evening (18:30). …76

Fig. 4-10. Atmospheric photochemical reactions and O_3 formation. …80

Fig. 4-11. O_3 formation potential from measured and calculated OH reacctivity. ...81

Fig. 4-12. O_3 formation potential (ϕ) obtained for FM TAMA and Tokyo Metropolitan Area (TMA). (ϕ for TMA is adopted from Yoshino et al., 2012). ...82

List of Tables

Table 2-1. Average mixing ratio of species …16

Table.2-2. Linear regression analysis coefficient (r^2) for the inter-correlation of species and the correlation with temperature and J(NO_2) …33

Table.2-3. Linear regression analysis coefficient (r^2) for ozone with VOCs, meteorological conditions. …34

Table 2-4. Mixing ratio of BVOCs measured in WFRS and SMEAR-II. …35

Table 2-5. Lifetime of BVOCs measured in WFRS and SMEAR-II in daytime. ([a]Hakola et al., 2003, [b]Patokoski et al., 2015). ...37

Table 2-5. Lifetime of BVOCs measured in WFRS and SMEAR-II in night-time. ([a]Hakola et al., 2003, [b]Patokoski et al., 2015). ...38

Table 3-1. Summary of total OH reactivity measurements in forest sites: vegetation type, measurement values, and fractions of missing OH reactivity …40

Table 3-2. Linear regression analysis coefficient (r^2) for the missing OH reactivity with trace species, meteorological conditions and total OH reactivity. …53

Table 4-1. Mixing ratios (ppb) VOCs and inorganics measured during AQUAS-TAMA campaign. …67

Table 4-2. Linear regression analysis coefficient (r^2) for missing OH reactivity vs. trace species. …77

1. Introduction

Earth's envelope is surrounded by its main constituents, nitrogen (~78 %), oxygen (~21 %) and a small amount of argon (~1%), variable water vapour (~ 1-2 %) and a trace amount of other gases. Even though main constituents remaining consistent trace gas composition changing continuously and that plays an important role in the air quality and climate. The industrial revolution in Europe and America in the 18-19th century and extending to the other parts of the world resulted in increasing of the air pollutants. Human activities such as industrialisation, transportation and energy consumption lead to the direct emission and secondary formation of climate-changing greenhouse gases, volatile organic compounds (VOCs), nitrogen oxides (NO_X = NO + NO_2), sulphur dioxide (SO_2), ozone (O_3) and particulate matters. London smog in 1952, due to strong temperature inversion and the sulphur dioxide emission from coal usage in home and factories caused 4000 premature deaths and ~ 100 000 causalities. In Los Angeles City, the 1940s to early 50's a new type of smog recognized as photochemical smog was first observed due to rapid increasing of vehicles, strong sunlight and unique meteorological factors such as land. Haagan-Smit (1952) firstly found that the photochemical reactions of volatile organic compounds (VOCs) and nitrogen oxides (NO_X = NO + NO_2) involved in the formation of photochemical smog that containing O_3 and aerosols. Los Angeles kind of photochemical smog was observed in many cities such as Mexico, Beijing, Delhi, and Tokyo.

1.1. Air pollution issues and countermeasures in Japan

As a result of rapid industrialisation in Japan since the middle of the 20th century, air pollution problems have emerged. In between 1960 and 1969, more than six hundred patients with respiratory diseases such as chronic bronchitis, allergic asthma bronchitis were found in the city of Yokkaichi due to high concentration (~1 ppm) sulphur dioxide (Kitagawa, 1984; Guo et al., 2008). After the implementation of total emission control system in 1972 and use of desulfurization technologies lead to the remarkable decrease in sulphur oxide air pollution in this region and by the end of the 1970s, it reached the same level as that in uncontaminated areas (Yoshida et al., 2007). Even though exhaust

emission control (1970), Automobile NO_X Reduction Law (1993) and the development and adoption of low emission cars and the improvement of fuels, increase in vehicles (8 million in 1968 to 78 million in 2005) caused steady NO_2 concentration during 1979-1995 and slight decrease until 2005 (MLIT, 2016; Wakamatsu et al, 2013).

Fig. 1-1. Annual average concentrations of NO_2 (1970-2012). (Adopted from Wakamatsu et al., 2013).

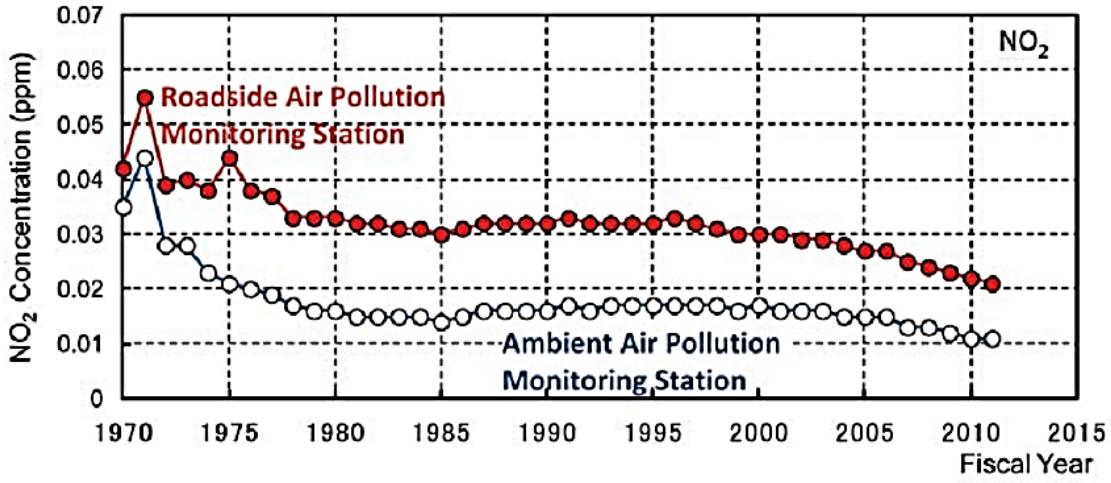

However, after implementation of automobile NO_X/PM Law (2001) and further improvements and much smaller increment of vehicles (78 million in 2005 – 80 million in 2015) resulted in a rapid decrease in NO_2 concentration from 2005 (Fig. 1-1). However, continuous increasing trend in surface ozone (O_3) has been observed for long time in most of the cities in Japan (Fig. 1-2), even though the precursors VOCs and NO_X have decreased 40-50 % and 51-54 % respectively from 1990-2010 after several strict regulations for anthropogenic emission (Akimoto et al., 2015; Wakamatsu et al., 2013). Previous studies in Japan, have suggested that increasing of O_3 may be due to the existence of unknown VOCs which might have involved in O_3 formation and subsequent consumption of NO_X (Sadanaga et al., 2005; Kajii et al., 2006; Yoshino et al, 2012), increase in the background O_3 concentration by transboundary transport and decrease in the NO titration effect (Akimoto et al, 2015). Growing surface ozone level has an important concern because of harmful effect on the human respiratory system (Patz et al., 2005; Godish, 2004), radiative forcing (Stocker et al., 2013) and damage to the vegetation (Fuhrer et al., 1997; Booker et al., 2009).

Fig. 1-2. Annual average of daily maximum concentrations of Ox (1976-2012) and annual average concentrations of NMHC between 6 am and 9 am (1976-2012). (Adopted from Wakamatsu et al., 2013).

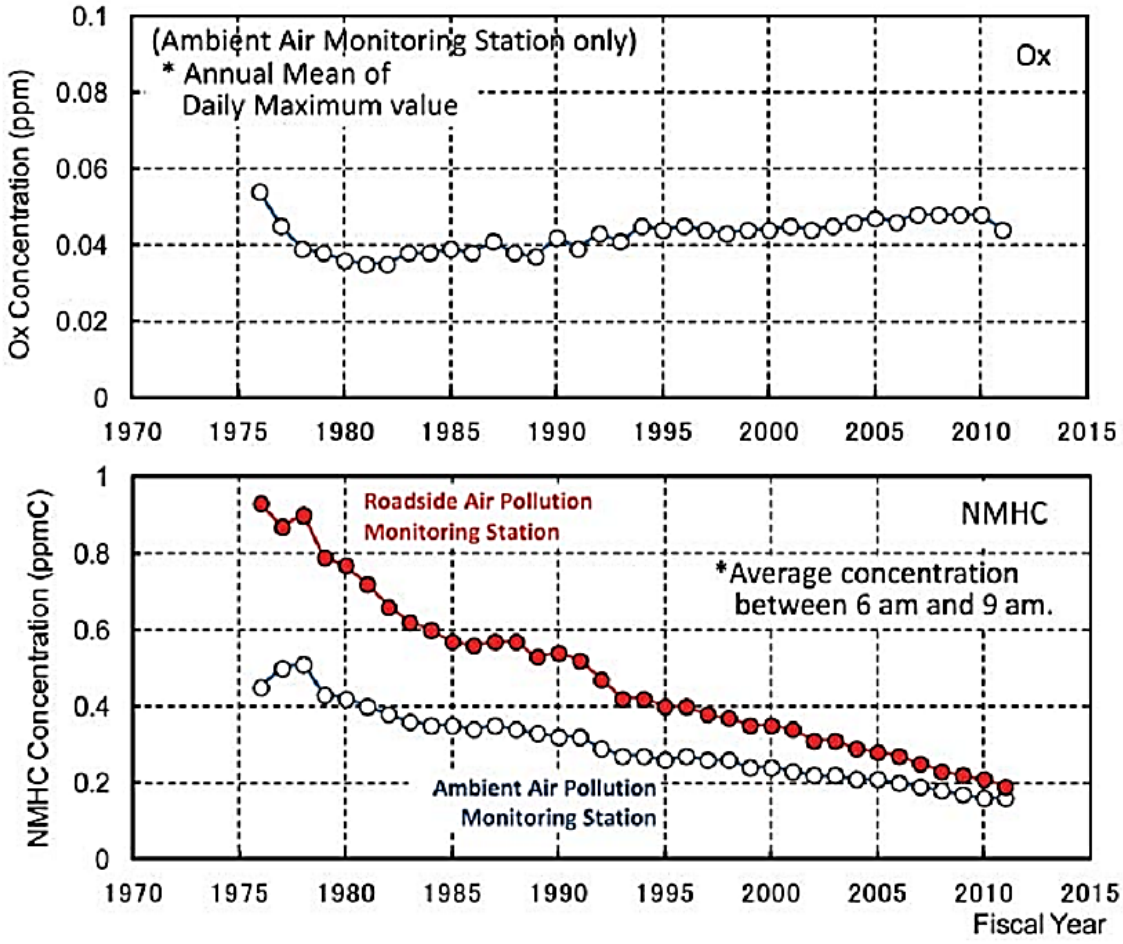

1.2. Importance of Biogenic VOCs emission and photochemical O_3 formation

Although regulations control anthropogenic VOCs, plants also emit a significant amount of reactive biogenic volatile organic compounds. Even though plants serve in many ways to the environment such as conversion of carbon dioxide through photosynthesis into energy, removal of pollutants such as NO_2, particulate matters (Pugh et al., 2012) and oxygenated VOCs (Karl et al., 2010) through deposition, they release potentially reactive BOVCs to the atmosphere that are synthesized through metabolic pathway (Kesselmeier and Staudt, 1999). Estimations have shown that biogenic emissions contribute larger fraction (1000 Tg C yr^{-1}) to the overall global

VOC emissions (Guenther et al., 2012), compared to anthropogenic emission (50-100Tg C yr^{-1}) (Holzke et al., 2006). Recently Sindelarova et al., (2014) estimated global BVOC flux as 760 Tg C yr^{-1} which comprised of 70 % isoprene and 11 % monoterpenes (Fig. 1-3).

Fig. 1-3. Spatial distribution of monthly mean emissions of (a) isoprene, (b) monoterpenes, (mg m^{-2} day^{-1}) for January (top) and July (bottom) averaged over the modelled period 1980–2010 calculated by the MEGAN model. (Adopted from Sindelarova et al., 2014).

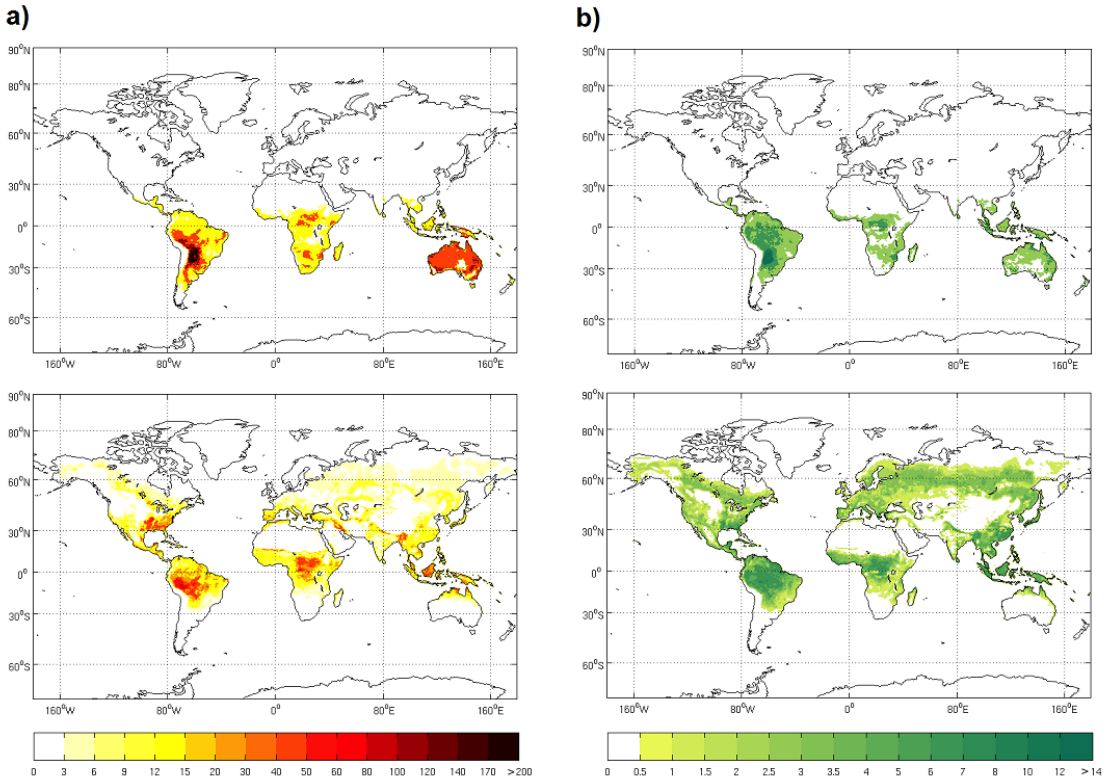

Biogenic volatile organic compounds (BVOC) with high reactivity towards atmospheric oxidants such as hydroxyl radicals (OH), ozone (O_3) and nitrate radicals (NO_3) are supplied to the atmosphere in a vast amount by forests (Guenther et al., 2000, 2012, Atkinson and Arey, 2003). If the abundance of reactive biogenic volatile organic compounds such as isoprene and monoterpene significant, near urban areas, where NO_X comes from anthropogenic emission will lead to the faster HO_X recycling and higher photochemical O_3 production in daytime.

Along with anthropogenic sources, isoprene also observed as a major sink of hydroxyl radical in many recent studies conducted in East Asian suburban areas near Beijing (Ran et al., 2011), Seoul (Kim et al., 2013; Kim et al., 2013a) and Taipei (Chang et al., 2014). Additionally, the modelling study evaluated that isoprene photochemistry efficiently involved in O_3 production in Kinki region, Japan (Bao et al., 2010). Observed and modelled O_3 mixing ratio in Kanto region including Tokyo metropolitan area (TMA) was reported as higher in mountain regions in addition to the urban areas (Watanabe et al., 2016).

The loss rate measurement of OH which is defined as OH reactivity provides the overall reactivity of air mass which is comprised of atmospheric trace species. The relative fraction of individual VOCs and other species can be determined by the comparison of directly measured OH reactivity with the OH reactivity calculated from simultaneous trace gas measurement. Our group has previously studied OH reactivity in the urban and suburban area in Tokyo Metropolitan area and found a discrepancy between measured and calculated OH reactivity due to the presence of unmeasured VOCs (Sadanaga et al., 2005, Yoshino et al. 2006 & 2012). The greater extent of discrepancy was observed in summer due to enhanced photochemical activity and subsequent oxygenated VOCs formation which were not measured.

1.3. Nature of BVOCs emission

Depending on the nature of the plants and the physiochemical and physiological environment plant emissions consist of a wide variety of terpenoids (isoprene, monoterpenes, and sesquiterpenes), oxygenated VOCs and aromatics, (Kesselmeier and Staudt, 1999; Niinemets et al., 2004; Laothawornkitkul et al., 2009). The main classification of terpenoid emissions from plants are 1) pool emission (emission from special storage structures) and 2) *de novo* synthesis (emission immediately after synthesis). Storage structures in plants such as the resin duct (e.g. coniferous trees) and the glandular cells lead to pool emission, which mainly depends on the temperature and accounts for both the day-time and night-time emission of monoterpenes and sesquiterpenes (Loreto et al., 2000; Karl et al., 2009; Taipale et al., 2011). On the other hand, isoprene and some monoterpenes can be emitted from *de novo* synthesis if plants do not have special storage structures that depending on light and temperature

conditions (Kesselmeier and Staudt, 1999). Various stresses such as heat and drought, herbivore attack, elevated CO_2 and ozone exposure can alter BVOC emissions, in addition to the above constitutive emission (Constable et al., 1999; Heiden et al., 1999; Loreto and Schnitzler, 2010; Niinemets, 2010; Copolovici et al., 2011).

1.4. Photochemical oxidation and trace gas removal in the atmosphere

The primary mechanism that involves the formation of OH radicals in the troposphere is photodissociation of O_3 by solar UV light ($\lambda < 320$ nm) into excited oxygen atom (O^1D) and further reaction with water vapour.

$$O_3 + h\nu \rightarrow O(^1D) + O_2 \quad (1\text{-}1)$$

$$O(^1D) + H_2O \rightarrow 2OH^{\bullet} \quad (1\text{-}2)$$

While major fraction of $O(^1D)$ are quenched back to $O(^3P)$ by N_2 and O_2, a small fraction of $O(^1D)$ will result in OH (marine boundary layer, about 10 % of $O(^1D)$ to OH) (Monks, 2005) and it depends on the H_2O concentration. There are some other photolysis reactions such as HCHO, HONO and H_2O_2 can produce OH significantly.

Additionally, ozonolysis of alkenes can also produce OH and it mainly active in night time since in daytime destruction of alkenes by OH is predominant.

OH loss process involves either in the formation of long living species which act as permanent sinks or short-living species which recycle back into OH.

Methane (CH_4) and CO are the most abundant species in the atmosphere to react with hydroxyl radicals if the environment is very clean (Eisele et al., 1994; Sadanaga et al., 2005).

$$OH^{\bullet} + CO(+ O_2) \rightarrow HO_2^{\bullet} + CO_2 \quad (1\text{-}3)$$

$$OH^{\bullet} + CH_4 (+ O_2) \rightarrow CH_3O_2^{\bullet} + H_2O \quad (1\text{-}4)$$

Fig. 1-4. Primary biogenic and anthropogenic emissions and atmospheric photochemical process. (Controls of BVOC emission, Ref.: Laothawornkitkul et al., 2009).

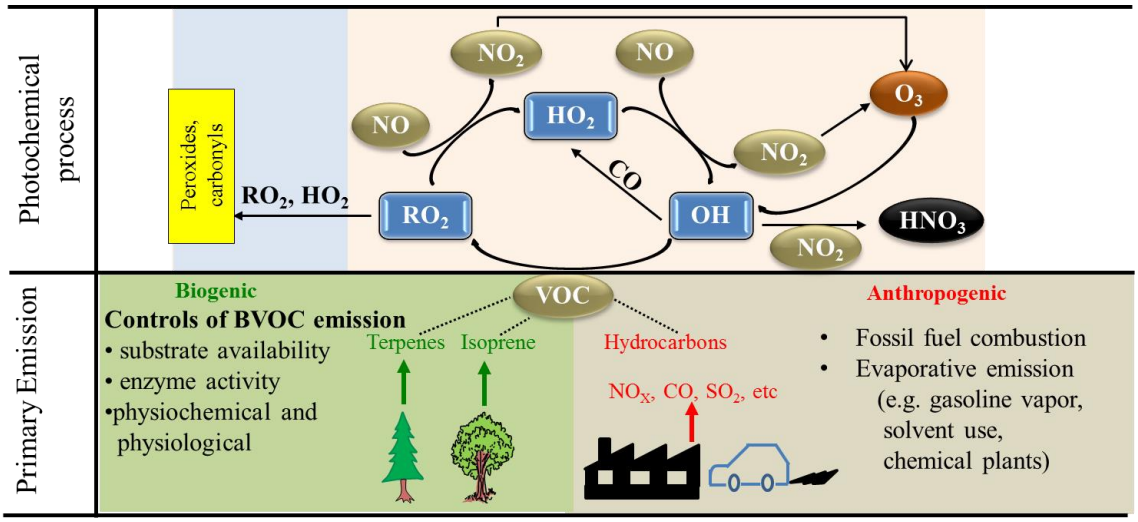

In the urban atmosphere, nitrogen oxides (NO and NO_2) and volatile organic compounds control the loss and recycling process of OH radicals.

The main reaction between VOCs and $OH^{\bullet}$ involves abstraction of H or addition of $OH^{\bullet}$ and formation of peroxides. For generalisation, the reaction 4 can be written as follows.

$$OH^{\bullet} + RH\ (+ O_2) \rightarrow RO_2^{\bullet} + H_2O \qquad (1\text{-}5)$$

Whereas R represents methyl, alkyl, aryl, carbonyl compounds. These peroxides rapidly recycle back OH radical with the production of photochemical O_3.

$$OH^{\bullet} + R{=}CH_2\ (+ O_2) \rightarrow R(O_2^{\bullet}){-}CH_2\ OH \qquad (1\text{-}6)$$

$$RO_2^{\bullet} + NO \rightarrow NO_2 + RO^{\bullet} \qquad (1\text{-}7)$$

$$RO^{\bullet} + O_2 \rightarrow R'CHO + HO_2^{\bullet} \qquad (1\text{-}8)$$

$$HO_2^{\bullet} + NO \rightarrow NO_2 + OH^{\bullet} \qquad (1\text{-}9)$$

Meanwhile NO_2 is photolyzed to O_3.

$NO_2 + hv(\lambda < 420\ nm) \rightarrow NO + O_3$ (1-10)

Recycling of peroxy radicals to OH radicals is affected by self-reactions of radicals, and it leads to the chain termination.

$HO_2^\bullet + HO_2^\bullet \rightarrow H_2O_2 + O_2$ (1-11)

$RO_2^\bullet + HO_2^\bullet \rightarrow ROOH + O_2$ (1-12)

$OH^\bullet + HO_2^\bullet \rightarrow H_2O + O_2$ (1-13)

Competition between chain termination and recycling determines the photochemical production of O_3

Usually recycling process is much faster than both HO_X ($OH + HO_2$) production and HO_X loss if optimum NO_X ($NO+NO_2$) and sufficient photochemical active radiation available.

Under high NO_X conditions, typically > 10 ppb OH loss by NO_X mainly is predominant.

$NO_2 + OH^\bullet\ (+M) \rightarrow HNO_3$ (1-14)

$NO + OH^\bullet\ (+M) \rightarrow HONO$ (1-15)

$NO_2 + HO_2^\bullet\ (+M) \rightarrow HNO_4$ (1-16)

M is the medium (O_2 or N_2)

The OH radical is often referred to as the tropospheric detergent as it reacts with almost all species present in the atmosphere, except for some extremely unreactive species such as N_2O, halocarbons, etc. Total OH reactivity, which is the loss rate measurement of the OH radical, indirectly evaluates the overall reactive species comprised in an air mass. In addition to this direct measurement, the OH reactivity is also calculated using the sum of the product of the OH reactive rate coefficients (k_{OH+N_i}) of all species with their respective mixing ratio [N_i] as shown below.

$$k_{calc} = \sum_i k_{OH+N_i}[N_i] \quad (1-17)$$

The discrepancy between the measured and calculated OH reactivity, which is referred to as missing OH reactivity, highlights the potential new sources of OH reactivity yet to be quantified.

1.5. Scope of this research work

Open questions:

- Reasons why increasing of O_3 in Japan, especially higher concentration in suburban areas near densely populated cities is still not clear, even though decreasing trend in the precursors VOCs and NO_X.
- Substantial uncertainty in BVOCs distribution due to limited measurements and quantification techniques.
- What kind of combination of instruments will describe well the distribution of trace species, photochemical process and meteorological controls is a matter of question?
- Which place will give a clear picture and serve as a representative place is also subject to question?

So that precise quantification of trace gas composition from both biogenic and anthropogenic sources and interpretation with meteorological controls is essential to understand the photochemical formation of secondary product O_3. Since BVOCs are highly reactive, a complete understanding of their supply to the atmosphere from biosphere near urban area is very complicated due to faster removal by oxidants. Therefore, recently developed improved BVOCs quantification tool BVOC GC-FID (Jones et al., 2014) with other trace gas measurement tools and well established OH reactivity instrument was deployed in remote forest site Wakayama Research Forest Station (WFRS) for two weeks during summer, 2014. This forest has chosen to study because of unique characteristics such as far away from anthropogenic emission sources, a larger area (8.42 km^2), more than 50 % area covered by coniferous trees namely Japanese cedar and Japanese cypress which are also major trees in Japan and predominant clean air mass flow from the Pacific Ocean. Due to these factors, this forest was expected to give a good picture of reactive trace gas distribution over an unpolluted atmosphere. The measurement was conducted in summer because biogenic species monoterpenes and isoprene are strongly sensitive to light and temperature, and

also both broad-leaved and coniferous trees host maxim leaves. Enhanced emission in summer can help to quantify several biogenic species and to understand the responses of biogenic VOCs to the meteorological driving forces. Isoprene and 12 monoterpenes such as α-pinene myrcene and Δ-3-carene and other trace gases were quantified. Measured OH reactivity in this campaign was much lower (7 s^{-1}) and consistent with that made in similar environments.

In another work, I have interpreted the trace gas composition and OH reactivity measured by our group at suburban forest site located in Tama Hills during early autumn during early autumn-2012 and summer-2013. This site was chosen because it located 30 km away from Tokyo and expected to receive both biogenic and anthropogenic sources. Japanese oak and Japanese cedar located in this forest supply biogenic sources additionally surrounding residential, traffic and urban air outflow provide anthropogenic sources. Sophisticated instruments such as OH reactivity measurement system to provide overall reactivity of ambient air, GC-FID to measure VOCs, and other inorganic pollutant measurement instruments were deployed during the measurement campaigns. Measurements were conducted in autumn and summer to understand the change in trace gas composition and photochemical products due to meteorological factors such as temperature and light.

2. Identification and characterisation of VOCs in Wakayama forest

In this chapter, identification of biogenic VOCs, oxygenated BVOCs, OVOCs in Wakayama Forest Research Station (WFRS) and the characteristics of those species such as response to meteorological conditions (temperature and light) and inter-relationship are discussed. Additionally, BVOCs measured in WFRS are compared with that measured in the boreal forest.

2.1. Observation

2.1.1. Field site description

During the summer period of July 27th to August 8th, 2014 an intensive campaign of measurement was conducted at WFRS (34°01' N, 135°01' E and 560 m a.s.l.) which belongs to Kyoto University (Fig.2-1)

The forest is located in the middle of the Kii peninsula, the largest in Honshu Island and the total area is 8.42 km^2. More than half of the forest is covered with coniferous trees, namely sugi (*Cryptomeria japonica*) and hinoki (*Chamaecyparis obutsa*) and the forest area mainly has a steep mountainous topography (altitude 445-1261 m). Previous studies have reported that *Cryptomeria japonica* and *Chamaecyparis obutsa* are strong monoterpene emitters, emitting especially high concentrations of α-pinene (Bao et al., 2008; Matsunaga, et al., 2011; Mochizuki, et al., 2011). Apart from these dominant trees, the other coniferous trees found in this region are momi (*Abies firma*) and tsuga (*Tsuga sieboldii*). In the higher altitudes broad-leaved deciduous trees are located, the most dominant of them being akagashi (*Quercus acuta*), urazirogashi (*Quercus salicina*), soyogo (*Ilex pondunclosa*) and mizunara (*Quercus crispula*). The middle of May to the beginning of September is considered as the summer season, during which it is generally wet and humid with August being the hottest month (average temperature 27.6 °C).

Fig. 2-1. Measurement site located at Wakayama forest research station (WFRS)

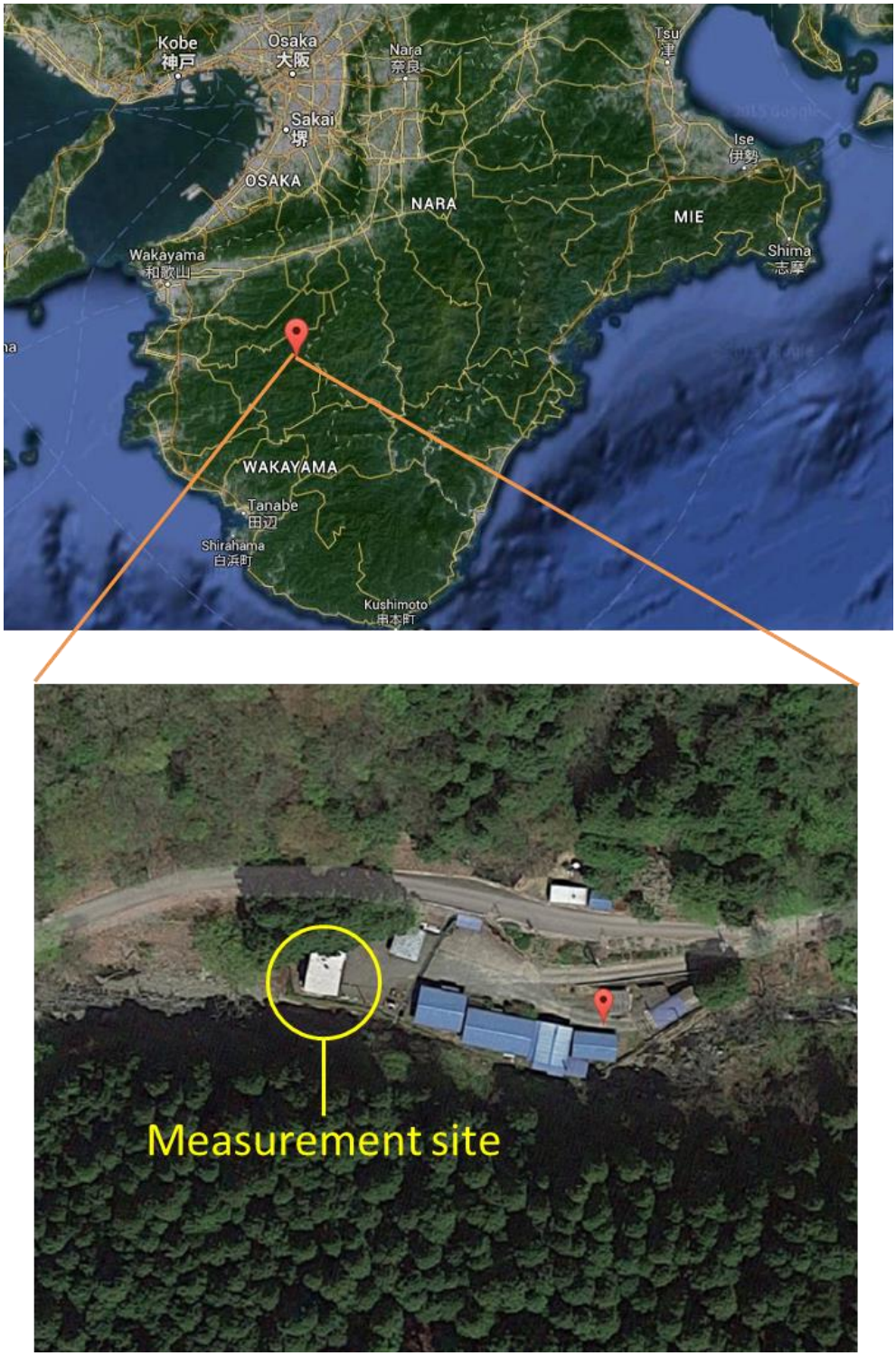

2.1.2. Measurement of VOCs

Monoterpenes, sesquiterpenes and oxygenated biogenic VOCs (OBVOCs) were measured *in situ* every ~27 minutes using a BVOC gas chromatography-flame ionisation detector (BVOC GC-FID) (300 Series GC, Ellutia) (Jones et al., 2014).

Fig. 2-2. Schematic diagram of BVOC-GCFID.

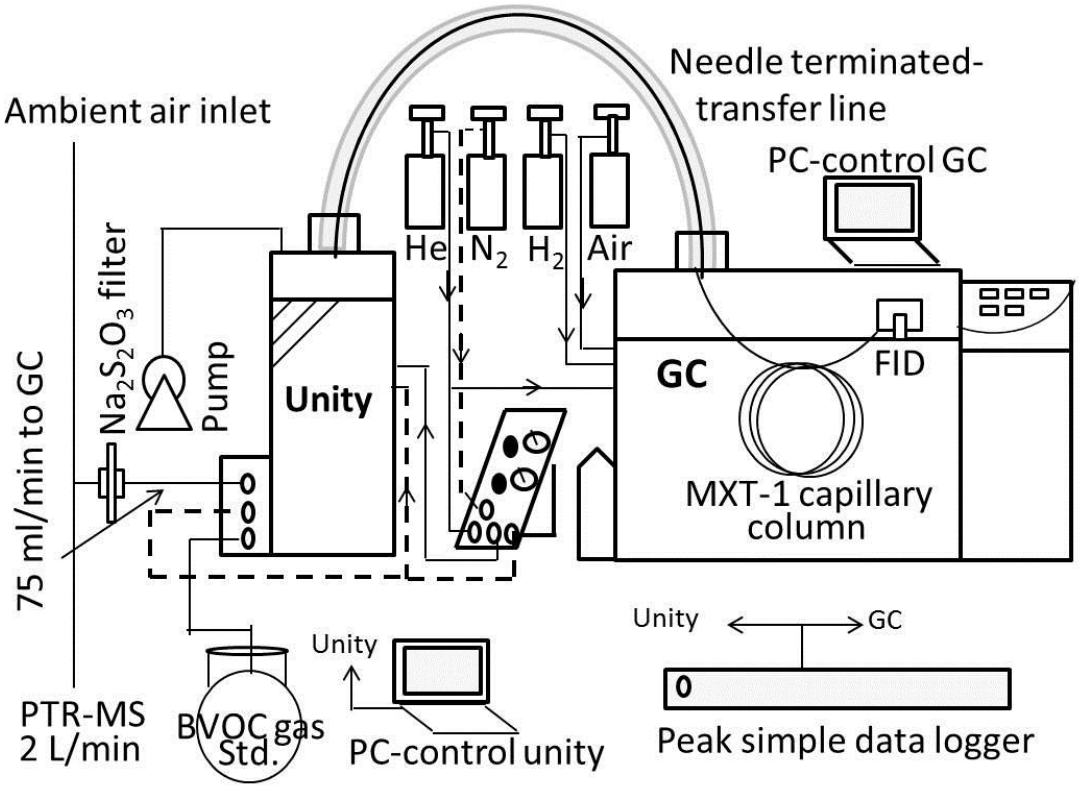

An air sample was pre-concentrated for 10 minutes, at a flow rate of 75 mL min^{-1}, in a peltier-cooled tenax cold trap settled in a Unity 2™ thermal desorber (Markers, UK). After sampling, to eliminate moisture, the cold trap was backflushed for 2 minutes with dry helium gas at a frequency of 30 mL min^{-1} and rapidly heated to 300 °C (~100 °C s^{-1}), then transferred through a heated needle terminated transfer line (deactivated silica capillary, 130 °C) to the GC injector port. An inert coated steel capillary, non-polar MXT-5 column (15 m × 0.25 mm ID, 0.25 µm film thickness) was resistively heated, instead of using a conventional large GC oven, to minimise GC cycle time (rapid heating during GC analysis and rapid post-analysis cooling). Sample volumes of 100 mL working terpene gas standards were directly calibrated against small quantities

(10–20 mL) of the 1 ppm (PAMS-J58, Sumitomo Seika Chemicals) primary standards and 100 mL volumes of the freshly diluted secondary standards for α-pinene and β-pinene. For the other components in the terpene gas standard, the mixing ratios were obtained based on the ratio of their respective FID responses to the α-pinene response factor. The overall uncertainties were assessed to be: ±8–12% for monoterpenes, ±14–26% for OBVOC and ±15–20% for sesquiterpenes. Limit of detection of monoterpenes and OBVOCs is 4-5 ppt. The ambient air samples were pulled through a (1/4″ (0.64 cm) OD) PFA manifold at a flow rate of 2 L min^{-1} from an inlet and subdivided into subsample lines. One of them was used to provide the air supply for the proton transfer reaction-quadrupole mass spectrometer (PTR-MS, Ionicon analystik, Austria) at a flow rate of 50 mL min^{-1} and another was applied to the BVOC GC-FID through a $Na_2S_2O_3$ ozone filter. The detailed discussion about the loss of terpenes due to ozone filter and correction are given elsewhere (Jones et.al, 2014). The residence time of ambient air in sample line from the inlet to BVOC GC-FID is <25 s and hence ozone destruction was not significant within the sample line. Diluted α-pinene gas was generated using a permeater (Gastec PD-1B) and supplied to the OH reactivity system and BVOC GC-FID. Mixing ratio of α-pinene was obtained from OH decay rate measured using OH reactivity system and reaction rate coefficient of α-pinene with OH. α-pinene mixing ratio obtained from BVOC GC-FID was cross-calibrated with that obtained from OH reactivity system.

Isoprene (*m*/*z* = 69), total monoterpenes (*m*/*z*=81, 137) and oxygenated volatile organic compounds (OVOCs), acetaldehyde (*m*/*z*=45), acetone (m/z=59), acetic acid (m/z=61), methyl vinyl ketone (MVK) + methacrolein (MACR) (*m*/*z*=71), methyl ethyl ketone (MEK) (*m*/*z*=73) and ethyl vinyl ketone (EVK) (*m*/*z*=85), were measured using a PTR-MS (Kato et al., 2004). Zero air, VOC free gas generated by the heated Pt catalyst, was measured periodically and subtracted as the background signal. The isoprene concentration was determined by comparison of the canister to GC-FID measurement. Although signal at *m*/*z* 69 is considered to be mainly isoprene, the slight interaction of the other species such as furan to this signal cannot be ruled out. A standard gas cylinder (Taiyo Toyo Sanso, Japan) was used for the calibration of acetaldehyde and acetone. MVK+MACR, MEK, EVK and acetic acid, were not calibrated by gas standards. The mixing ratios of non-calibrated OVOCs were obtained by assuming a similar calibration factor as calibrated OVOCs.

During the measurement campaign, the pressurized ambient air samples were collected seven times at the following times and dates: on the 3rd at,13:30 and 21:06, 5th at 16:02, 6th at 15:21, 7th at 10:30 and 14:40 and the 8th at 14:38, in 6 L stainless canisters for non-methane hydrocarbon (NMHCs) analysis. GC-FID (HP 6890, Hewlett Packard) was used to analyse approximately 60 species of C_2–C_{11} NMHCs present in the canister and the detailed description of analysis is given elsewhere (Kato et al., 2001). NMHCs were concentrated by introducing 0.5 L of the sample into a three-stage preconcentrator (Model 7000, Entech) before injection into the GC-FID. The injected sample was introduced into the HP-1 Column (60 m length, 0.32 mm internal diameter, 1-mm film thickness, Agilent J&W) to analyse hydrocarbons. Initially, the GC oven temperature was kept at -50 °C (for 8 min) and then increased to 40 °C at a rate of 5 °C min^{-1}, after that the temperature was further increased to 150 °C at a rate of 15 °C min^{-1}. NMHC concentrations were calibrated with a 1 ppmv standard gas containing 58 species (PAMS-J58, Sumitomoseika). Detection limits of the NMHCs are in the range of 1-3 pptv with 2-13% accuracy and 2-15% precision.

Ambient air was collected every day, three times, at 08:30, 12:30 and 16:30 using silica-gel coated 2,4-dinitrophenylhydrazine (DNPH) scrubbers (Inertsep mini aero DNPH, GL Sciences) for carbonyl compounds measurement. Prior to the DNPH scrubbers, a potassium iodide (KI) scrubber (Inertsep mini aero ozone scrubber, GL Sciences) was attached. Ambient air was pulled through the scrubbers using a pump at a rate of 0.5 L min^{-1}, and the total sampling time was one hour. 5 mL of high-grade acetonitrile was used to extract the DNPH derivative, and the extraction was analysed using a high-performance liquid chromatograph (HPLC) (L-7000, Hitachi High-Technologies) coupled with a UV absorption spectrometer at 360 nm (Hitachi L-7455 Diode Array Detector). A 100 μL volume of the sample solution was introduced into the column (LaChrom C18, Hitachi High-Tech Fielding) via an autosampler and carbonyls were separated in the column with a mobile phase of acetonitrile/water (1:1) and a flow rate of 1.0 mL min^{-1}. The column oven temperature was kept at 40 °C. Calibration and quantification of carbonyls were done using standard samples (SPELCO).

Table 2-1. Average mixing ratio of species

[a]Average mixing ratio of species with standard deviation (1σ)

species	[a]average mixing ratio
Biogenics (mixing ratio unit: ppt)	
isoprene	595 ± 502
Monoterpenes	
α-pinene	259 ± 105
camphene	48 ± 26
β-pinene	98 ± 39
myrcene	56 ± 27
α-phellandrene	10 ± 9
Δ-3-carene	97 ± 48
α-terpinene	2 ± 3
p-cymene	16 ±10
limonene	47 ± 18
ocimene	49 ± 27
γ- terpinene	13 ± 8
terpinolene	12 ± 8
monoterpenes (total)	709 ± 213
OBVOCs	
linalool	34 ± 46
limonene oxide	13 ± 10
Sesquiterpenes	
β-caryophellene	27 ± 8
OVOCs (mixing ratio unit: ppb)	
acetaldehyde (m/z 59)	3.6 ± 2.3
MVK+MACR (m/z 71)	3.3 ± 2.2
EVK (m/z 85)	1.4 ± 0.7
acetone (m/z 45)	7.9 ± 4.3
MEK (m/z 73)	1.1 ± 5.6
acetic acid (m/z 61)	5.4 ± 3.9
Inorganics (mixing ratio unit: ppb)	
CO	114 (assumed)
O_3	7.7 ± 10.5
NO	0.7 ± 0.7
NO_2	0.3 ± 0.3
CH_4	1710 (assumed)

2. 2. Results and discussion

2.2.1. Anthropogenic VOCs and Carbonyl Species

Anthropogenic VOCs measured using canister/GC-FID were found to be in the lower order of mixing ratios (e.g. average mixing ratios of propane 50 ppt, n-pentane 18 ppt, trans-2-butene 8 ppt and ethylbenzene 4 ppt). Unfortunately, carbonyl compounds that were collected using DNPH scrubbers were not available. Due to the very high humidity (the average relative humidity% was ~90%) the KI scrubber used prior to the DNPH scrubber to trap O_3 may have trapped the carbonyls before they reached the DNPH scrubber or reactive KI_3 may have been formed from the reaction of KI thus destroying the carbonyls in the DNPH scrubber.

2.2.2. Monoterpenes, sesquiterpenes, and OBVOCs diurnal profile

For the first time in this forest, 12 monoterpenes, 2 OBVOCs, and one sesquiterpene (Fig. 2-3) were quantified *in situ*. The mixing ratios of α-pinene, camphene, β-pinene, myrcene, α-phellandrene, Δ-3-carene, α-terpinene, ρ-cymene, limonene, ocimene, γ-terpene, terpinolene (monoterpenes), linalool, limonene oxide (oxygenated BVOCs) and β- caryophyllene (sesquiterpene) were measured using BVOC GC-FID are shown in Figures 2-4 to 2-7. Since coniferous trees monoterpene emitters are the dominant species in this forest, the average mixing ratio of monoterpene (709 ppt) was higher than that of isoprene (595 ppt). Despite the average mixing ratio of isoprene during the day-time was higher (835 ppt) than that of the total monoterpenes (622 ppt), the night-time average mixing ratio of total monoterpenes was much higher (782 ppt) than that of isoprene (168 ppt). This can be attributed to the combination of the nocturnal boundary layer and the temperature dependent emission of terpene and the absence of isoprene emission in darkness.

Fig. 2-3. Molecular structure of monoterpenes, sesquiterpene and oxygenated biogenic volatile organic compounds (OBVOCs).

Monoterpenes

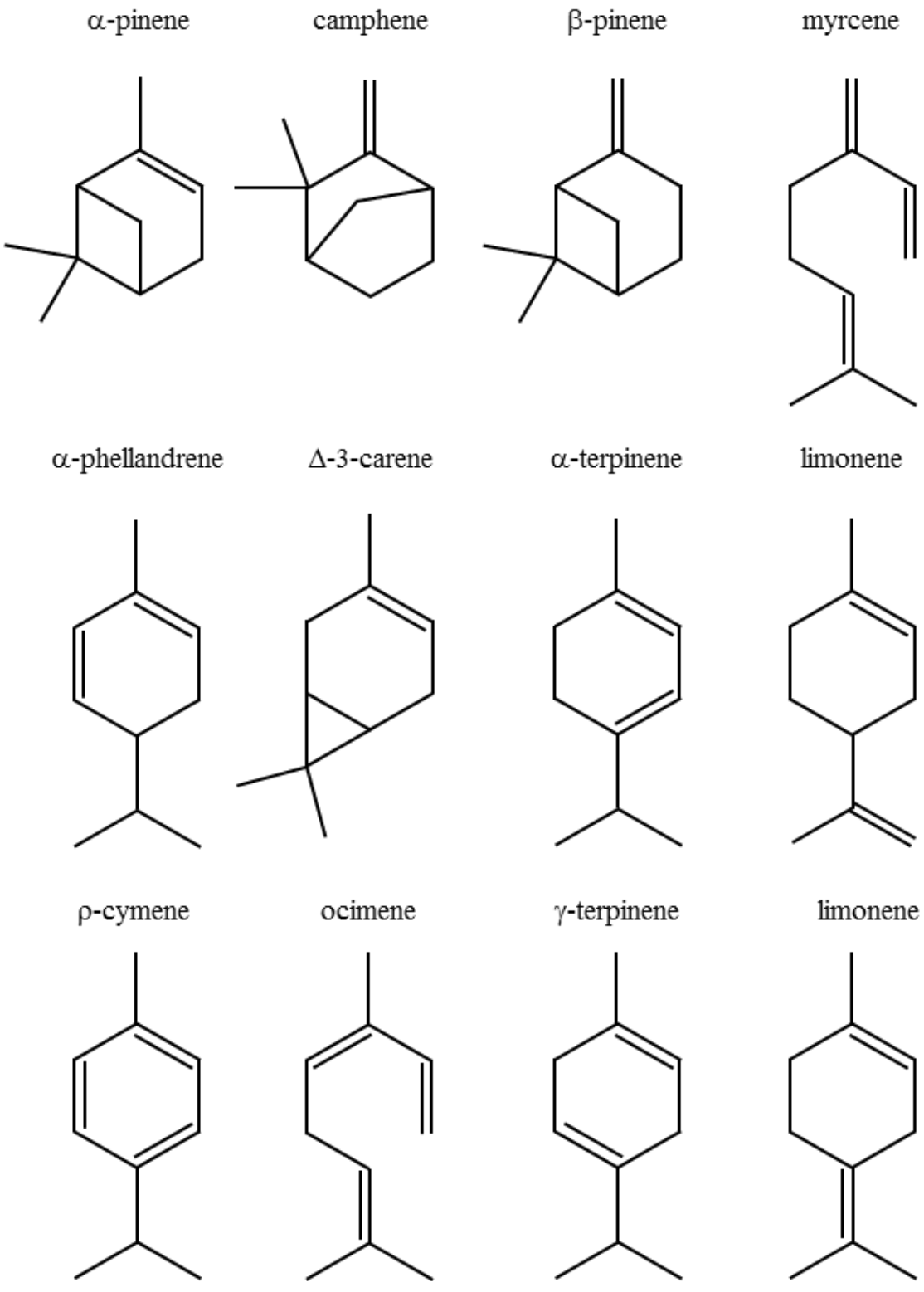

Sesquiterpene

β-caryophyllene

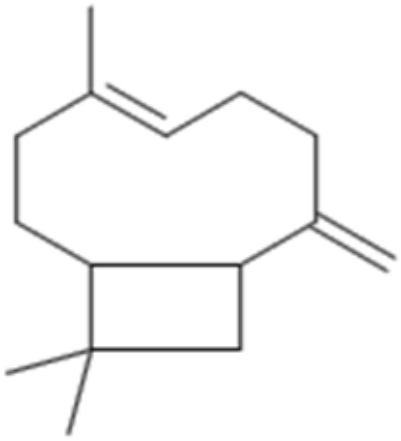

Oxygenated biogenic volatile organic compounds (OBVOCs)

linalool

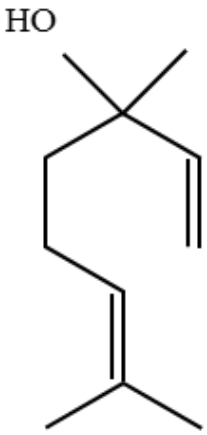

Limonene oxide

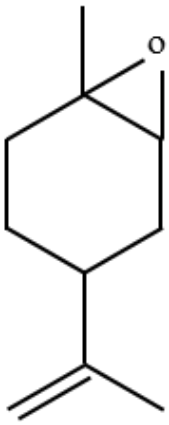

Fig. 2-4. Time series of mixing ratio (ppt) of monoterpenes (α-pinene, camphene, β-pinene, myrcene) measured using BVOC GC-FID.

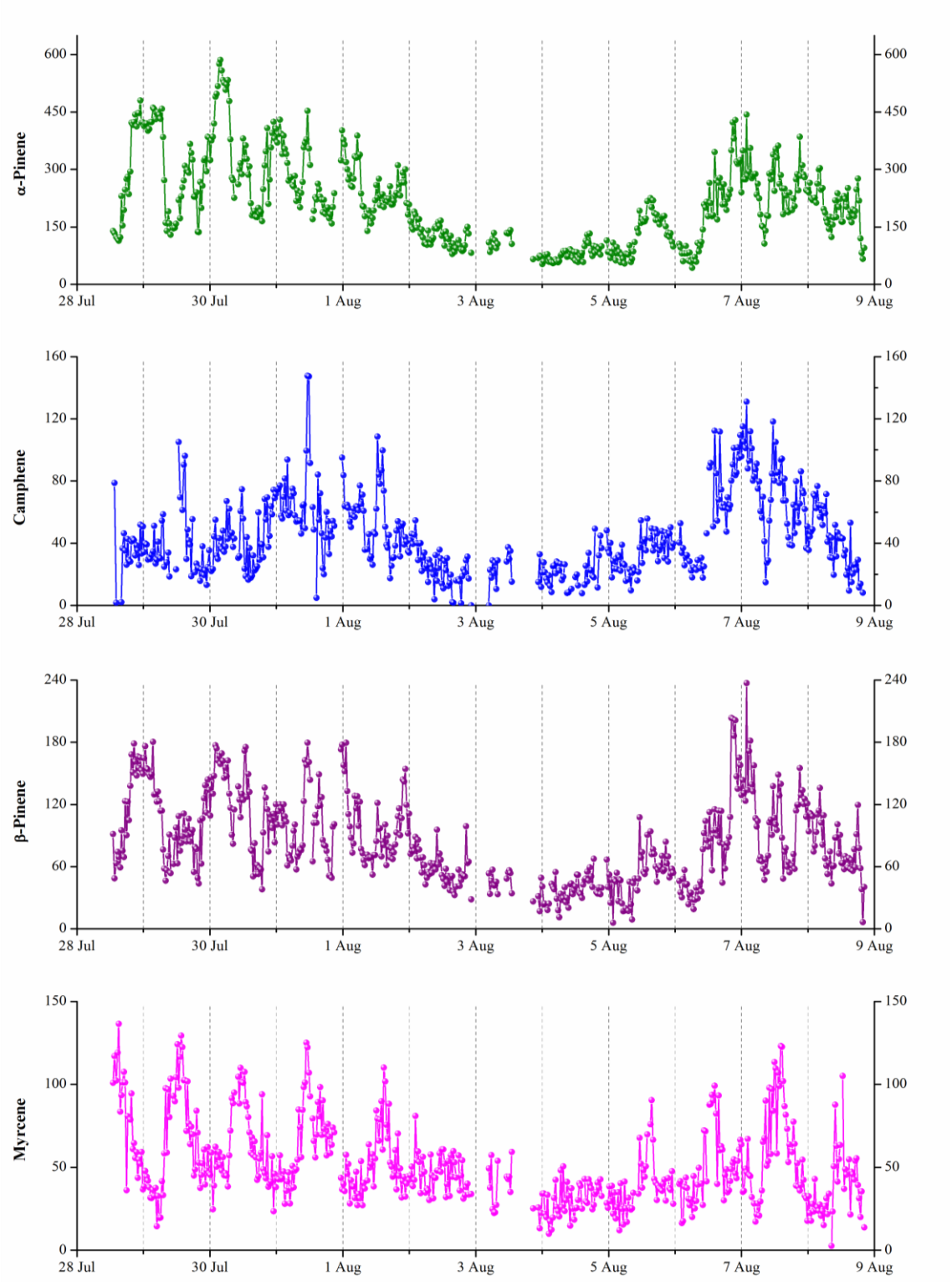

Fig. 2-5. Time series of mixing ratio (ppt) of monoterpenes α-phellandrene, Δ-3-carene, α-terpinene, ρ-cymene) measured using BVOC GC-FID.

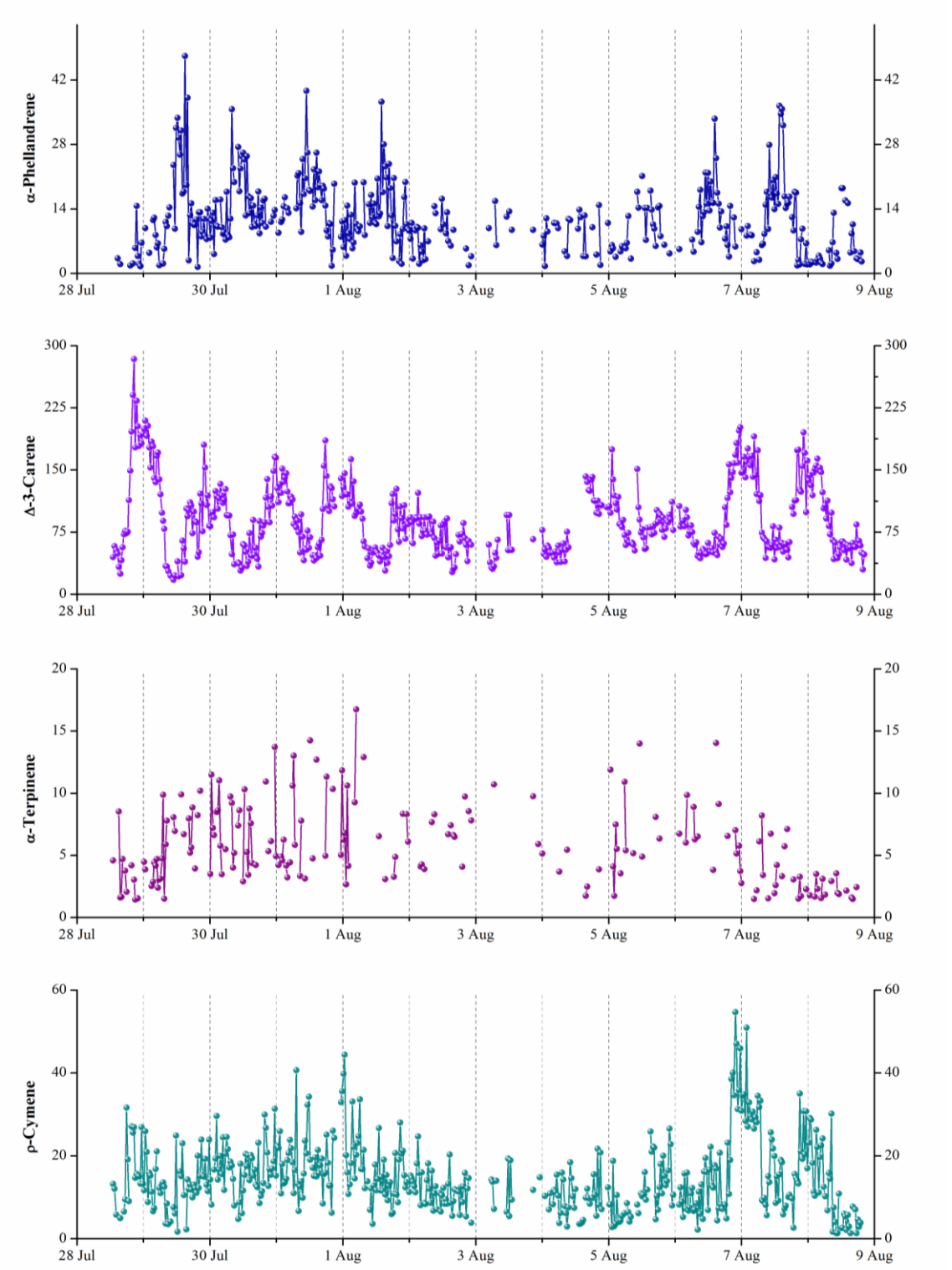

Fig. 2-6. Time series of mixing ratio (ppt) of monoterpenes limonene, ocimene, γ-terpinene, terpinolene measured using the BVOC-GCFID.

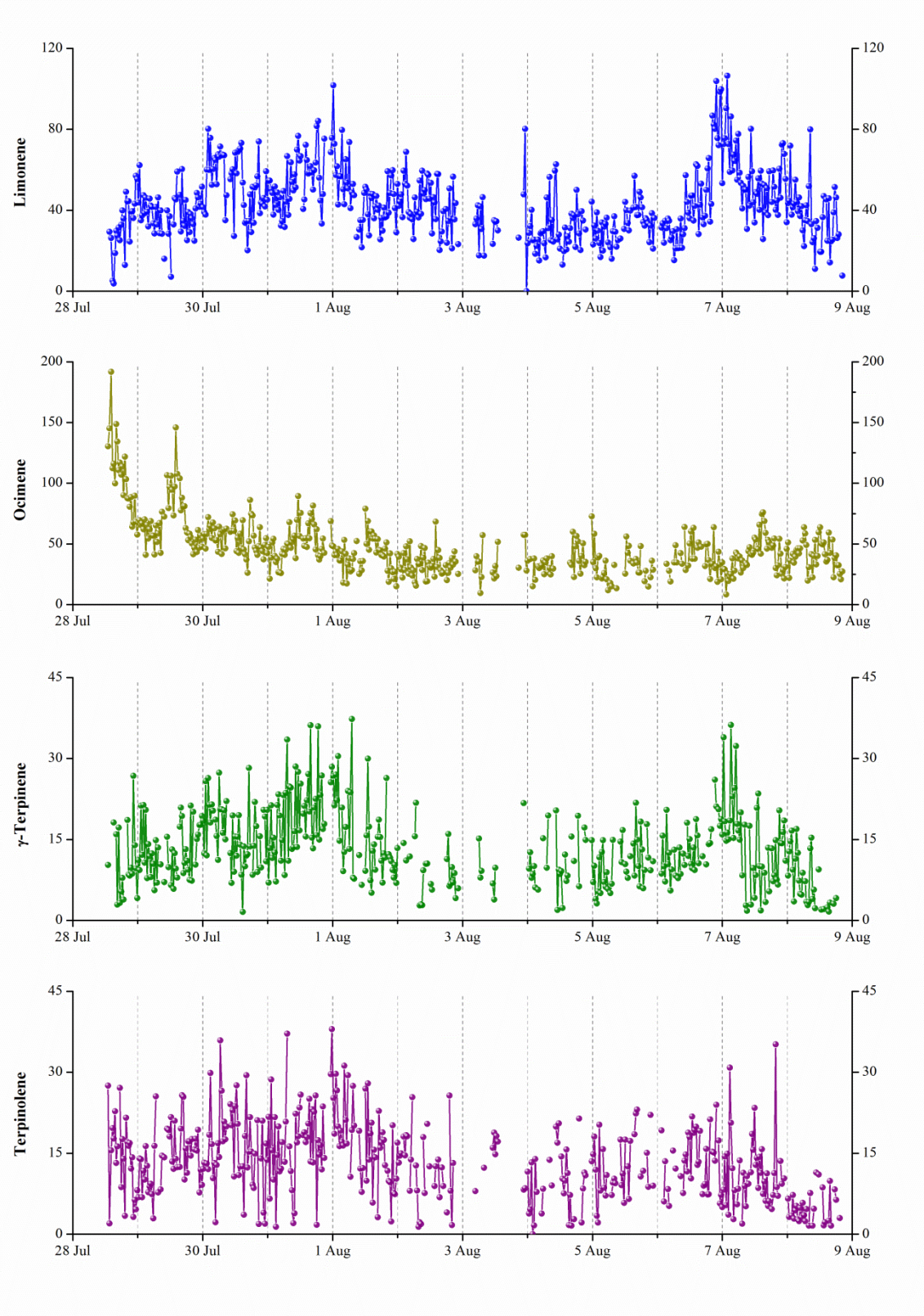

Fig. 2-7. Time series of mixing ratio (ppt) of OBVOCs (linalool, limonene oxide) and sesquiterpene (β-caryophyllene), measured using the Fast-GC.

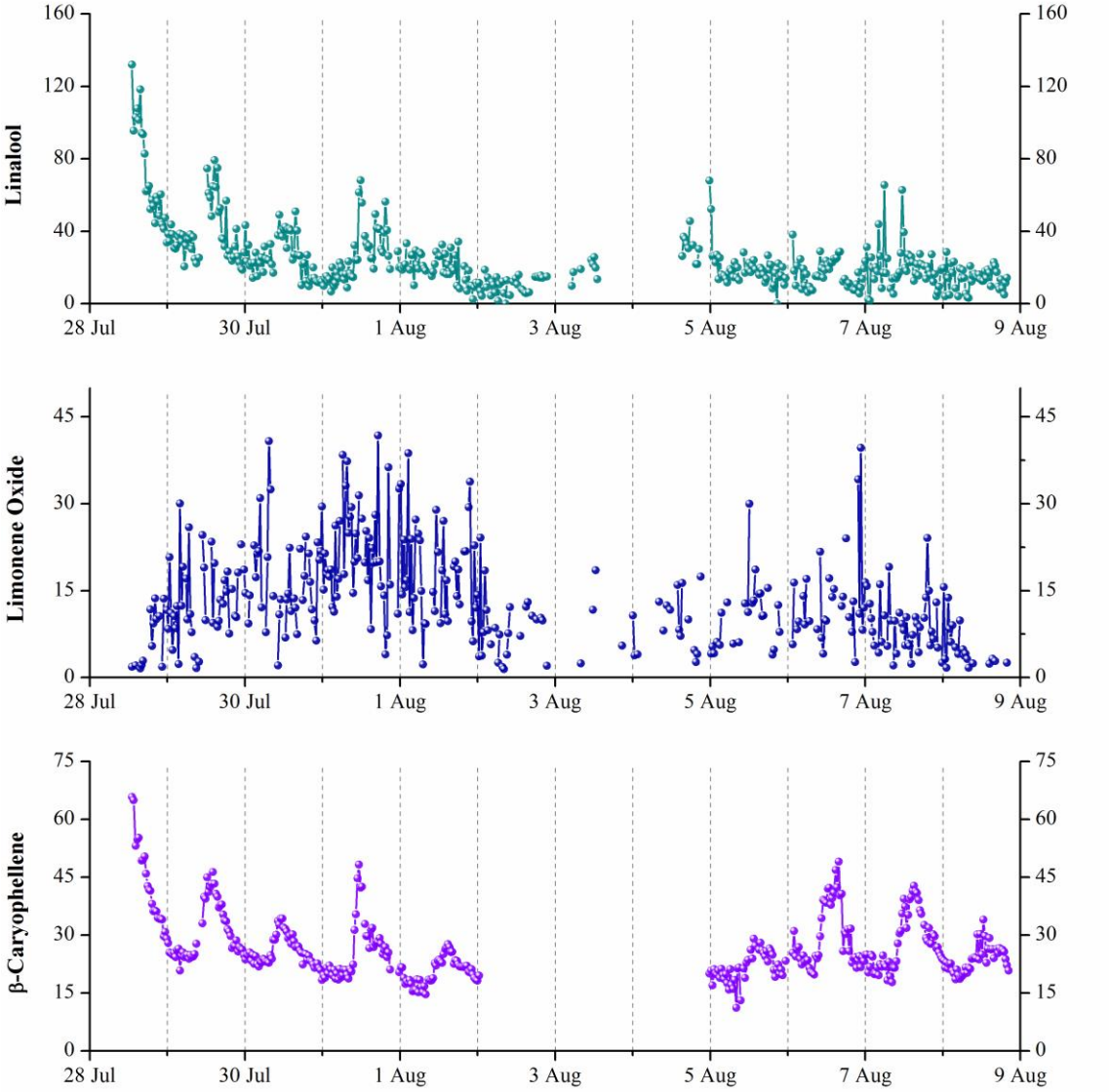

In the summer (June to September), both coniferous trees and deciduous broadleaf trees in the Kinki region (including this site) host a maximum number of leaves compared to other seasons (Fig. 2-8)(Bao et al., 2008). Therefore, BVOCs emission potential can be enhanced due to maximum leaf quantity in the summer along with maximum temperatures (Bao et al., 2008). Another study reported (Fig. 2-9) that the maximum leaf oil level and maximum terpene emissions occur over the summer for important species, such as *Cryptomeria japonica* and *Chamaecyparis obutsa*, (Yatagai et al., 1995).

Fig. 2-8. Seasonal ratio of leaves calculated as, V [quantity of leaves]/[maximum quantity of leaves in summer] (Adopted from Bao et al., 2008).

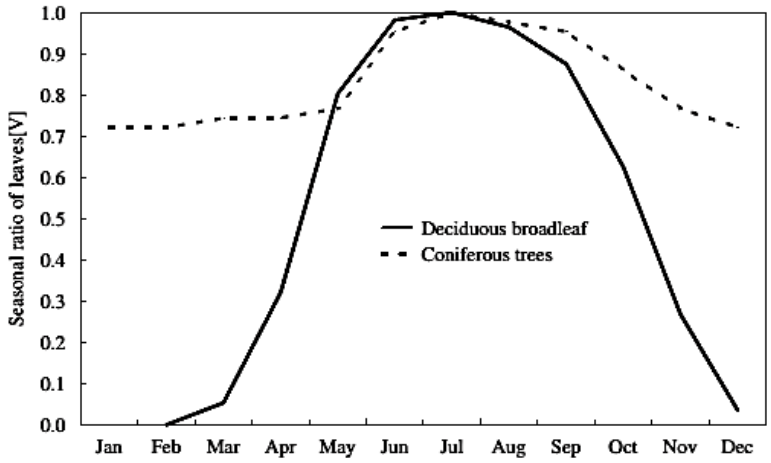

Fig. 2-9. Leaf oil contents and the amounts of terpene emission from *Cryptomeria japonica* and *Chamaecyparis obtusa* (Adopted from Yatagai et al., 1995).

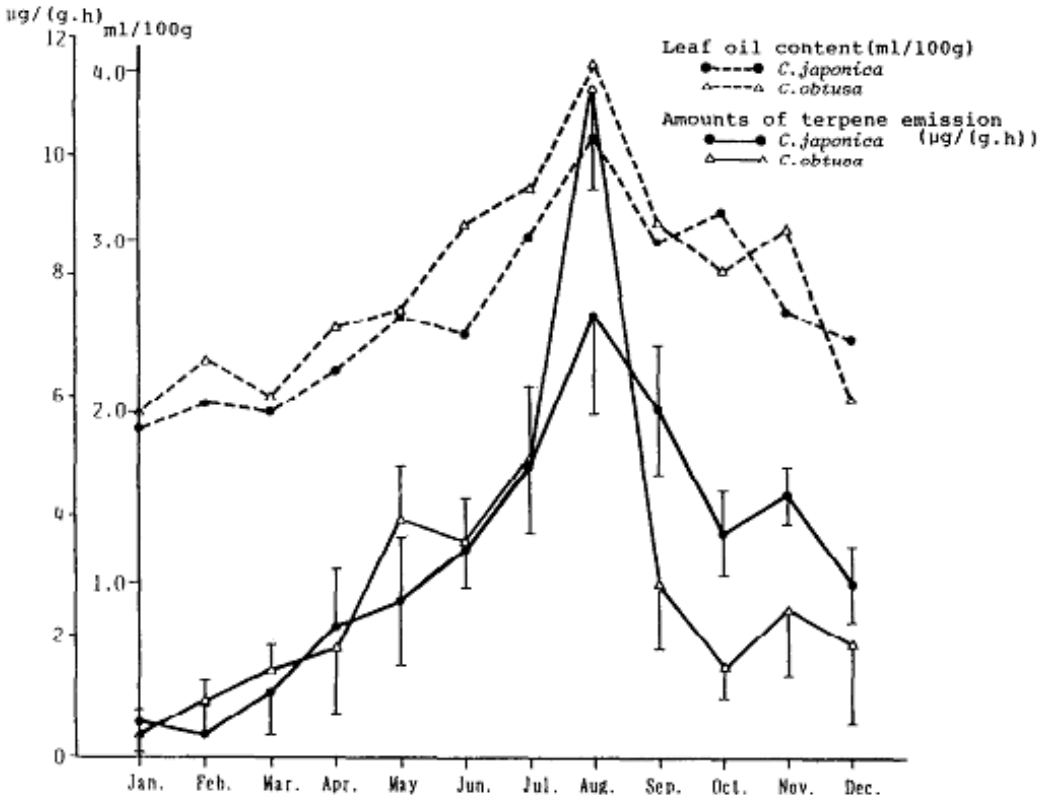

The average mixing ratio of 12 monoterpenes is shown in Table 2-1. α-Pinene was the most abundant (average mixing ratio of 259 ppt) monoterpene during the entire campaign, amongst those that were measured. Δ-3-carene (97 ppt), β-pinene (98 ppt), myrcene (56 ppt), limonene (47 ppt), camphene (48 ppt), and ocimene (49 ppt) were other monoterpenes with significant abundance. The average mixing ratios of β-pinene and Δ-3-carene were 2.5 times, limonene, camphene, and ocimene were 5 times lower than that of α-pinene, for the campaign as a whole. It should be noted that even though abundance of α-pinene is much higher than that of the other terpenes, the reactivity of terpenes with OH is widely variable, for example, myrcene, ocimene, α-phellandrene are 4 to 6 times more reactive with OH than α-pinene. The abundance of ρ-cymene, α-phellandrene, terpinolene, α-terpinene and γ-terpinene were low and sometimes the concentration went below the detection limit.

The average diurnal profiles of monoterpenes, sesquiterpenes and OBVOCs are shown in Fig.2-10 to 2-13. The average diurnal profile of α-pinene, β-pinene, limonene, ρ-cymene and Δ-3-carene demonstrates a maximum level at night-time. This characteristic profile designates that pool-type emission is most likely dominant. Despite the fact that the light intensity dropped quickly and reached zero soon after sunset, the ambient temperature persisted high and diminished slowly (Fig. 2-10 & 2-11). The mean time boundary layer also contracted so that the mixing ratio of the aforementioned monoterpenes increased from 18:00 to 00:00. The average diurnal cycle of myrcene, ocimene and α-phellandrene displayed a day-time maximum which indicates that *de novo* synthesis emission may be dominant (Fig. 2-12). Although they showed the light dependent emission difference between day-time and night-time was not as high as isoprene. This may have been caused by the low light saturation of terpene emissions (Rinne et al., 2009) and their high reactivity with oxidants, mainly OH. Linear regression analysis showed that myrcene emissions (r^2=0.43) moderately correlated with isoprene emissions, whereas α-phellandrene emissions (r^2=0.30) and ocimene emissions (r^2=0.30) were weakly correlated.

Fig. 2-10. Average diurnal profile of mixing ratio (ppt) of monoterpenes (α-pinene, camphene, β-pinene). Error bars indicate standard deviation (1σ)

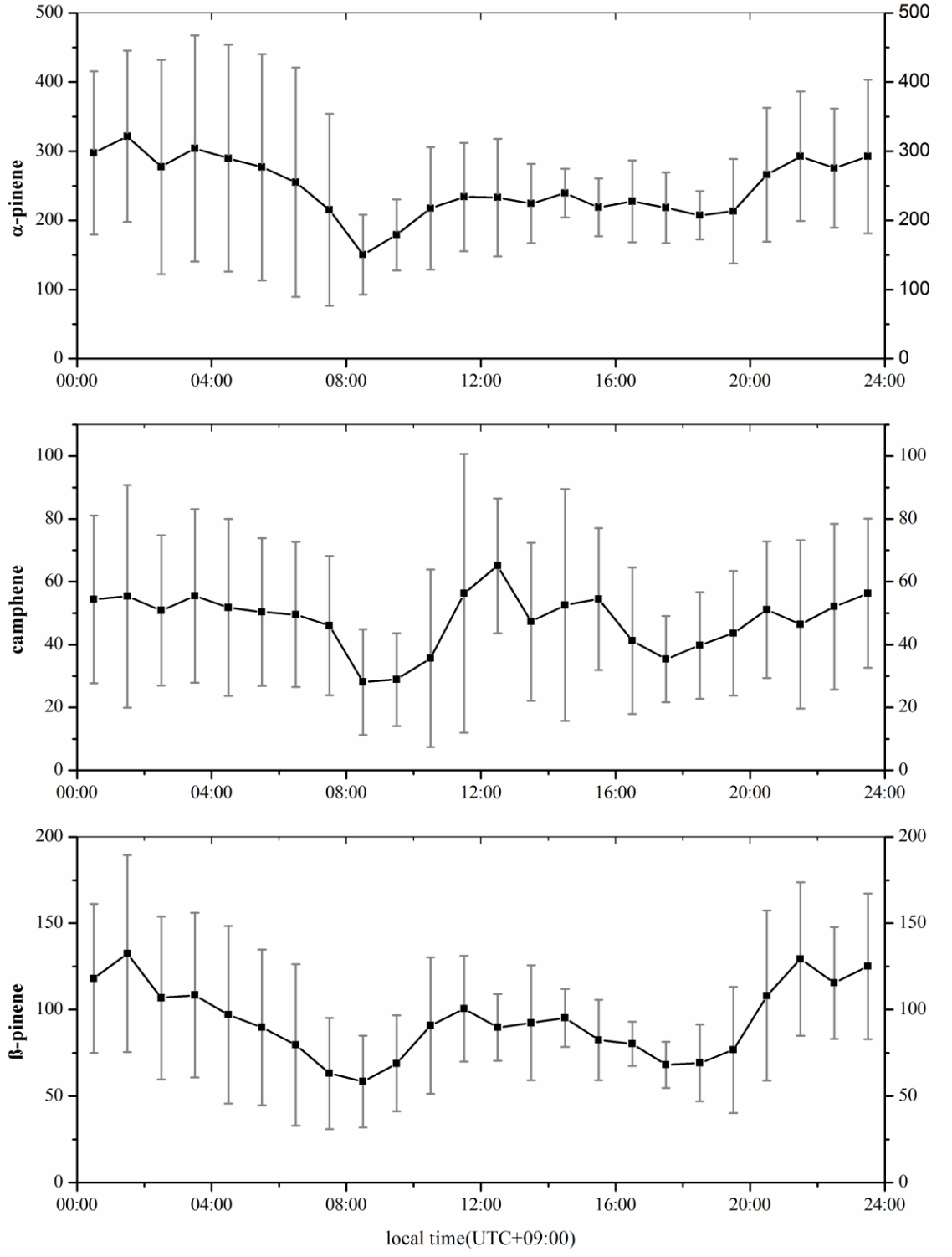

Fig. 2-11. Average diurnal profile of mixing ratio (ppt) of monoterpenes ρ-cymene, limonene, Δ-3-carene. Error bars indicate standard deviation (1σ).

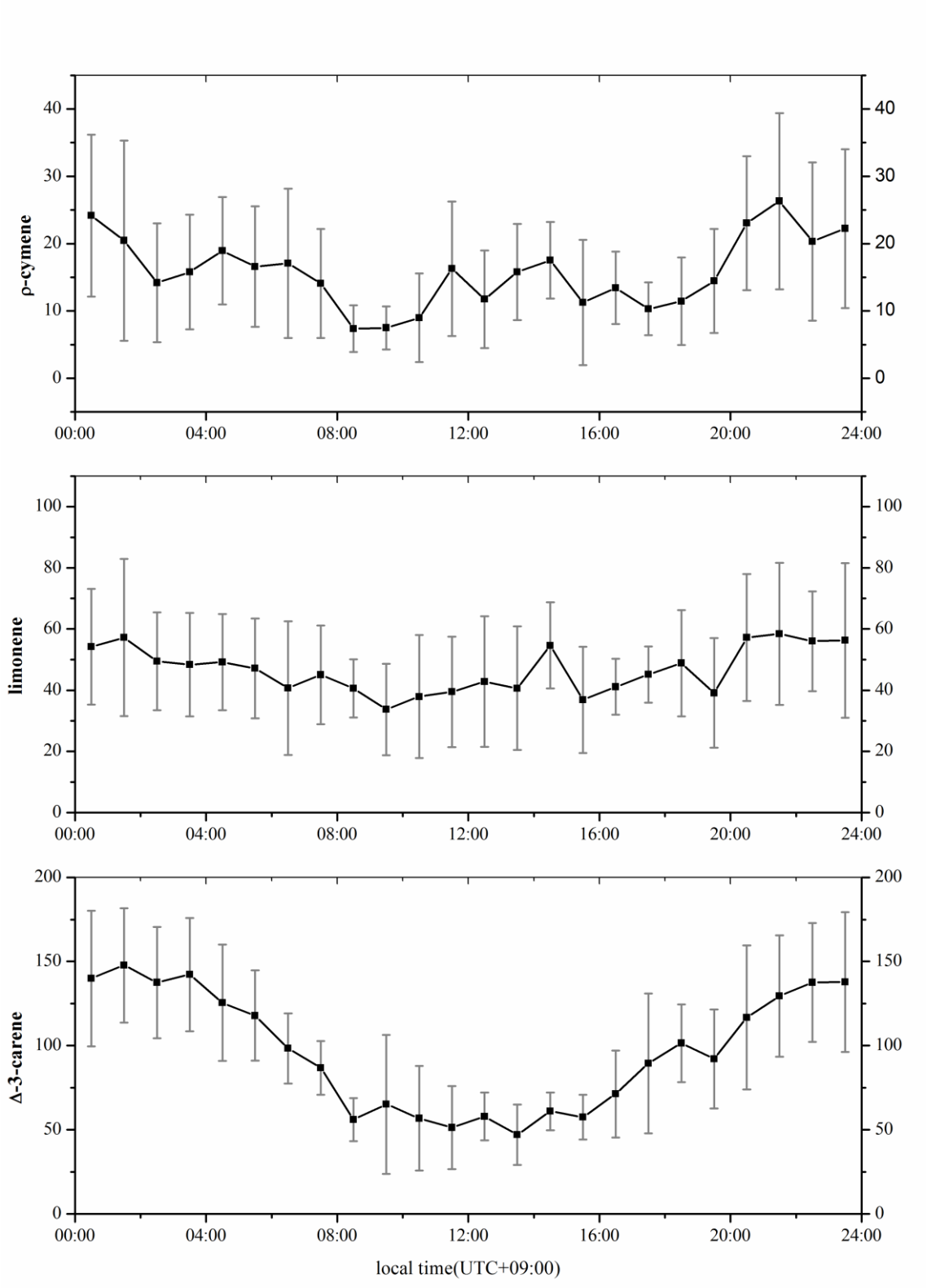

Fig. 2-12. Average diurnal profile of mixing ratio (ppt) of monoterpenes myrcene, α-phellandrene, ocimene). Error bars indicate standard deviation (1σ).

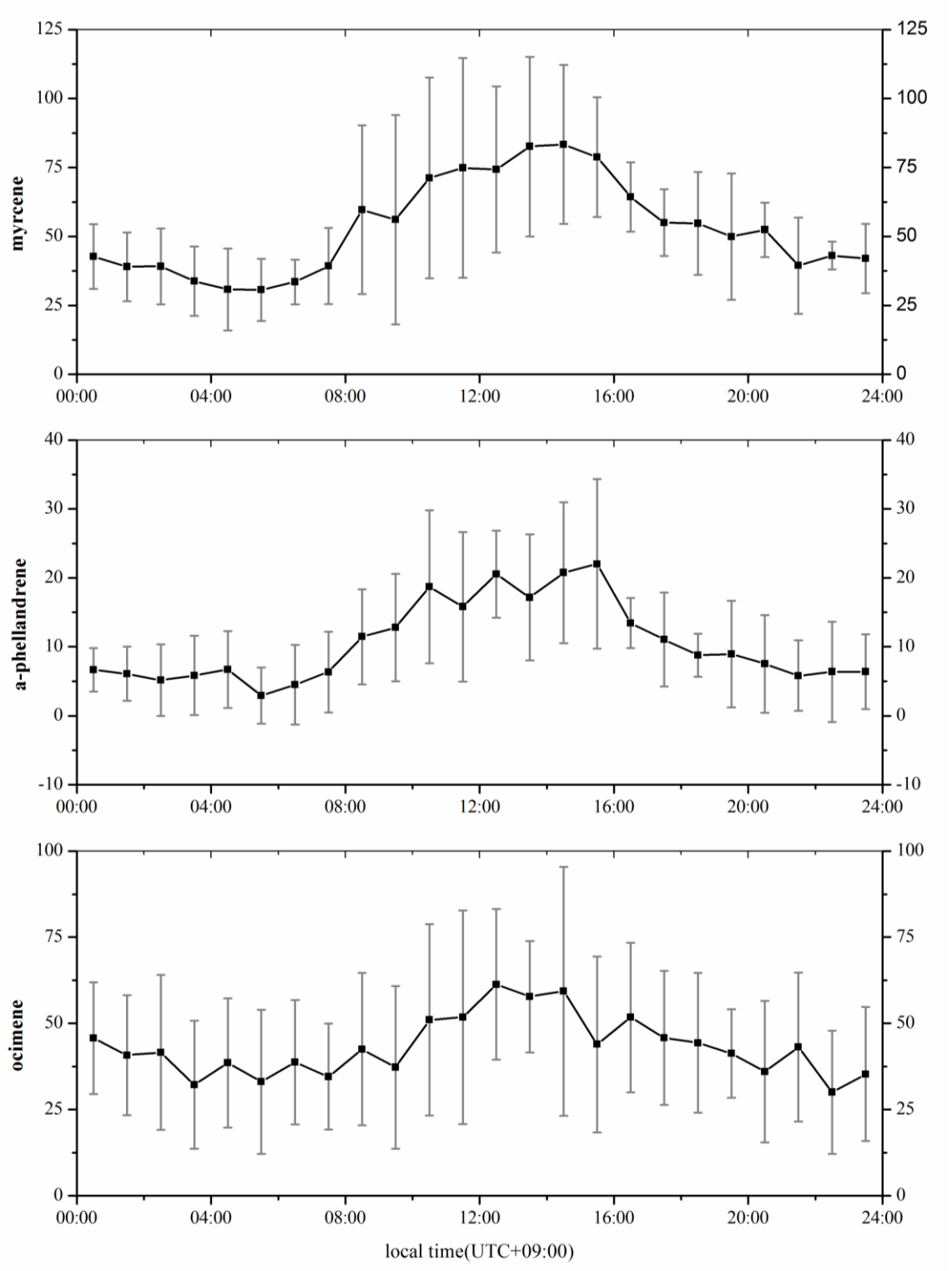

Fig. 2-13. Average diurnal profile of mixing ratio (ppt) of monoterpene (terpinolene), OBVOC (linalool) and sesquiterpene (β-caryophyllene). Error bars indicate standard deviation (1σ).

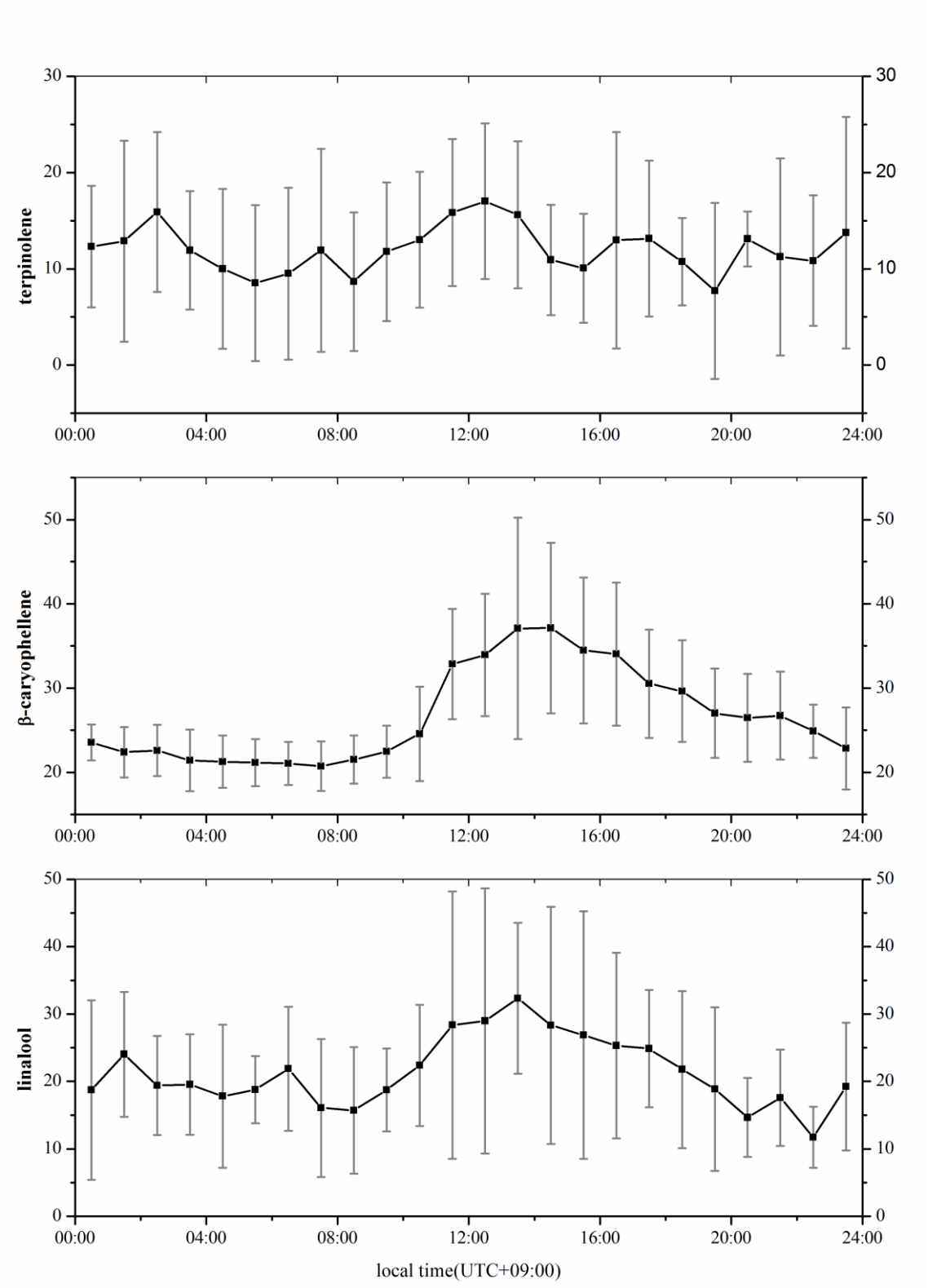

The average diurnal cycle of linalool showed a late afternoon peak. Linalool (r^2=0.25) and β-caryophyllene emissions (r^2=0.30) were also weakly correlated with isoprene. During the night-time the average diurnal cycles of α-pinene, β-pinene, camphene, limonene and ρ-cymene were closely related to boreal forest measurements (Hakola et al., 2012; Yassaa et al., 2012) but the day-time average mixing ratio was still significant, probably due to less available oxidants.

2.2.3. Isoprene and OVOCs diurnal profile

Isoprene (*m*/*z* 69), acetaldehyde (*m*/*z* 45), acetone (*m*/*z* 59), CH_3COOH (*m*/*z* 61), MVK+MACR (*m*/*z* 71), MEK (*m*/*z* 73), EVK (*m*/*z* 85) measured by PTR-MS are shown in Figs.2-14 and 2-15. In contrast to monoterpenes, isoprene and OVOCs show strong diurnal cycles with temperature and light variation. Non-calibrated OVOCs, such as MEK (*m*/*z* 73), EVK (*m*/*z* 85), MVK+MACR (*m*/*z* 71) correlated well with $J(NO_2)$, temperature and calibrated OVOCs, acetaldehyde, and acetone (Table 3). Isoprene increased and decreased covariantly with $J(NO_2)$, whereas isoprene oxidation products MVK+MACR (*m*/*z* 71) concentrations increased and decreased shortly after $J(NO_2)$, due to the time lag on product formation. One of the main sources of furan, the biomass burning, is generally very less in Japan during summer time (Kumagai et al., 2010). Mostly around midnight times isoprene mixing ratio reached very low (< 100 ppt). The lower mixing ratios of inorganic pollutants O_3, NO_X (except July 28th & 29th) and anthropogenic VOCs (August 3rd - 8th) and also clean marine air to the field site (July 30th – August 8th) support possible interference of furan with isoprene at *m*/*z* 29 to be low. The average mixing ratio of isoprene and isoprene products (MVK+MACR) (*m*/*z* 71) were 0.7 and 0.3 ppb (Table 2-1). Isoprene emissions demonstrated moderate linear correlation with $J(NO_2)$ (r^2= 0.57) and comparatively good correlation with temperature (r^2=0.69). Despite isoprene emissions being strongly covariant with light intensity, light initiated degradation also simultaneously occurred which limited the correlation. The most abundant OVOC was acetone, with an average recorded mixing ratio of 7.6 ppb followed by acetaldehyde with 3.5 ppb. Isoprene and monoterpene are emitted from primary sources whereas OVOCs have both primary and secondary, via oxidation sources.

Fig. 2-14. Time series of average (1 hour) meteorological parameters (temperature, relative humidity), J(NO_2), and mixing ratios of isoprene and (MVK+MACR) (*m*/*z* 71).

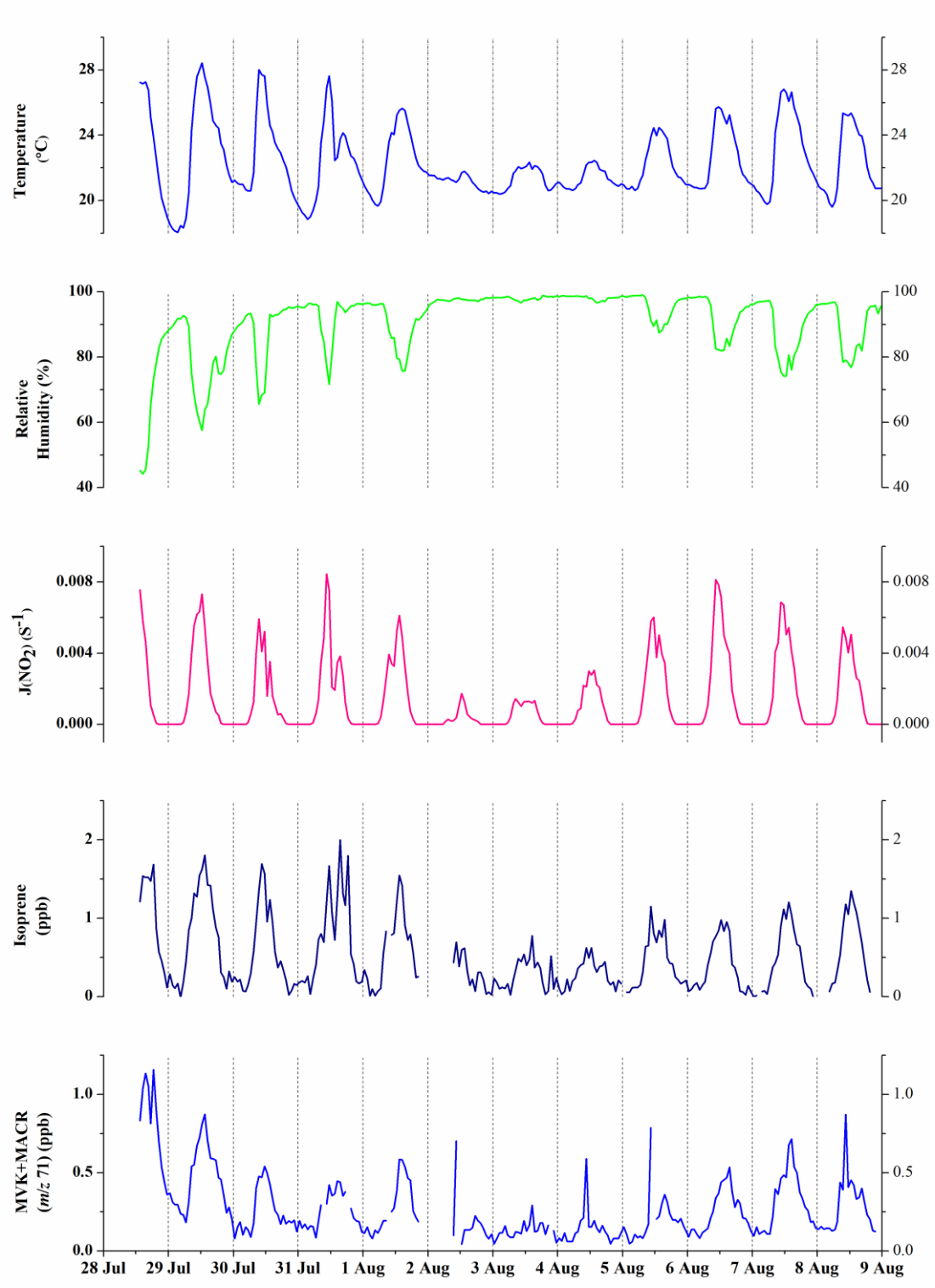

Fig. 2-15. Time series of average (1 hour) mixing ratio (ppb) of acetaldehyde, acetone, MEK (*m*/*z* 73), EVK (*m*/*z* 85) and acetic acid (*m*/*z* 61).

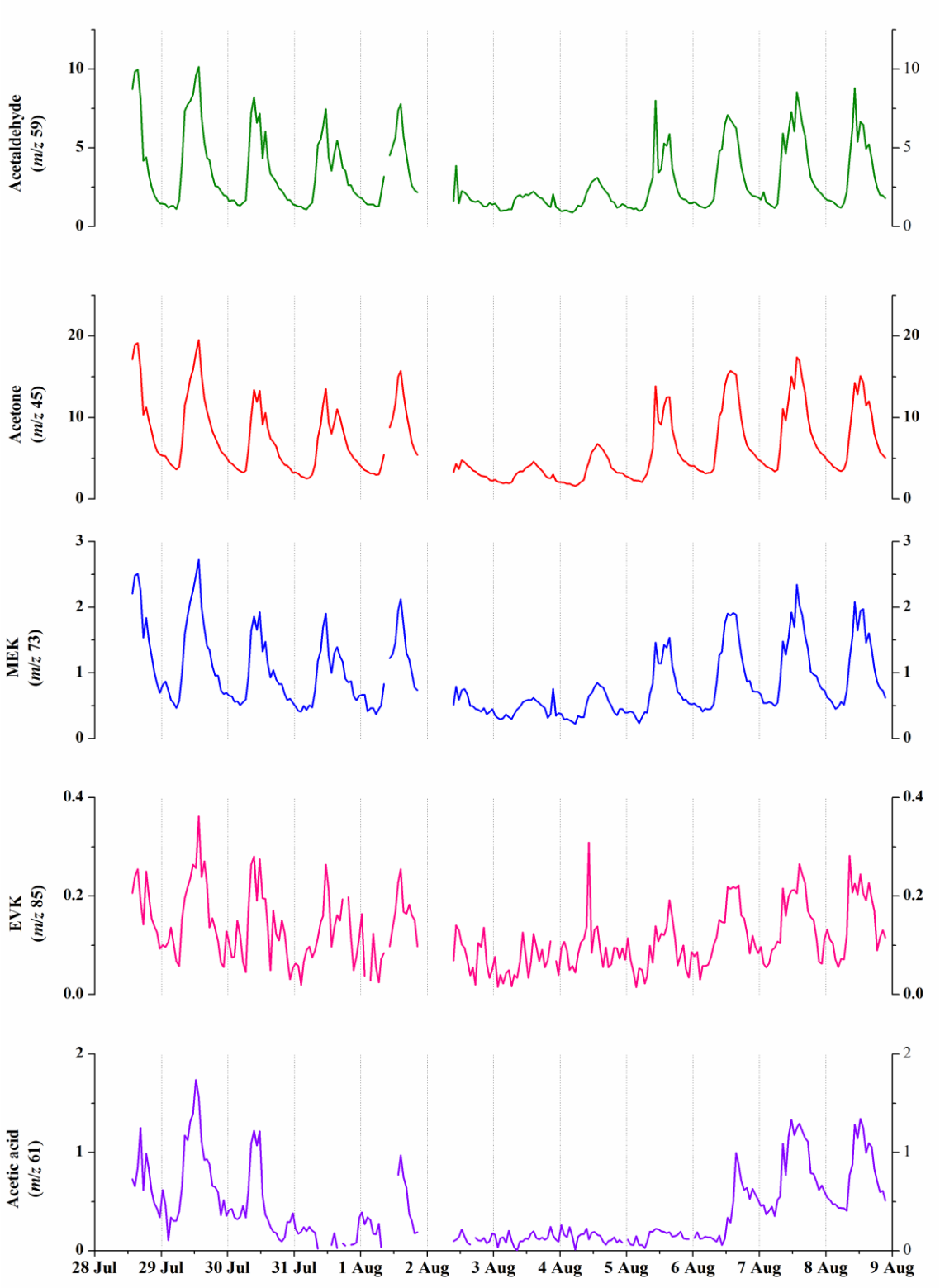

Table.2-2. Linear regression analysis coefficient (r^2) for the inter-correlation of species and the correlation with temperature and $J(NO_2)$.

	$J(NO_2)$	Temperature	MVK+ MACR	Acetaldehyde	Acetone	MEK	EVK	Acetic acid
Isoprene (*m/z* 69)	0.57	0.69	0.53	0.75	0.71	0.74	0.54	0.31
MVK+ MACR (*m/z* 71)	0.33	0.50		0.68	0.70	0.77	0.60	0.48
Acetaldehyde (*m/z* 59)	0.79	0.84			0.93	0.94	0.69	0.47
Acetone (*m/z* 45)	0.71	0.82				0.97	0.72	0.50
MEK (*m/z* 73)	0.71	0.82					0.76	0.55
EVK (*m/z* 85)	0.46	0.63						0.54
Acetic acid (*m/z* 61)	0.25	0.42						

2.2.4. Correlations of O_3 with VOCs

The ambient O_3 level can stimulate sesquiterpene emission especially when exceeds 36.6 ± 3.9 ppbv (Bourtsoukidis et al., 2012). To understand the stimulation of sesquiterpene and other VOCs by O_3, the correlation of those species with O_3 were checked and the results are shown in supplementary material (Table.2-3). During transported pollution event (period 1 a: 28 & 29th July) β-caryophyllene showed only weak correlation (r^2 = 0.18) with O_3 and relatively better correlation (r^2= 0.29 and 0.42) with light and temperature respectively. Moreover, also, the notable range of correlations was observed with temperature in the whole campaign (r^2= 0.36), period 1b (r^2= 0.40) and period 2 (r^2= 0.48) indicate that temperature played dominant role on sesquiterpenes emission. Several other primary and secondary VOCs showed only weak correlation with O_3 except the isoprene oxidation product MVK+MACR that demonstrated a good correlation with O_3 (r^2= 0.49). Except the initial days (28 & 29th), very low mixing ratio of O_3 (< 12 ppb) was observed in the rest of the campaign. Therefore the stimulation effect of O_3 on sesquiterpenes seems to be insignificant in this campaign.

Table 2-3. Linear regression analysis coefficient (r^2) for ozone with VOCs, meteorological conditions.

Ozone	Whole campaign (n=156)	Period 1a (n=34)	Period 1b (n=46)	Period 2 (n=76)
$J(NO_2)$	0.02	0.08	0.06	0.54
temperature	0.04	0.09	0.07	0.66
α-pinene	0.03	-0.13	0.02	0.001
camphene	-0.07	-0.03	-0.02	-0.001
β-pinene	0.03	0.002	0.03	-0.01
myrcene	0.07	0.06	0.10	0.25
α-phellandrene	0.001	0.04	0.08	0.46
Δ-3-carene	0.002	0.001	-0.14	-0.42
α-terpinene	-0.002	-0.22	0.01	0.01
p-cymene	-0.01	0.07	-0.08	-0.10
limonene	-0.07	-0.07	0.001	0.05
ocimene	0.45	0.39	0.09	0.26
γ- terpinene	-0.03	-0.14	-0.001	-0.05
terpinolene	0.03	0.08	0.06	0.01
monoterpenes (total)	0.08	0.03	0.02	0.02
Linalool	0.37	0.14	0.06	0.15
β-caryophellene	0.26	0.18	0.16	0.43
isoprene	0.10	0.11	0.03	0.55
MVK+ MACR (*m/z* 71)	0.46	0.49	0.23	0.55
acetaldehyde (*m/z* 59)	0.06	0.06	0.09	0.66
acetone (*m/z* 45)	0.11	0.13	0.09	0.65
MEK (*m/z* 73)	0.15	0.19	0.09	0.65
EVK (*m/z* 85)	0.12	0.08	0.11	0.57
acetic acid (*m/z* 61)	0.17	0.22	0.10	0.01

2.2.5. Comparison of BVOCs in WFRS with that in boreal forest

BVOCs measured in this forest are compared with that of boreal forest site (Fig. 2-16) Station for Measuring Forest Ecosystem-Atmospheric Relations (SMEAR-II) because both forests have several similarities. WFRS is dominated by coniferous trees Japanese cedar (*Cryptomeria japonica*) and Japanese cypress (*Chamaecyparis obutsa*) (more than 50 %), similarly SMEAR is dominated by coniferous trees Scots pine (*Pinus*

sylvestris) and Norway spruce (*Picea abies*) (Aaltonen et al., 2010; Hakola et al., 2012) and both forests possess trees aged ~50 years.

Fig. 2-16. Station for Measuring Ecosystem–Atmosphere Relations (SMEAR). (https://www.atm.helsinki.fi/SMEAR/)

Table 2-4. Mixing ratio of BVOCs measured in WFRS and SMEAR-II.

Monoterpene	SMEAR-2,	WFRS,
α-pinene	259	259
camphene	28	48
β-pinene	72	98
Δ-3-carene	109	97
P-cymene	7	16
limonene	29	47

Fig. 2-17. Diurnal profiles of BVOCs measured in WFRS (left side) and SMEAR-II (right side).

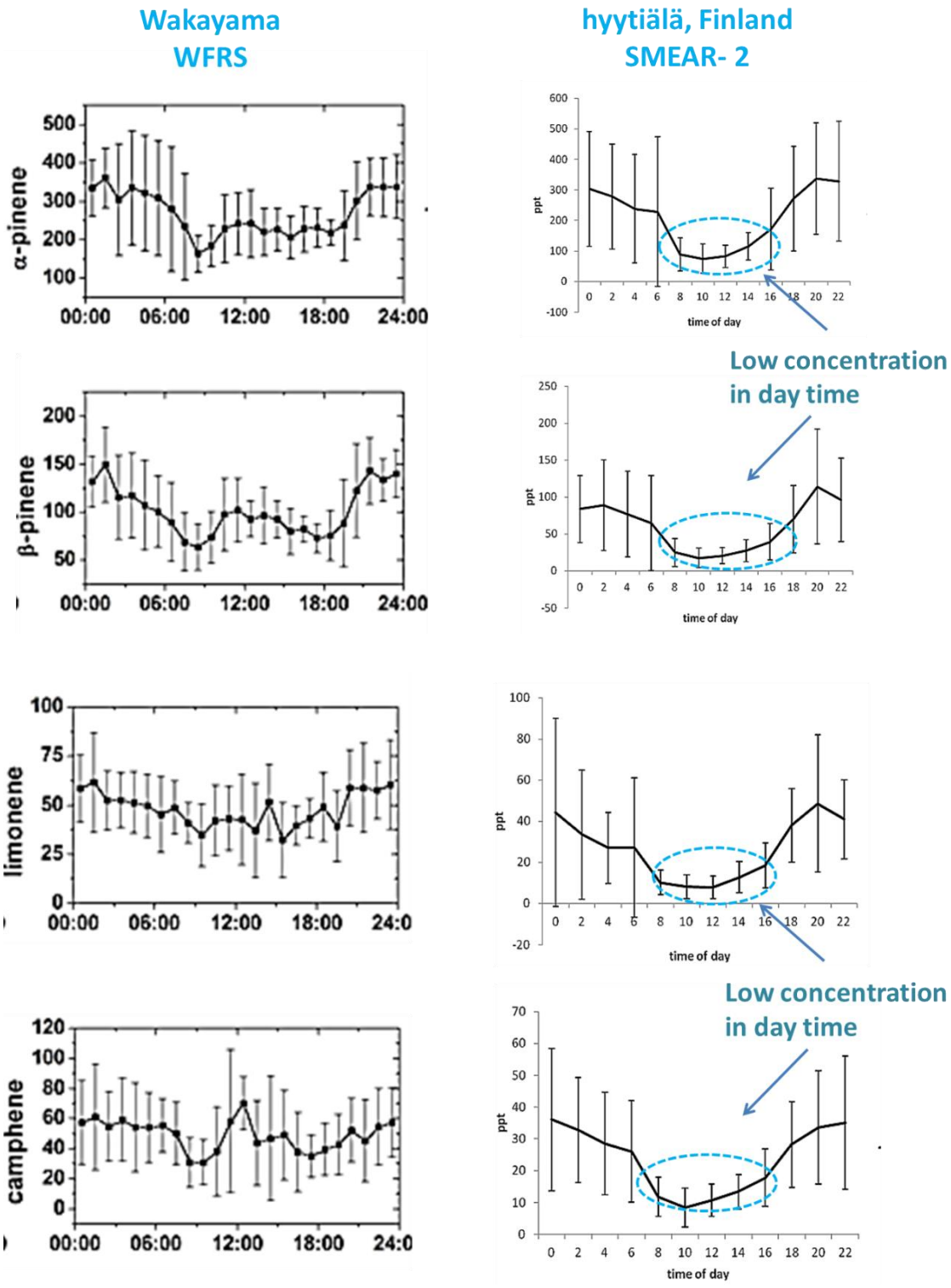

Interestingly in both the forests, summer time average mixing ratio (Table 2-4) of monoterpenes such as α-pinene, β-pinene and Δ-3-carene are found almost. Moreover, average diurnal profile in WFRS and SMEAR-II also resembling each other and both have shown that night-time maximum (Fig. 2-17). However, the day-time average mixing ratio in SMEAR-II was found to be much lower than that of WFRS. Therefore, BVOCs lifetime against tropospheric oxidant OH and O_3 in both forests are compared. The day-time average mixing ratio of O_3 in WFRS is much lower (~ 7 times) compared to that of SMEAR-II and so the lifetime of BVOCs in WFRS relatively longer.

Table 2-5. Lifetime of BVOCs measured in WFRS and SMEAR-II in daytime. ([a]Hakola et al., 2003, [b]Patokoski et al., 2015).

Monoterpenes	SMEAR-2, summer, 2011		WFRS, Summer, 2014
	Day/OH[a]	Day/O_3[b]	Day/ O_3
	$1.5*10^6$ molec/cm^3	35 ppb	4.8 ppb
α-pinene	3.5 h	3.7 h	27 h
camphene	3.5 h	15 day	110 day
β-pinene	2.3 h	21.5 h	6.6 day
Δ-3-carene	2.1 h	8.7 h	64 h
myrcene	0.86 h	3.7 h	27 h
limonene	1.08 h	1.6 h	12 h

Table 2-6. Lifetime of BVOCs measured in WFRS and SMEAR-II in night-time. ([b]Patokoski et al., 2015).

Monoterpenes	SMEAR-2, summer, 2011	WFRS, Summer, 2014
	Night/O_3[b]	Night/O_3
	29 ppb	1.7 ppb
α-pinene	4.5 h	76 h
camphene	18 day	306 day
β-pinene	26 h	18.4 day
Δ-3-carene	10.6 h	179 h
myrcene	4.5 h	76 h
limonene	2 h	33 h

In WFRS BVOCs lifetime against O_3 were varying 12 hours to several days whereas in SMEAR-II lifetime of BVOCs against O_3 were much shorter (varying 1.6 hours to 15 days). Additionally, in SMEAR-II, the lifetime of BVOCs in day-time against primary oxidant OH also very short. A similar difference in the lifetime of BVOCs against O_3 between two sites was observed in the night-time. However in night time lifetime of BVOCs against O_3 in SMEAR-II relatively long compared to day-time and since O_3 is the main oxidant in night-time BVOCs may have removed slowly. Therefore night-time diurnal profile of BVOCs in WFRS and SMEAR-II are comparable, but daytime mixing ratios of BVOCs in SMEAR-II were much lower compared to WFRS.

2.4. Summary

The 12 monoterpenes, two oxygenated BVOCs, and one sesquiterpene were quantified in situ in this forest for the first time. α-pinene was the major specie among

monoterpenes measured. The majority of the monoterpenes showed night-time maximum because the forest is dominated by coniferous trees Japanese cedar (*Cryptomeria japonica*) and Japanese cypress (*Chamaecyparis obutsa*) which are reported to emit a copious amount of monoterpene from their storage structures depending on the ambient temperature. Some of the monoterpenes such as myrcene, ocimene and α-phellandrene showed day-time maximum as the result of *de novo* synthesis. Isoprene and OVOCs demonstrated clear diurnal cycle and strong correlation with light and temperature due to light dependent emission and photochemistry. Most of monoterpenes measured in WFRS have shown similar night-time diurnal cycle as boreal forest (SMEAR-II). However, daytime average mixing ratio in WFRS was higher than that of SMEAR-II due to lower oxidant level.

3. Total OH reactivity measurement in Wakayama forest

3.1 Ambient OH reactivity measurements

Table 3-1. Summary of total OH reactivity measurements in forest sites: vegetation type, measurement values, and fractions of missing OH reactivity.

Publication	Measurement site	Measured OH reactivity (S^{-1})	Fraction of missing OH reactivity
Ren et al. (2006), Summer 2002	Whiteface mountain, mixed forest	2-12	0 %
Sinha et al. (2008), Summer 2005	Surinam, tropical forest	28-72	70 %
Edwards et al. (2013), Summer 2008	Borneo, tropical forest	7-84	48 %
Nakashima et al. (2014), Summer 2008	South rocky mountain, pine forest	2-26	30 %
Ingham et al. (2009), Spring 2008	Borneo, tropical forest	10-60	50 %
Sinha et al. (2010), Spring 2008	Finland, boreal forest	5-12	50 %
Nolscher et al. (2012), Summer 2010	Finland, boreal forest	3-76	68 %
This work, Summer (2014)	WFRS, Coniferous temperate forest	2-21	29 %

High missing OH reactivity in forested regions often reported for total OH reactivity measurements conducted. The presence of unidentified sinks that may be unmeasured BVOC emissions (Di Carlo et al., 2004; Sinha et al., 2010) or unmeasured secondary products produced from the reactions of primarily emitted BVOCs with atmospheric oxidants (Edwards et al., 2013; Hansen et al., 2014; Lou et al., 2010;

Nakashima et al., 2014; Taraborrelli et al., 2012) or both (Nölscher et al., 2012) may be the reasons for missing OH reactivity. Reported total OH reactivity measurements in the forested atmospheres are presented in Table 3-1.

In this chapter, the measurements of OH reactivity along with various trace species such as O_3, NO, NO_2 and VOCs in a Wakayama Forest Research Station (WFRS) are discussed. A detailed description of measurement site is given in Chapter 2 (section 2.2.1). Calculated OH reactivity, measured OH reactivity, meteorological conditions, and air mass history were considered to investigate the contribution of primary and secondary trace species to the atmospheric oxidant budget and to examine how primary emissions respond to meteorological conditions and anthropogenic influences. The possible origin of sinks related to the missing OH reactivity is also discussed.

3.2. Observation

3.2.1. Details of OH reactivity measurement

Continuous OH reactivity measurement was carried out using a laser induced pump and probe technique (Sadanaga et al., (2004, 2005). Ambient air was pulled into a reaction cell (made from aluminium, 1.4 m length, 40 mm inner diameter) by a diaphragm pump (DA-60S, ULVAC) from the inlet placed at a height of 5 m height on an aluminium pole through a ~15 m long (1/2″ (1.27 cm) OD) PFA tube. In the reaction cell, the flow rate of the sample air was 12 SLM, controlled by a mass flow controller placed just before the diaphragm pump and monitored by a mass flow sensor (Model 3660, Kofloc) placed at the entrance of the reaction cell. Approximately 1 atm (1.01 X 10^5 Pa) pressure was maintained in the reaction cell. To generate artificial OH radicals in the reaction cell, it was irradiated with a pulsed 266 nm laser beam from the fourth harmonic of a flash-lamp pumped Nd:YAG laser (Tempest 300, New Wave Research) that proceeds the photolysis of O_3 and the successive reaction with water vapour present in the sample air as shown below:

$$O_3 + h\upsilon\ (266\ nm) \rightarrow O_2 + O\ (^1D) \quad (1\text{-}1)$$

$$O\ (^1D) + H_2O \rightarrow 2OH \quad (1\text{-}2)$$

Fig. 3-1. OH reactivity measurement system diagram.

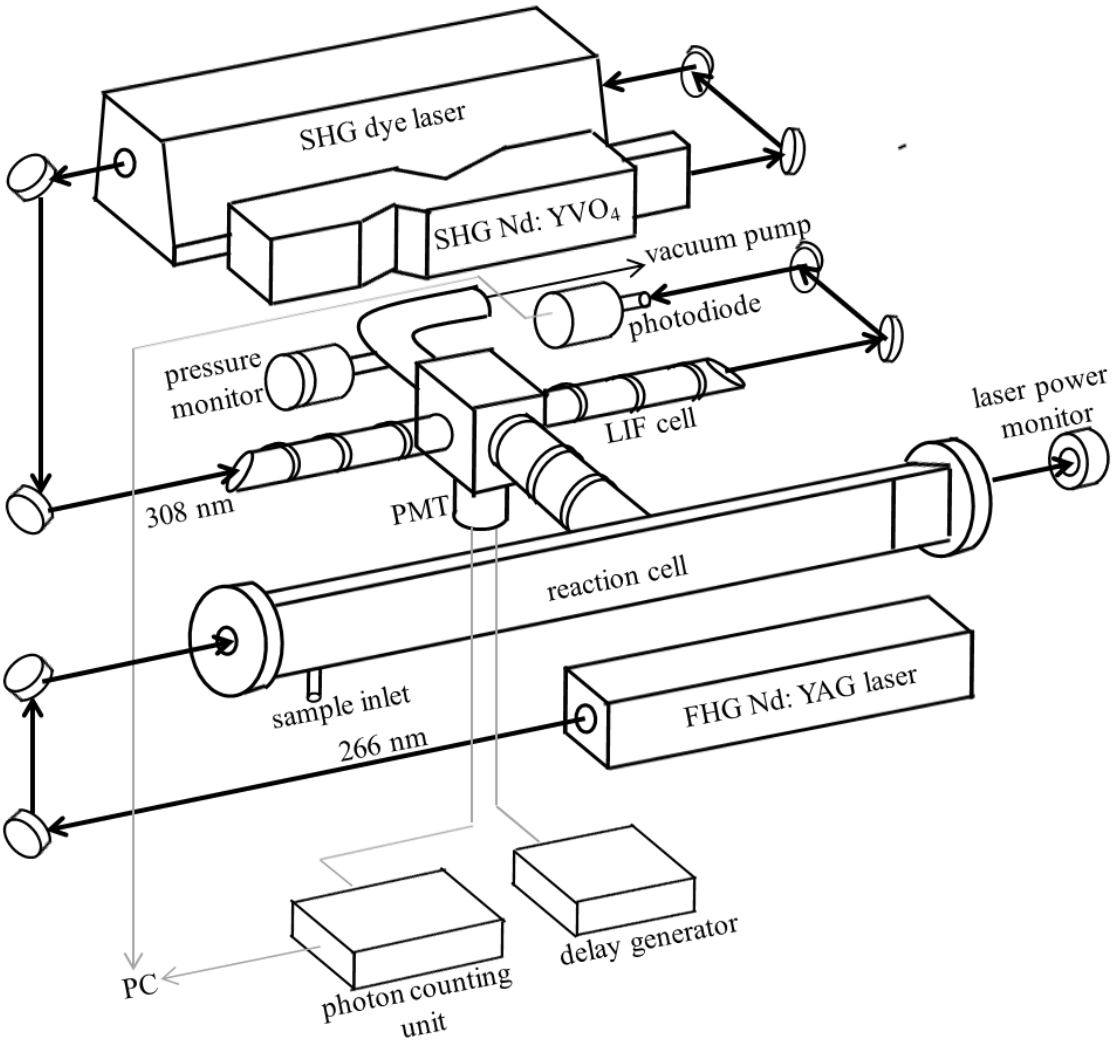

The repetition rate of the laser beam was set to 2 Hz, and the energy was approximately 20 mJ/pulse. The number of OH radicals produced decreased with time as a result of reactions with trace species in the sample air. The laser-induced fluorescence technique (LIF) was used to detect the changes in the concentration of OH radicals. A portion of sample air was introduced into the LIF cell through a 0.5 mm orifice which was placed 0.8 m downstream of the inlet of the reaction cell by using an oil rotatory pump (D-950K, ULVAC). The pressure in the LIF cell was kept at around 2.67 X 10^2 Pa. A second harmonic pulsed dye laser (Credo, Sirah), pumped by a second harmonic pulsed Nd:YVO_4 laser (YHP-40-532Q, Spectra Physics), was used to excite

the $A^2\Sigma^+$ - $X^2\prod(0,0)$ Q1(2) rotational line (308 nm) of OH in the sample air, to detect the fluorescence of OH. The repetition rate and power of the laser beam were set to 10 Hz and around 2-3 mW, respectively. A photomultiplier tube (R2256P, Hamamatsu) equipped with a dynode gating system was used to detect the fluorescence signal, and a photon counting method was used to record the signal.

3.2.2. Simultaneous measurements of trace species, aerosol particles, and meteorological conditions

Measurements of the trace species present in the ambient air and weather conditions were performed together with OH reactivity measurements. O_3, CO, and NOX were measured by UV absorption (Model 49C, Thermo Electron), non-dispersive infrared spectroscopy (Model 48C, Thermo Electron) and O_3 chemiluminescence (Model 42i-TL, Thermo Electron) respectively. Lower detection limit of O_3, CO, NO_X by thermo instruments is 1 ppb, 40 ppb, and 50 ppt respectively. These instruments were placed on the basement floor of a two-storey building, and ambient air was supplied through a (1/4″ (0.64 cm) OD) PFA tube from an inlet which was located at the same position as the inlet for the OH reactivity instrument. NO_2 was measured using a cavity attenuated phase shift (CAPS, Teledyne API Model T500U) instrument. Lower detection limit of NO_2 is 40 ppt. The ambient temperature and the relative humidity were measured using a thermo recorder (Ondotori TR-77Ui, T&D Corporation) and $J(NO_2)$ was measured using a spectroradiometer. Aerosol was aspirated through a cyclone (cutpoint: 2.5 μm) and the number-size distributions under dehumidified conditions (<6% RH) in the range of 14.1–736.5 nm in diameter were measured using a scanning mobility particle sizer (SMPS).

3.3. Results and discussion

3.3.1. Classification of measurement campaign

Time series of one-hour average mixing ratio of inorganic species NO, NO_2, O_3 is shown in the Fig. 3-2. A relatively high O_3 mixing ratio (average 25 ppb) was observed at the beginning of the campaign, July 28th, and 29th. The relatively high mixing ratio of O_3 despite the forest is far remote from direct anthropogenic emission sources, is indicative of influence from transported air mass. The O_3 mixing ratio after these first

two days, exhibited a diurnal trend, with a maximum noon-time mixing ratio, except August second and third. From August second to August fourth, continuous rain due to a typhoon affected the measurement campaign. For the whole campaign, typically low mixing ratios of NO and NO_2, with an average of 0.71 and 0.29 ppb respectively, were observed.

Fig. 3-2. Time series of average (1 hour) mixing ratio of NO, NO_2, and O_3.

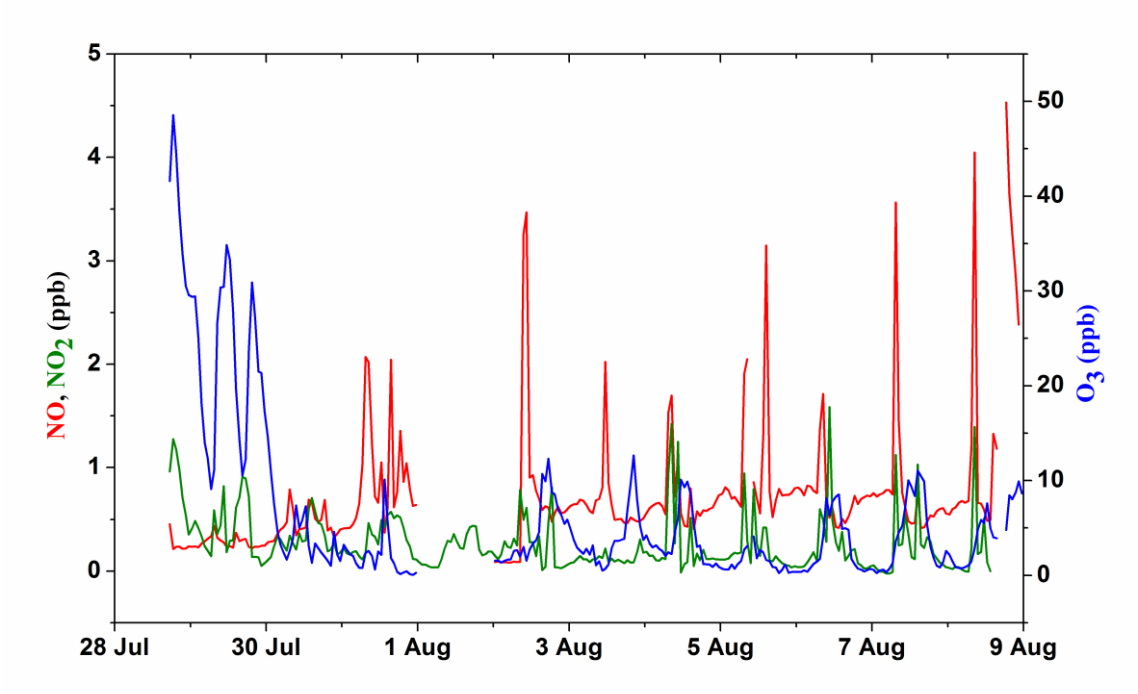

Several spikes of NO and NO_2 mixing ratios were observed due to vehicles used for our transportation. From late evening to early morning NO and O_3 were anti-correlated. During these hours, NO mixing ratio was over 0.5 ppb, but the O_3 mixing ratio was very low and mostly close to zero. The mixing ratio of the OH radical, which is a major sink for BVOCs, was low during the night, and the high mixing ratio of BVOCs consumed O_3 so that the NO mixing ratio remained significant through the nights.

Air mass flow history (Fig. 3-3) to the site was calculated by backward trajectory analysis with the NOAA HYSPLIT model (Draxler and Rolph, 2014) to understand the influence of anthropogenic emission, photochemical aging, and mixing of clean marine air. For the entire period, backward trajectory analysis was calculated at two height levels (500 m, 1000 m) at one-hour intervals. Backward trajectory analysis calculated at

noon-time [UTC+9] is shown in Fig. 3-3. for clarity. Symbols on the line indicate every six hours. From the beginning of the campaign to 01:00 [UTC+9] on July 29th a north-west and northerly wind passed through urban areas such as Kyoto and Osaka, which brought polluted continental air to the campaign site. During these hours, the wind speed was low, and the polluted air spent more than 12 hours inland. From July 29th at 01:00 [UTC+9] to July 30th at 02:00 [UTC+9], a northerly wind passed through the continent and onto the sea and reached the campaign site from a south-eastern direction.

Fig. 3-3. Backward trajectory analysis (noon-time [UTC+9]) at 500 m height. Black lines (Period 1a- July 28th, and 29th, 2014), red lines (Period 1b- July 30th to August 1st, 2014), green lines (Period 2- August 5th to the 8th, 2014) and blue lines (continuous rainy days- August 2nd to 4th).

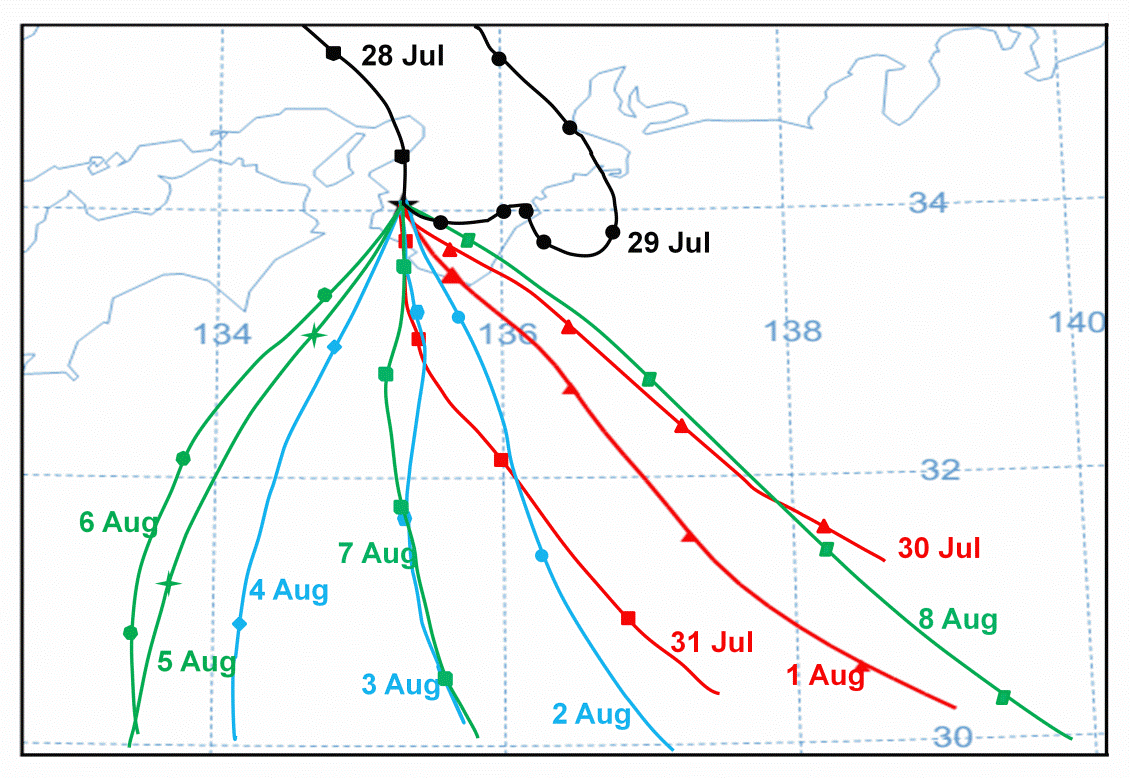

From July 30th to the end of the campaign, the field site received a clean air mass from the Pacific Ocean. The field campaign measurements were classified into two periods based on the wind direction, anthropogenic influence, and rainfall. Period 1 depicts the time before the continuous rainfall (August 2nd to 4th) and period 2 denotes the time after the continuous rainfall. Period 1 is sub-classified into period 1a and 1b. Period 1a covers July 28th & 29th (anthropogenic pollution influence), period 1b covers

July 30th to August 1st and finally, period 2 covers August 5th to August 8th (after continuous rainfall). In Fig. 3-3 the black lines depict period 1a, red lines depict period 1b, and green lines depict period 2. Blue lines depict the continuous rainy period due to typhoon conditions. CO measurement was available for only the last three days of the campaign, so the average mixing ratio 114 ppb is used.

3.3.2. Total OH reactivity

When the entire campaign is considered, a 2 minute average of measured OH reactivity varied diurnally in the range of 2 to 21 s^{-1}. The average OH reactivity for the entire campaign was 7.1 ± 3.4 s^{-1}. This average OH reactivity is comparable with coniferous pine forests, 10 s^{-1}, as reported by Nakashima et al., (2014) and boreal forests, 9 s^{-1}, as reported by (Sinha et al., 2010). Conversely, the average is much lower than that of tropical forest measurements such as the Suriname rainforest, 53 s^{-1}, as reported by (Sinha et al., 2008) and the Borneo rainforest 20 s^{-1}, as reported by (Edwards et al., 2013). The average day-time OH reactivity was 1.7 times higher than that of the night-time.

Fig. 3-4. Linear regression analysis coefficient (r^2) for OH reactivity with temperature.

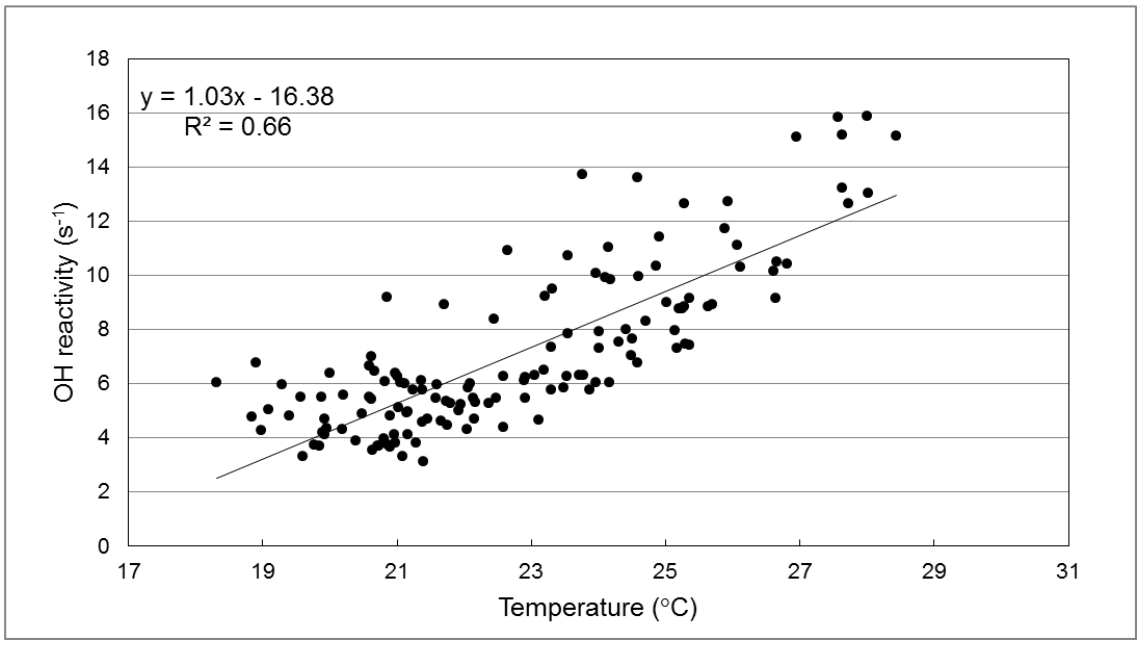

The total OH reactivity varied diurnally with light and temperature and reached a maximum at noon-time, after which it decreased. The observed ambient temperature during the campaign ranged from between 18 to 30 °C, with an average recorded temperature of 22 °C. Linear regression analysis indicated that the measured OH reactivity moderately correlated with temperature (r^2= 0.66) (Fig. 3-4) and light J(NO_2) (r^2= 0.56) (Fig. 3-5).

Fig. 3-5. Linear regression analysis coefficient (r^2) for OH reactivity with J(NO_2).

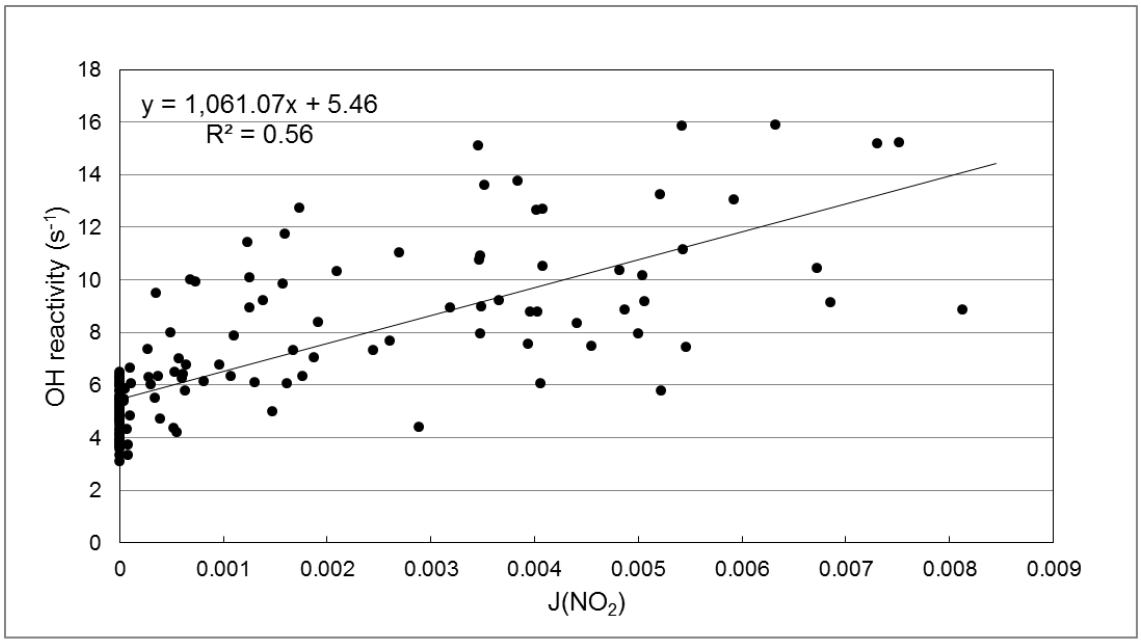

Diel cycle of total OH reactivity is shown in the Fig. 3-6. The average and median ranged in greater extent in day-time (6 to 13 s^{-1}) than night time (4 to 8 s^{-1}). Whiskers extend to a large range during midday to midnight because of high OH reactivity during transported pollution especially on 28th July 13:00- 22:00 and 29th July 11:00-18:00. Day to day variability for the same hours (relative standard deviation = standard deviation/mean hourly average value) ranged relatively higher for the whole campaign (0.19–0.51) than for polluted period 1a excluded part (0.10 to 0.39).

Due to the influence of polluted continental air, the measured OH reactivity observed during period 1a was very high. OH reactivity ranged from 4 to 21 s^{-1} and the average OH reactivity was 9.8 ± 4.6 s^{-1}. The average temperature during this period was 23 °C

and the maximum hourly average temperature of 28.4 °C was observed during July 29th from 12:00 to 13:00.

Fig. 3-6 Diel cycle of OH reactivity during the campaign. Dots, open squares, the boxes and the whiskers indicate medians, averages, 25-75 % and 10-90 % of the data respectively.

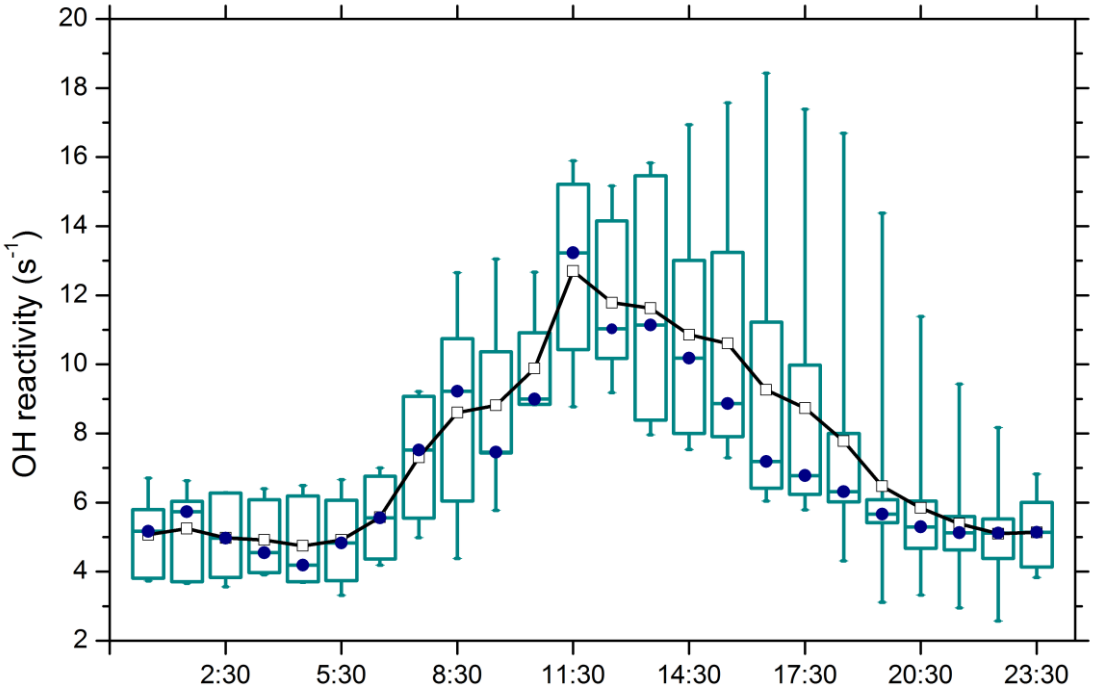

The maximum hourly average OH reactivity of 18 s^{-1} was observed at 16:00 [UTC+9] during period 1a. The measured OH reactivity during period 1b ranged from 3 to 20 s^{-1} with the average being 8.06 ± 3.31 s^{-1}, slightly less than period 1a. The average temperature was 22.6 °C, close to period 1a, but August 1st was cooler with a maximum recorded daytime temperature of 25.5 °C. Rainy day measurements, conducted from August 2nd to 4th, were not available due to instrument failures.

Period 2 was marked by cool and clean marine air from the Pacific Ocean, after the continuous rainy period. Although the average temperature during the period 2 was 23 °C, which was equal to period 1, the maximum day-time temperature was 2-3 °C lower than that of period 1. The OH reactivity ranged from 2 to 14 s^{-1} and the average OH reactivity was 6 s^{-1}. This average OH reactivity is close to the coastal site measurements of 5 s^{-1} as reported by (Ingham et al., 2009) and (Lee et al., 2009) and the air mass from the ocean sector, 6 s^{-1}, as reported by (Sinha et al., 2012). The OH

reactivity in period 2 was 30% and 26% lower than the same in periods 1a and 1b, respectively.

3.3.3. Contribution to the total OH reactivity

Fig. 3-7. Measured (lines) and calculated (stacked area) OH reactivity. Measured total OH reactivity 2-minute data (grey line) and 1 hour average (red line). Rainy days measurements (August 2nd to 4th, 2014) was not available due to instrument failure.

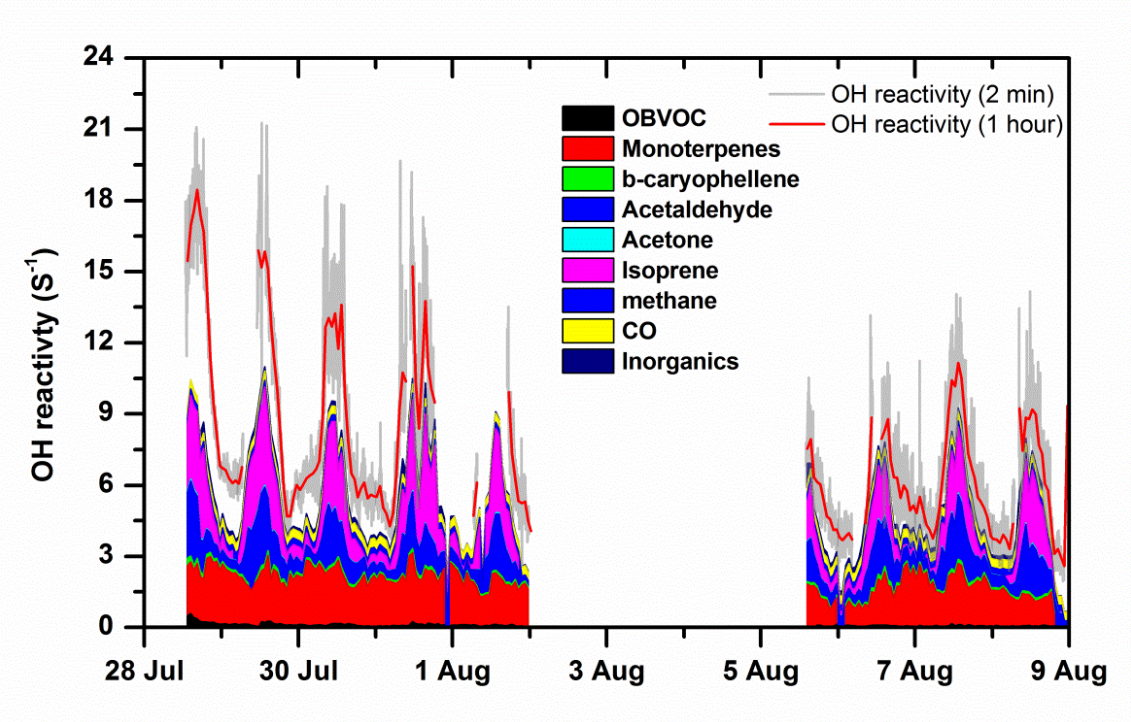

The OH reactivity for the trace gas species such as VOCs, NO_X and O_3 is calculated by multiplying their concentration [N_i] with their respective OH reactive rate constants (k_{OH+N_i}) as Eq. (1). The reaction rate constants were taken from literature (Atkinson, 1994, 1997, 2003; Atkinson et al., 1995, 1997; Calvert et al., 2000; Sander et al., 2002). OH reactivity calculated for every individual trace gas species is shown in Table. 2. The mixing ratio of methane was assumed to be 1780 ppb.

In Fig. 3-7, the grey, and red lines represent respectively the two-minute average and the one hour average of measured OH reactivity. The stacked area, shown in various colours, shows the one hour calculated OH reactivity average. The discrepancy between measured and calculated OH reactivity can be attributed to missing OH sinks. Fig. 3-8. Shows the contribution of trace species to the total OH reactivity for the entire

campaign and different periods. When considering the whole campaign, monoterpenes are the major contributor to the total OH reactivity, accounting for 23.7% of the total OH reactivity.

Fig. 3-8. Contribution of trace species to the total OH reactivity for the whole campaign and different periods.

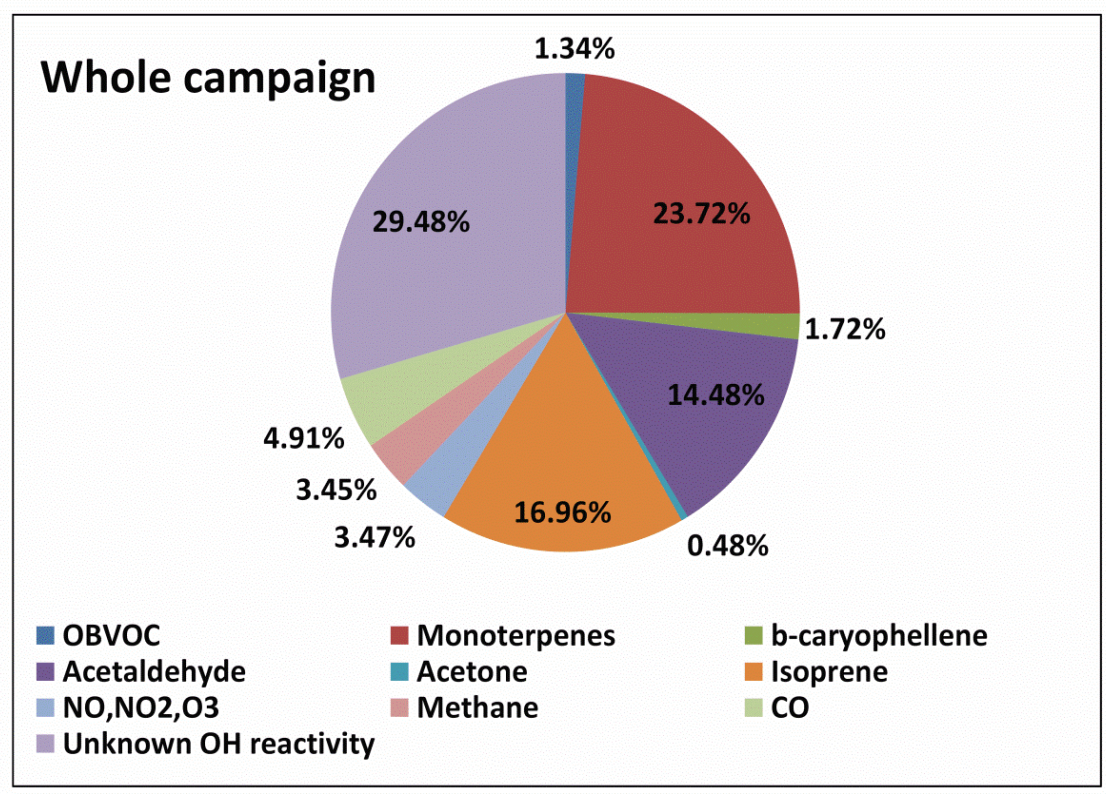

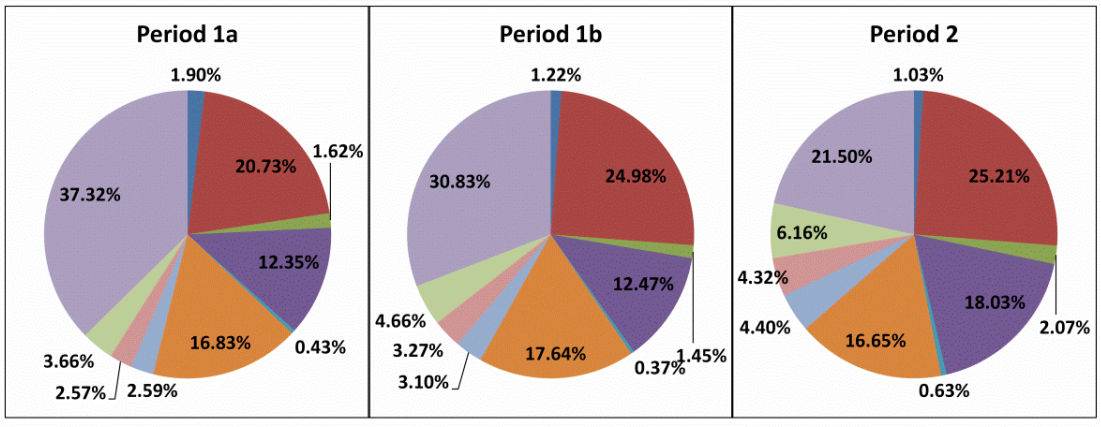

Quantification of the main abundant monoterpenes significantly improved the identification of a significant fraction of the OH reactivity sinks. Several previous OH reactivity measurement studies only measured the total monoterpene mixing ratio, which made it difficult to calculate the OH reactivity, since monoterpenes react with OH at very different rates. From the monoterpene group α-pinene was the highest contributor to OH reactivity, accounting for, on its own, 4.5%. As explained in section 2.2.2. ocimene and myrcene made up 4.0%, 3.9% of OH reactivity, respectively, even though their abundance is five times lower than that of α-pinene due to their much higher reactivity with OH. Δ-3-carene, β-pinene and limonene were also good contributors to the OH reactivity when we consider the monoterpene group, accounting for 2.8%, 2.5%, 2.6%, respectively.

Fig. 3-9. Average diurnal variation in the calculated OH reactivity of each species and missing OH reactivity.

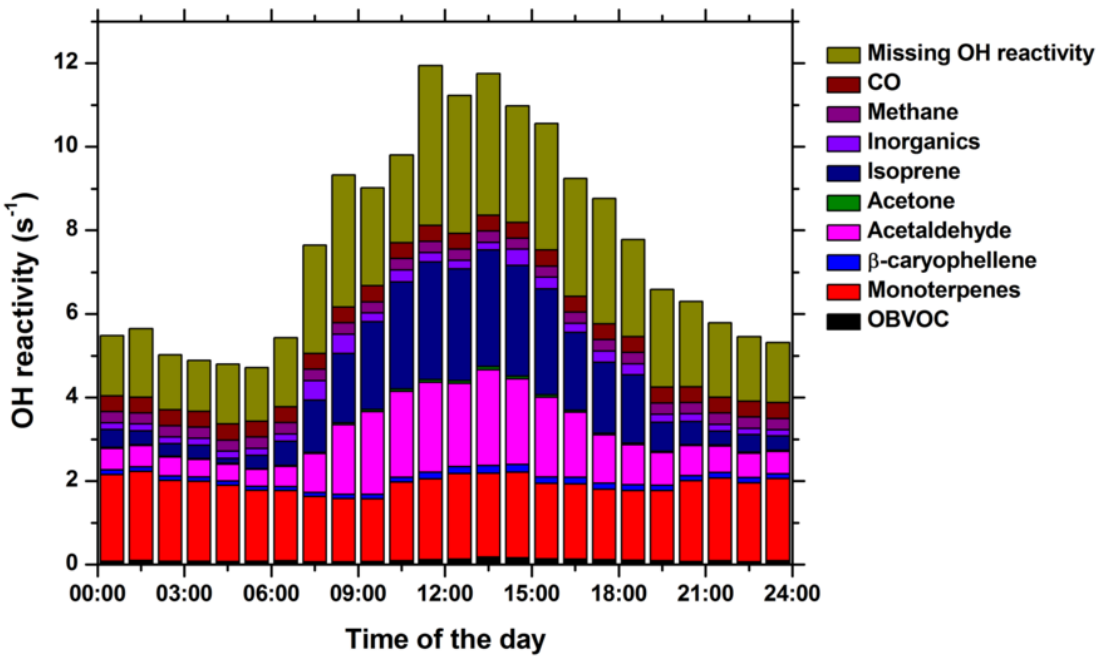

Among the least abundant monoterpenes, α-phellandrene accounted for 1.0% of the total OH reactivity due to its relatively higher reactivity. Next to monoterpenes, isoprene and acetaldehyde contributed 17.0% and 14.5%, respectively. These were the major contributors to the total OH reactivity. Inorganic pollutants NO, NO_2 and O_3 made up only 3.5% of the total OH reactivity. Methane and CO accounted for 3.5 and

4.9%, respectively. Monoterpenes accounted for 20.7% of the total OH reactivity during period 1a which was lower than the campaign average value of 23.7%, due to the high oxidant concentration which converted them into secondary products.

3.3.4. Missing OH reactivity

The average missing OH reactivity for the whole campaign was 29.5%. The missing OH reactivity was 37.3%, 30.8% and 21.5% during period 1a, 1b and period 2, respectively. The average OH reactivity calculated from the anthropogenic VOCs measured in-between August 2nd to 8th (mainly period 2) using canister only accounts for 0.27 s^{-1}. This could contribute 4.5% to the average total OH reactivity during period 2 reducing missing OH reactivity to 16.7%.

Before the continuous rainy period, high missing OH reactivity was observed and showed similar variance with total OH reactivity. Linear regression analysis between missing OH reactivity and the other trace species was calculated for the whole campaign and different periods to investigate the origin of the missing OH reactivity and the results are shown in Table 3-2. Average missing OH reactivity displayed a diurnal variation (Fig. 3-9) Missing OH reactivity showed a weak correlation with light (r^2= 0.29) and a slightly higher correlation with temperature (r^2 = 0.42) during period 1a. A better correlation was observed with light (r^2= 0.59) and temperature (r^2= 0.54) during Period 1b. Primary biogenic species isoprene (r^2 =0.40), ocimene (r^2= 0.59) and β-caryophyllene (r^2= 0.36) and secondary species MVK+MACR (*m*/*z* 71) (r^2= 0.59), linalool (r^2= 0.51) showed good correlation with the missing OH reactivity, when the whole campaign was considered (Table 4). Specifically, in periods 1a and 1b, primary biogenic compound isoprene, secondary species MVK+MACR (*m*/*z* 71), MEK (*m*/*z* 73) and other OVOCs showed a high level of correlation.

In addition, ocimene (r^2= 0.60) and β-caryophyllene (r^2= 0.57) correlated well with missing OH reactivity in period 1a, whereas myrcene (r^2= 0.44) and α-phellandrene (r^2= 0.39) moderately correlated in period 1b. These correlations suggest that light and temperature dependent unmeasured primary and secondary species may be responsible for the missing OH reactivity. However NO_2 (r^2= 0.50) and O_3 (r^2= 0.39) also demonstrated reasonably good correlation with missing OH reactivity and

meantime MVK+MACR correlated well with both O_3 (r^2= 0.49) and missing OH reactivity (r^2= 0.81) during transported pollution influence (period 1a) indicates that anthropogenic sources and secondary products formed from oxidation of primary VOCs may also responsible for the missing OH reactivity. However, the mixing ratio of NO_X during transported event was almost similar to the clean period only O_3 mixing ratio was relatively higher. Since O_3 lifetime is significantly higher than that of NO_X this may have happened. Therefore, it seems relatively long living and less reactive anthropogenic species only transported during polluted period 1a. So it seems that, unmeasured biogenic VOCs and secondary products due to higher oxidant level most likely contributed to the missing OH reactivity. Since MVK+MACR (*m*/*z* 71), MEK (*m*/*z* 73), EVK (*m*/*z* 85) and acetic acid (*m*/*z* 61) were not calibrated using standards they were not included in the total OH reactivity calculations.

Table 3-2. Linear regression analysis coefficient (r^2) for the missing OH reactivity with trace species, meteorological conditions and total OH reactivity.

Missing OH reactivity	Whole campaign (n=146)	Period 1a (n=33)	Period 1b (n=46)	Period 2 (n=68)
Total OH reactivity	0.80	0.91	0.75	0.36
J(NO_2)	0.13	0.30	0.60	0.16
Temperature	0.23	0.41	0.54	0.26
Monoterpenes (total)	0.14	0.04	0.12	0.003
Myrcene	0.22	0.25	0.44	0.05
α-phellandrene	0.02	0.005	0.39	0.05
Ocimene	0.59	0.60	0.25	0.05
β-caryophellene	0.36	0.57	0.22	0.08
Linalool	0.51	0.40	0.25	0.02
Isoprene	0.40	0.70	0.37	0.10
MVK+ MACR (*m*/*z* 71)	0.59	0.81	0.65	0.16
Acetaldehyde (*m*/*z* 59)	0.26	0.48	0.65	0.12
Acetone (*m*/*z* 45)	0.24	0.55	0.60	0.13
MEK (*m*/*z* 73)	0.32	0.62	0.65	0.14
EVK (*m*/*z* 85)	0.24	0.46	0.55	0.15
Acetic acid (*m*/*z* 61)	0.09	0.33	0.25	0.02
O_3	0.36	0.39	0.09	0.09
NO_2	0.35	0.50	0.16	0.25
NO	0.009	0.09	0.06	0.03

If they were included, they could contribute as follows. MVK+MACR (*m*/*z* 71) and EVK (*m*/*z* 85) contribute to the OH reactivity 3.2% and 1.6%, respectively. The other two OVOCs MEK (*m*/*z* 73) and acetic acid (*m*/*z* 61), due to their low reactivity with OH contribute only 0.4% and 0.1%, respectively. This result reduces the missing OH reactivity for the whole campaign to 23.8%. Similarly, when these four OVOCs contributions were included, the missing OH reactivity for period 1a and 1b and period two was reduced to 30.9%, 26.2%, and 11.5%, respectively. The OH loss by the uptake by aerosol particles was estimated to be small both in the ambient air and in the reaction cell. The loss was assessed using the SMPS data, with the assumptions of the uptake coefficient as unity, the OH diffusion coefficient as 0.234 cm^2 s^{-1} (Tang et al., 2014), and the particle hygroscopic growth with parameter κ as 0.3 (Andreae and Rosenfeld, 2008) under ambient RH conditions. To the total OH reactivity, the mean contribution of the calculated OH losses with the consideration of the precision of the RH measurement were 0.15% and 0.23% respectively. Considering the low percentages, the loss by the uptake was not discussed further.

3.3.5. Less photochemical O_3 formation

A recent study (Williams et al., 2015) reported that in Beijing along with high NO_X, the production of ozone is ten times higher than that of the Amazon rainforest even though OH reactivity in the Amazon rainforest is three times higher. Similarly in this study, although VOCs were emitted significantly, due to the absence anthropogenic emission, NO concentration was very low (Avg. 0.7 ppb) during the period 2 and the formation of NO_2 via $RO_2 + NO \rightarrow RO + NO_2$ also low. Consequently, O_3, which can be formed through photolysis of NO_2 was observed in low mixing ratio (avg. 4.8 ppb) during period 2. This suggests that when natural vegetation area unaffected by anthropogenic influence, produce much smaller harmful ozone than the urban areas are where anthropogenic VOCs emitted along with NO_X.

3.3.6. Average diurnal variation in the relative fraction of trace species

The hourly average fraction of trace species to the total OH reactivity is shown in Fig. 3-10. Monoterpene was the major contributor amongst the sinks that were measured on the site. In the night-time from 19:00 to 06:00, monoterpene showed a

maximum contribution of between 25 to 39%. The isoprene contribution rapidly increased from 7% to 26% between 05:00 and 10:00. The acetaldehyde contribution also increased rapidly from 9% to 22% in between 05:00 and 21:00. In the day-time in between 06:00 and 18:00, isoprene and acetaldehyde contributed a higher fraction, 22%, and 17%, respectively, to the total OH reactivity. In the morning, from 05:00 to 08:00, the breakdown of the nocturnal boundary layer and the rapid increase of the isoprene and acetaldehyde contribution led to a rapid decrease in the monoterpene contribution, from 36% to 16%. From 08:00 to late evening, 16:00, the monoterpene contribution remained between 16 and 19%. While in the day-time isoprene and acetaldehyde supplied a high fraction to the total OH reactivity, after 17:00 the isoprene fraction rapidly decreased, and the acetaldehyde emissions gradually decreased due to the large difference in their loss due to oxidants. Between 18:00 and 06:00 isoprene contributed only 7%.

Fig. 3-10. Average diurnal variation in the fraction of trace species and missing sinks to the total OH reactivity.

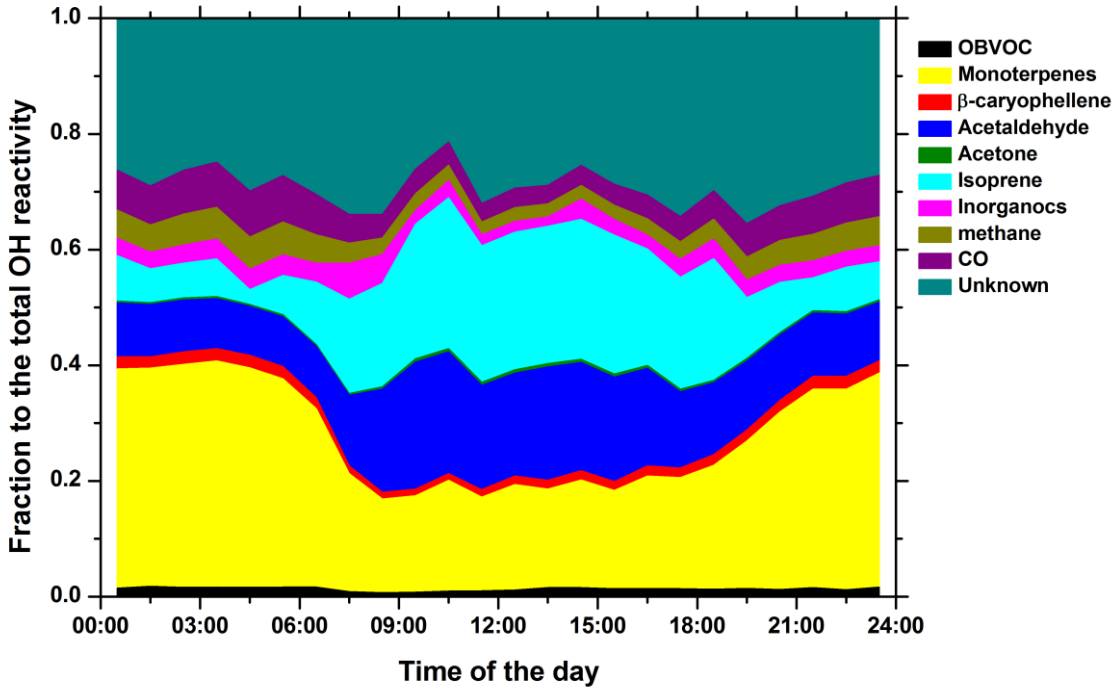

3.3.7. Average diurnal variation in the relative fraction of calculated monoterpenes OH reactivity

Fig. 3-11. Average diurnal variation in the fraction of monoterpenes which contribute to the OH reactivity.

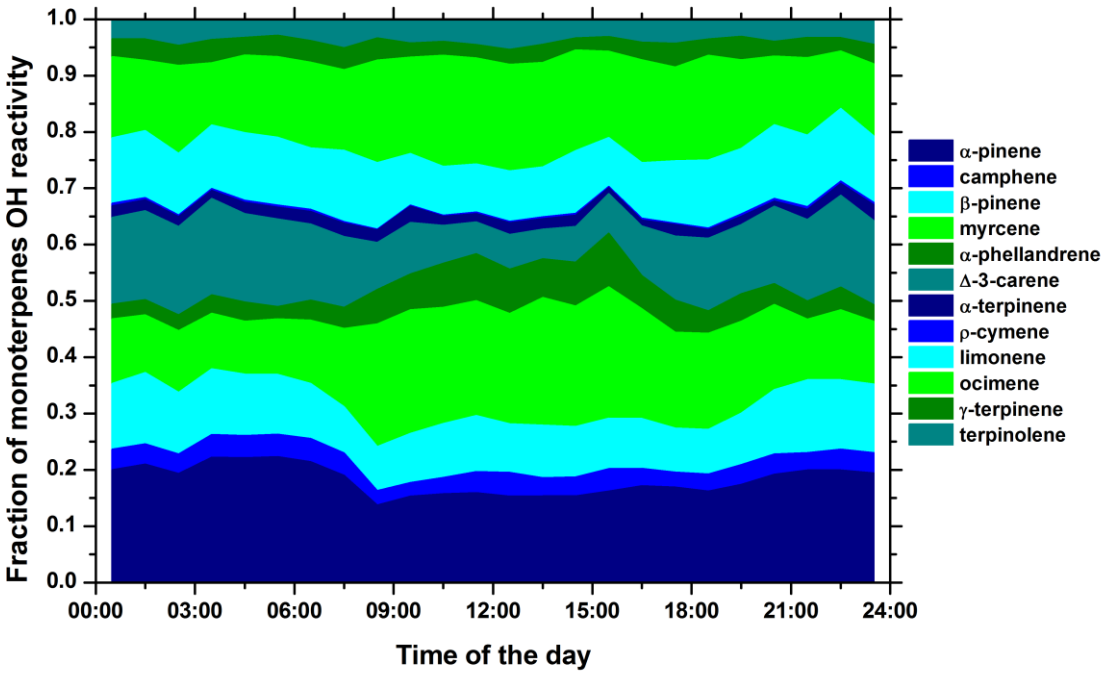

The fraction within monoterpenes to OH reactivity is shown in Fig. 3-11. α-pinene was the major contributor accounting for 19%. During the night-time α-pinene contributed between 19 and 22%. However, in the daytime, from 08:00 to 16:00, myrcene and ocimene contributed to a greater extent than α-pinene. During these hours, myrcene and ocimene contributed 19 to 23% and 15 to 20%, respectively whereas emissions of α-pinene accounted for only 15 to 17%. Between 19:00 and 06:00, Δ-3-carene, β-pinene, limonene contributed 15%, 11% and 11% respectively, but in the day-time they exhibited relatively low concentrations of 8%, 9% and 10%, respectively. The contribution of myrcene and α-phellandrene in the day-time was twice as much (20% and 6%) as their night-time contribution (12% and 3%). γ-terpinene, camphene and terpinolene were minor contributors and accounted for only 3%, 3.4%, and 3.7%, respectively.

3.3.8. OH steady state concentration ([OH]s.s molec cm^{-3})

3.3.8.1. Derivation of $J(O^1D)$

To calculate [OH]s.s concentration, $J(O^1D)$, H_2O concentration and O_3 concentration are needed. In the first half of the campaign (July 28th to August 1st, 2014) due to instrument problems $J(O^1D)$ measurement was not available sometimes as shown in Fig.3-12. Continuous rainy period due to typhoon was (August 2nd to 4th).

However, during in the second half of the campaign (August 5th to 8th) measurement was available all the time and it closely matches (highlighted in the green box) with electromagnetic radiation (mW m^{-2}). The linear correlation between $J(O^1D)$ and electromagnetic radiation (mW m^{-2}) during the second half of the campaign (August 5th to 8th) is shown in Fig. 3-13.

Using the correlation between $J(O^1D)$ and mW m^{-2} $J(O^1D)$ for the first half of the campaign is derived, and it is shown in the Fig. 3-14. The derived region is highlighted in the green box. This derived $J(O^1D)$ is used for calculating [OH]s.s. concentration.

Fig. 3-12. Time series of $J(O^1D)$ and electromagnetic radiation (mW m^{-2}).

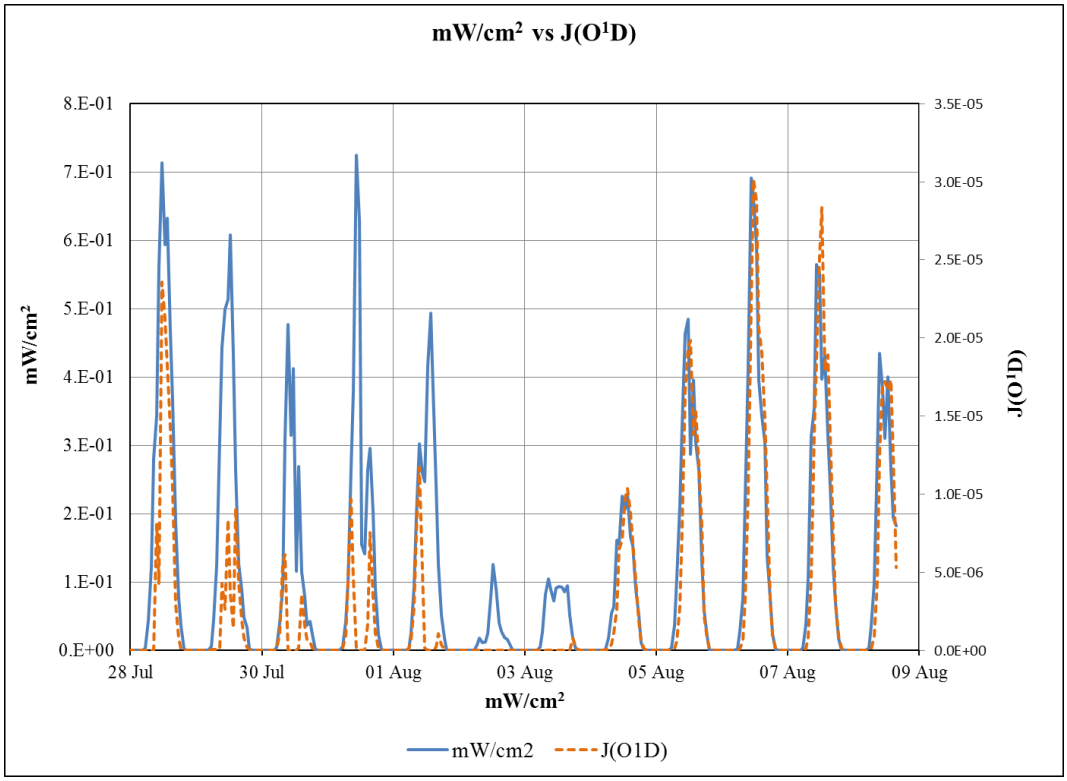

Fig. 3-13. Linear correlation between J(O^1D) and electromagnetic radiation (mW m^{-2}) during the second half of the campaign (August 5th to 8th).

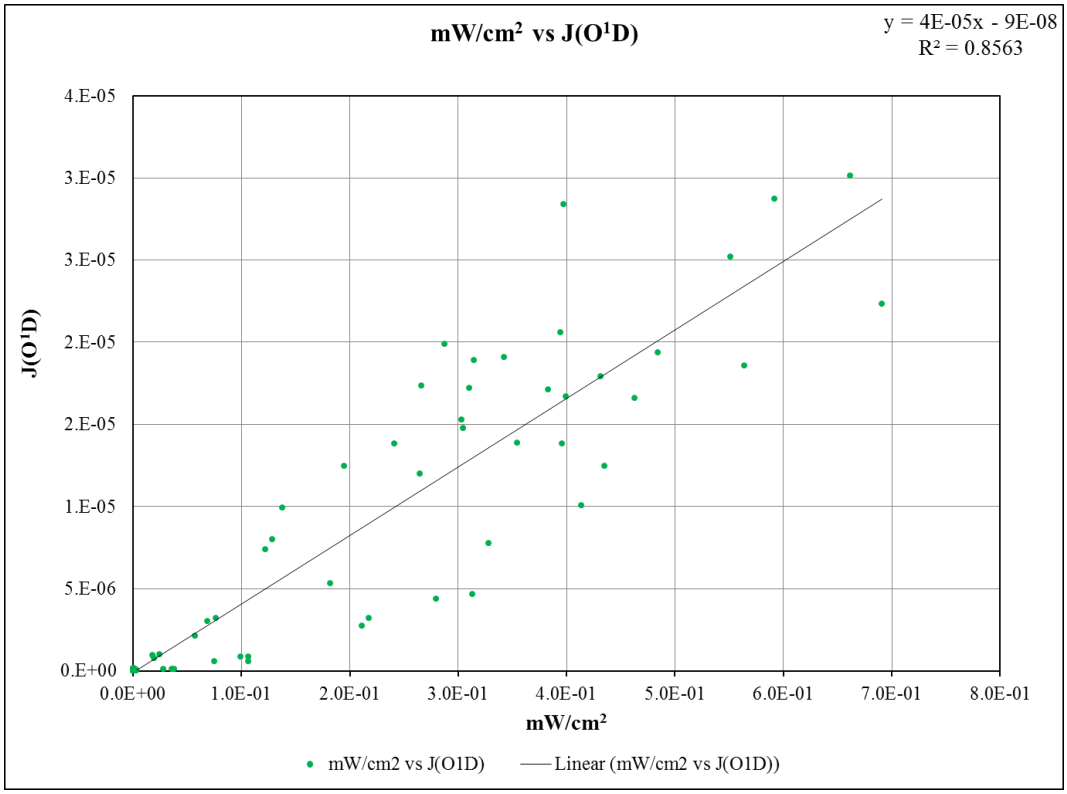

Fig. 3-14. Derived J(O^1D) using relationship between J(O^1D) and mW m^{-2}

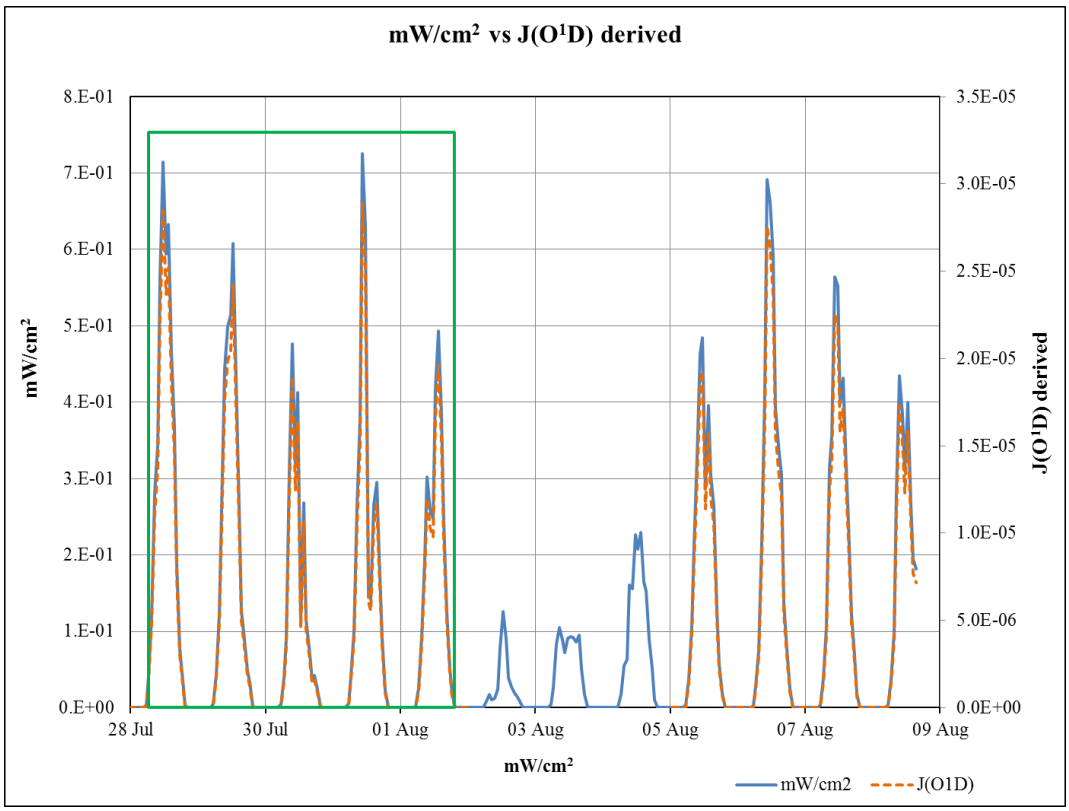

3.3.8.2. [H_2O] concentration calculation

Saturation vapour pressure, p_s, in pascals, is calculated using the following equation. (3-1)

$$P_s = 610.78 * \exp(t / (t + 238.3)*17.2694) \quad (3\text{-}1)$$

Where, **t** is the temperature in degrees Celsius

Then the actual pressure of water vapour (P) in pascals is calculated using the following equation. (3-2)

$$P = RH * P \quad (3\text{-}2)$$

Pressure in Pascal is converted to atmosphere (Pa= 9.8692 X 10^{-6} atm)

RH is relative humidity.

Moreover, Finally [H_2O] concentration (molec cm^{-3}) is calculated using the following equation.

$$\frac{n}{V} = \frac{P}{RT} \quad (3\text{-}3)$$

volume in cm^3, P= pressure in atm, T= temperature in K, R= gas constant (82.057338 cm^3 atm K^{-1} mol^{-1})

3.3.8.3. Calculation of [OH]s.s concentration

a) [OH] steady state concentration = production rate of OH/loss rate of OH

$$= P(OH)/OH \text{ reactivity } (s^{-1}) \quad (3\text{-}4)$$

[OH]s.s concentration can be expressed in molec cm^{-3}. loss rate of OH is OH reactivity (s^{-1})

b) Production of OH = P(OH) = $2Q * [O_3] * J(O1D)$ (3-5)

P(OH) is expressed in molec cm^{-3} s^{-1}

$$Q = (k_1[H_2O]/k_1[H_2O] + k_2 [N_2] + k_3 [O_2]) \quad (3\text{-}6)$$

Whereas, k_1, k_2 and k_3 are the rate constants for the reaction of H_2O, N_2, O_2 with O_3 respectively.

$k_1 = 2.2 \text{ X } 10^{-10}$ cm^3 molec^{-1} s^{-1} , $k_2 = 1.8 \text{ X } 10^{-11} \exp(107/T)$ cm^3 molec^{-1} s^{-1} ,
$k_3 = 1.8 \text{ X } 10^{-11} \exp(70/T)$ cm^3 molec^{-1} s^{-1}

Thus calculated [OH]s.s concentration is shown in the Fig. 3-15.

Fig. 3-15. Time series of calculated [OH]s.s. concentration.

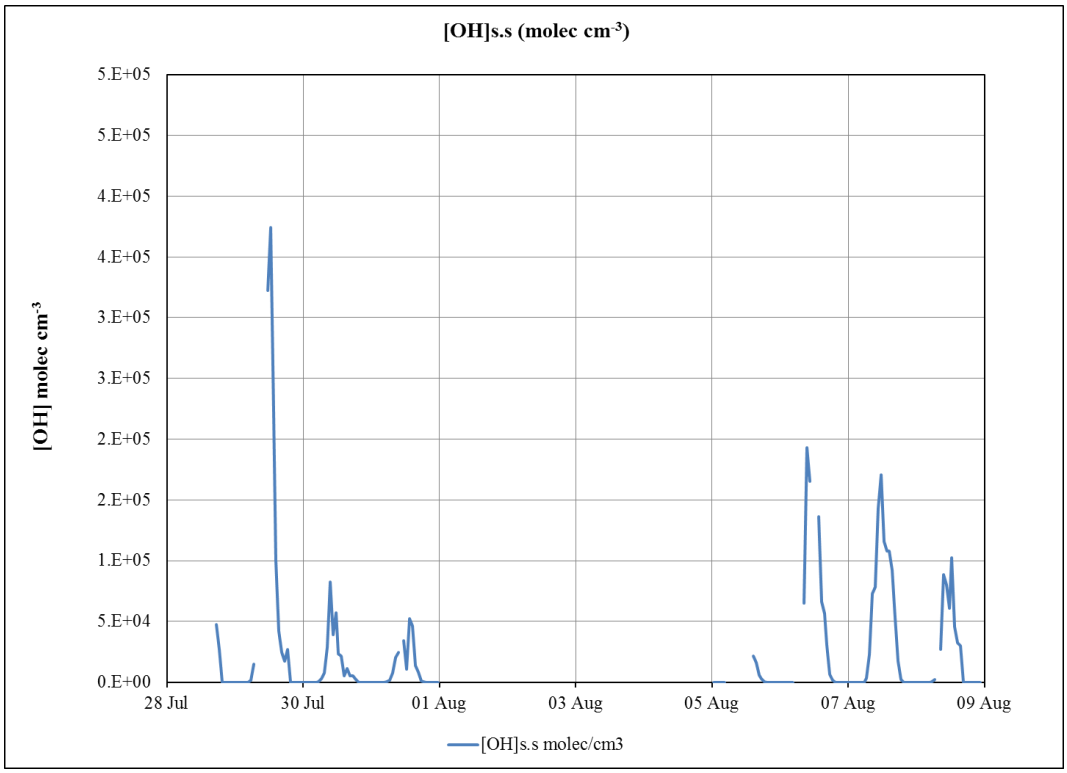

During polluted days (July 28th and 29th) high O_3 mixing ratio was measured. During these two days, [OH]s.s concentration is not available for many hours due to either no measured OH reactivity or O_3. Linear correlation between [OH]s.s concentration and P(OH) for 29th July 11:30 to 16:30 hrs is calculated (Fig. 3-16). Then this linear relationship is used for deriving the [OH]s.s concentration during 28th July 5:30 to 12:30 & 18:30 to 19:30 and 29th July 5:30 to 10:30 (Fig. 3-17).

Fig. 3-16. Calculation of linear correlation between [OH]s.s concentration and P(OH) during 29th July 11:30 to 16:30 and August 5th to 8th .

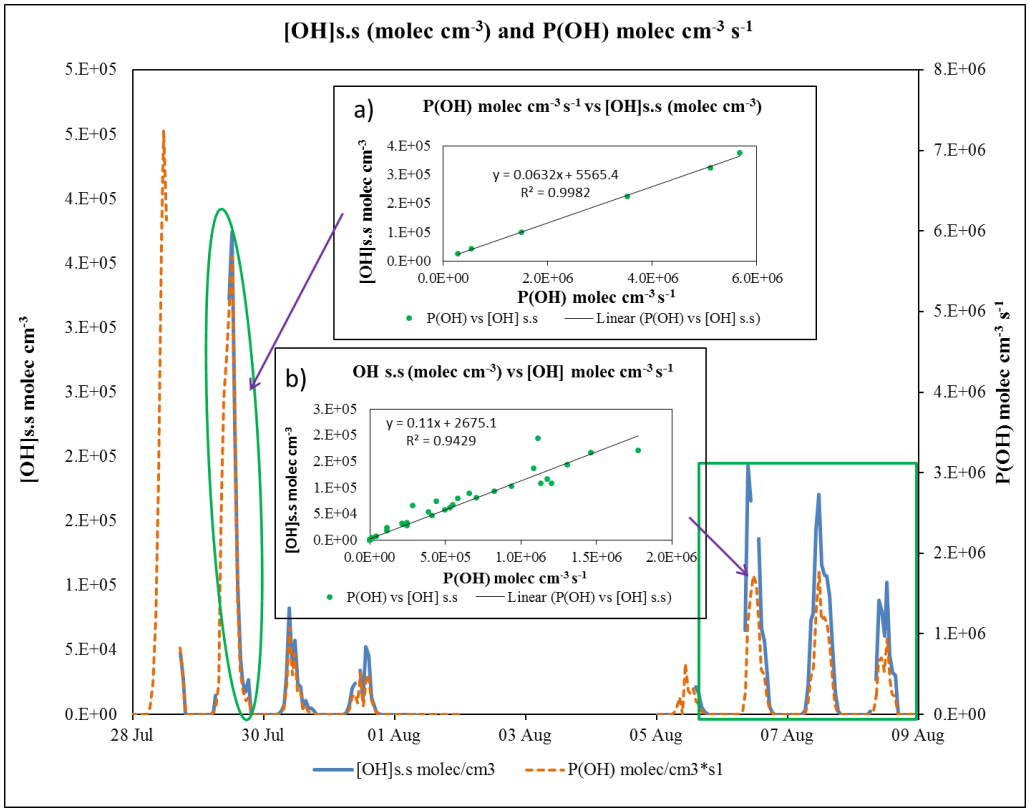

Fig. 3-17. Derived [OH]s.s concentration for missed hours.

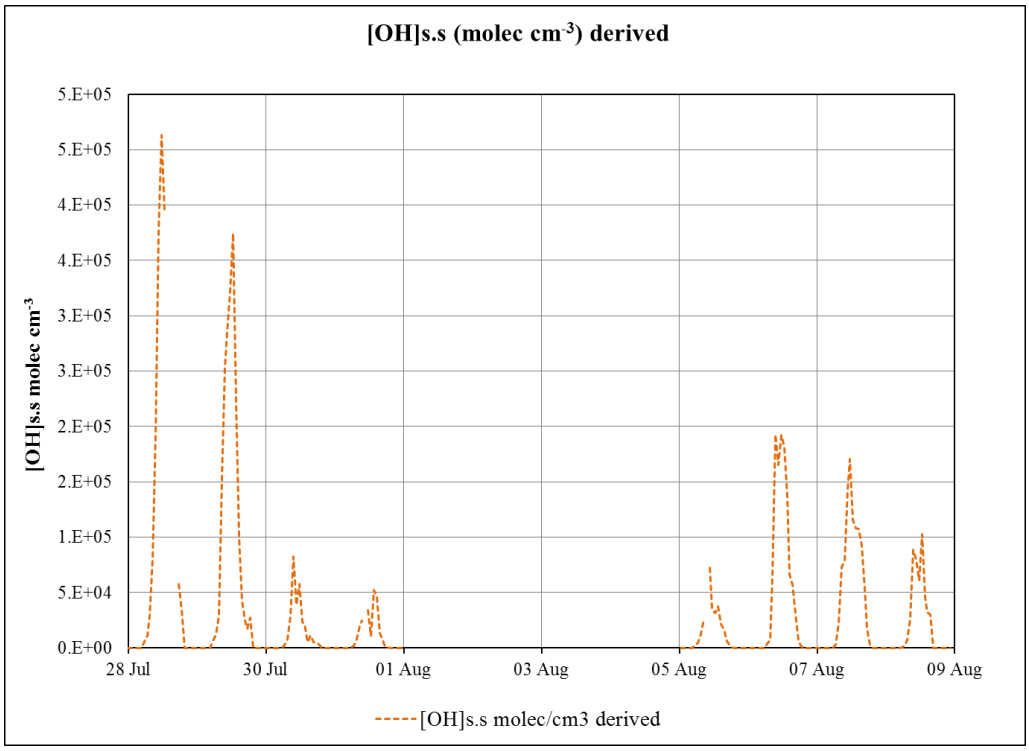

Similarly during the second half of the campaign (August 5th to 8th) the linear correlation between [OH]s.s concentration and P(OH) is used to derive [OH]s.s concentration in missed hours (Fig. 3-17). Calculated and derived [OH]s.s concentration is shown in Fig. 3-18. [OH]s.s. concentration is not derived when the O_3 mixing ratio is not available.

Fig. 3-18. Calculated and derived [OH]s.s concentration.

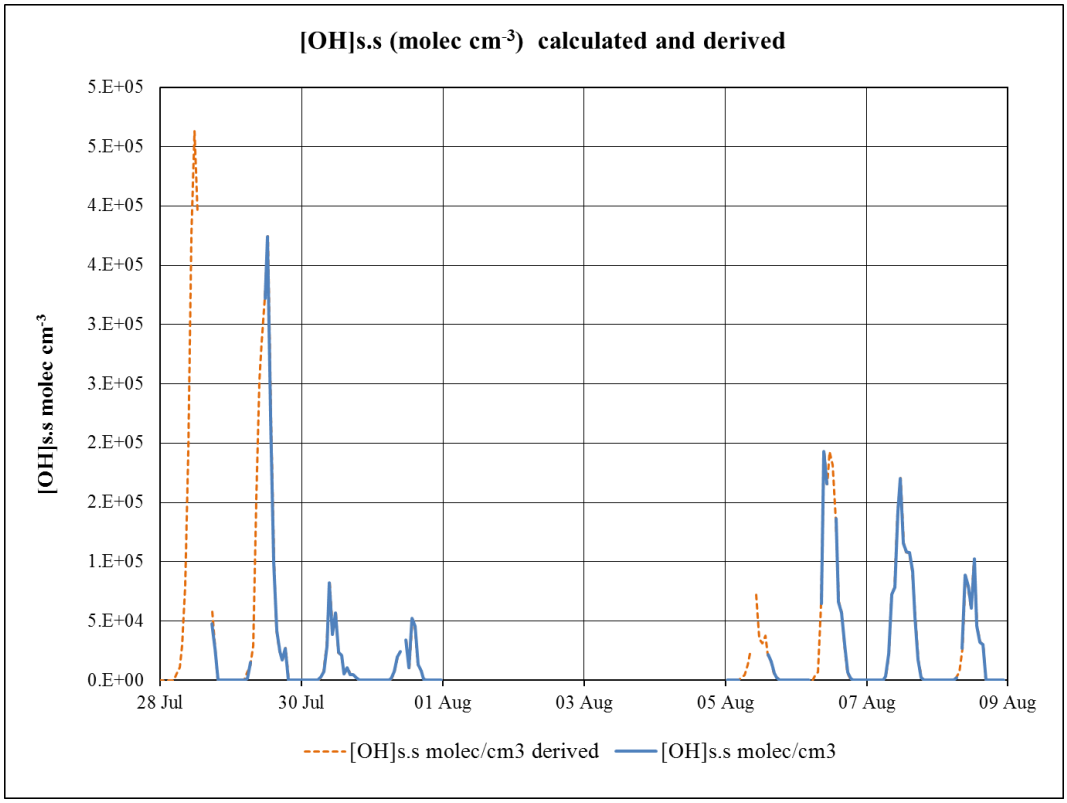

Calculated [OH]s.s concentration is closer to the background level (5 X 10^5 molec cm^{-3}) (Kim et al., 2013b) because of very low O_3 mixing ratio from which OH is produced and high loss rate of OH due to abundance of BVOCs. Even though night time O_3 and BVOCs reaction can produce OH, the O_3 mixing ratio in the night time is closer to zero. Therefore underestimation of OH production due to O_3 alkene reaction is insignificant. However, this calculation does not include additional OH producing sources such as HONO, HCHO. Also, atmospheric measurements and laboratory studies have reported that OH can be recycled from BVOCs such as isoprene oxidation in the clean atmosphere (Lelieveld et al., 2008; Fuchs et al., 2013). Therefore underestimation of OH production may also have led to low [OH]s.s concentration.

3.4. Summary

Total OH reactivity measurement was conducted together with simultaneous trace species measurements in WFRS, in Honshu Island, Japan. The field site was located inside the deep forest where biogenic emission was predominant, and far away from direct anthropogenic emissions. The average OH reactivity was comparable with those measured for other temperate and coniferous forests (Sinha et al., 2010; Nakashima et al., 2014) and very low compared to tropical rain forests (Sinha et al., 2008; Edwards et al., 2013).

The missing OH reactivity of 37.1% and the total OH reactivity of 9.8 s^{-1} were higher during the period 1a (July 28th and 29th) due to anthropogenic influences. Cleaner conditions, less warm daytime temperatures, and less anthropogenic influences in period 2 may account for less average OH reactivity at 6 s^{-1}, with very low missing OH reactivity. The mean measured OH reactivity during period 2 was comparable to that of coastal sites (Lee et al., 2009; Ingham et al., 2009; Sinha et al., 2012). In period 2, the production of low O_3 along with low NO_x concentration despite substantial emission of reactive BVOCs implies that forest generates much lesser harmful O_3 than the urban areas.

Due to the natural homogeneity of the forest and small anthropogenic influence, the measured OH reactivity showed very little short-time variability. The measurement of monoterpenes, which are major contributors to total OH reactivity, much improved the quantification and identification of sinks which contribute to the total OH reactivity. Monoterpenes contribute 30–40% to the total OH reactivity during the night-time as a result of temperature-dependent pool emission and low vertical dilution. Primarily emitted terpenoids (monoterpenes, isoprene and β-caryophyllene) accounted for 42% of the total OH reactivity.

4. OH reactivity and trace species measurement in a suburban forest near Tokyo during AQUAS-TAMA campaign

In this chapter, OH reactivity together with various trace species such as O_3, NO, NO_2 and VOCs measured in a suburban forest near Tokyo are discussed. VOCs are emitted in this measurement site by both anthropogenic sources such as vehicle exhaust and evaporative emissions and biogenic sources from the trees in the forest. VOCs and trace species emission, Calculated OH reactivity, measured OH reactivity was considered to investigate the contribution of primary and secondary trace species to the atmospheric oxidant budget and to investigate. The possible origin of sources related to the missing OH reactivity is also discussed.

4.1. Observation

4.1.1. Description of field site

Field measurements in consecutive years during 20th September to 4th October of early autumn 2012 and during 25th July to 6th August of summer 2013 were conducted in Field Museum Tama (35°64'N 139°38'E), a field experimental station of Tokyo University of Agriculture and Technology as a part of AQUAS-TAMA (Air QUAlity Study at FM TAMA) campaign (Figure 1). The field site is a small forest situated at the northeast boundary of the Tama Rolling Hills, which range to the southeast of the Kanto plane that includes densely populated Tokyo Metropolitan and neighbouring prefectures. The dominant tree species in this location are *Quercus serrata* (Japanese oak), *Cryptomeria japonica* (Japanese cedar) and *Chamaecyparis obutsa* (Japanese cypress).

4.1.2. OH reactivity measurement details

Continuous measurements of OH reactivity were made using laser induced pump and probe technique, and the detailed description have given elsewhere (Sadanaga et al., 2004, 2005). In brief, ambient air was introduced into a reaction cell (1.4 m length and 40 mm inner diameter aluminium cell) at a flow rate of 12 slm by a diaphragm pump

(DA-60S, ULVAC) and the pressure in the reaction cell was maintained at approximately 1 atm (1.01 X 10^5 Pa). A trace amount of ~ 50 ppb O_3 was generated by passing 0.1 slm zero air (VOC and NO_X free air) through a low-pressure Hg lamp and mixed with the ambient air flow.

Fig. 4-1. AQUAS-TAMA campaign suburban forest measurement site.

Along the whole length of the reaction cell uniform OH was produced by the photolysis of O_3 using a pulsed 266 nm laser beam (repetition rate 2Hz with energy ~ 20 mJ/pulse) from the fourth harmonic of a flash-lamp pumped Nd:YAG laser (Tempest 300, New Wave Research or Quanta-Ray INDI-40, Spectra Physics) and the successive reaction of $O(^1D)$ with water vapour present in the sample air as shown below:

$$O_3 + h\upsilon\ (266\ nm) \rightarrow O_2 + O(^1D) \qquad (1\text{-}1)$$

$$O(^1D) + H_2O \rightarrow 2OH \qquad (1\text{-}2)$$

Air from the reaction cell was sampled into LIF (Laser Induced Fluorescence) cell through a 0.5 mm pinhole using oil rotatory pump (D-950K, ULVAC) to detect the changes in OH radical concentrations due to pseudo first-order loss with species present in ambient air. The pressure in the LIF cell was kept at around 2.67 X 10^2 Pa. The 308 nm probe laser (repetition rate 10 kHz and energy 2-3 mW) from a second harmonic pulsed dye laser (Credo, Sirah), pumped by a second harmonic pulsed Nd:YVO4 laser (YHP-40- 532Q, Spectra Physics), passed across LIF cell to excite the $A^2\Sigma^+ - X^2\ \Pi(0,0)$ Q1(2) rotational line of OH radicals. Fluorescence signal of OH at ~308nm wavelength was detected using a photomultiplier tube (R2256P, Hamamatsu) furnished with a dynode gating system, and the resulting signal from photomultiplier tube was recorded using a photon counting method. OH reactivity finally derived from the single exponential fitting of OH decay curve which was integrated 240 times.

4.1.3. VOCs measurement

The ambient air samples were collected four times every day at local time 9:30, 12:30, 15:30 and 18:30 in 6 L stainless steel canisters and analysis performed using Gas Chromatography with Flame Ionisation Detector (GC-FID) (HP 6890, Hewlett Packard) for non-methane hydrocarbon (NMHCs). The details of this instrument were reported previously in (Kato et al., 2001). For the calibration of NMHCs, 1 ppmv standard gas containing 58 species (PAMS-J58, Sumitomo seika) was used. Limits of detection for NMHCs was in the range of 1–3 pptv with 2–13% accuracy and 2–15% precision. Benzene, toluene, isoprene, total monoterpenes and oxygenated VOCs were measured using Proton Transfer Reaction-quadrupole Mass Spectrometer (PTR-MS, Ionicon analystik, Austria). The details of measurement method have been described previously (Kato et al., 2004). Calibration was carried out using a standard gas cylinder (Taiyo Toyo Sanso, Japan). Individual monoterpenes and oxygenated biogenic VOCs were measured using BVOC GC-FID (300 Series GC, Ellutia). The details of measurement method and removal ozone from air sample have been described previously (Jones et al., 2014). Small volumes (10–20 mL) of the 1 ppm (PAMSJ58, Sumitomo Seika Chemicals) primary standards and 100 mL volumes of the freshly diluted secondary standards were used to calibrate sample volumes of 100 mL working terpene gas standards for α-pinene. Based upon the ratio of their respective FID responses to the a-pinene response factor, the mixing ratios of the other species in the terpene gas standard

were derived. The overall assessed uncertainties were ±8–12% for monoterpenes, ±15–20% for sesquiterpenes and ±14–26% for OBVOC.

Table 4-1. Average daytime mixing ratio (ppb) VOCs measured during AQUAS-TAMA campaign.

(group with * mark) 24 hours average mixing ratio (ppb) of species measured during AQUAS-TAMA campaign.

Species	**Autumn – 2012**		**Summer – 2013**	
Alkanes	**Avg. ± S.D**	**Med.**	**Avg. ± S.D**	**Med.**
Ethane	1.339 ± 0.522	1.350	1.662 ± 0.884	1.488
Propane	1.631 ± 0.840	1.503	2.651 ± 1.555	2.152
Isobutane	0.531 ± 0.294	0.460	1.123 ± 0.806	0.888
n-Butane	0.935 ± 0.499	0.817	1.880 ± 1.183	1.567
Isopentane	0.727 ± 0.510	0.571	1.121 ± 0.648	0.932
n-Pentane	0.325 ± 0.242	0.245	0.522 ± 0.351	0.398
2,2- dimethylbutane	0.018 ± 0.010	0.016	0.028 ± 0.015	0.028
Cyclopentane	0.048 ± 0.041	0.036	0.110 ± 0.058	0.103
2,3-Dimethylbutane	0.040 ± 0.024	0.033	0.062 ± 0.035	0.050
2-Methylpentane	0.180 ± 0.105	0.152	0.309 ± 0.174	0.281
3-Methylpentane	0.120 ± 0.070	0.094	0.211 ± 0.128	0.175
n-Hexane	0.172 ± 0.385	0.099	0.309 ± 0.273	0.224
Methylcyclopentane	0.055 ± 0.034	0.047	0.105 ± 0.075	0.077
2,4-Dimethylpentane	0.036 ± 0.022	0.032	0.011 ± 0.009	0.008
Cyclohexane	0.082 ± 0.060	0.058	0.125 ± 0.122	0.072
2-Methylhexane	0.049 ± 0.026	0.044	0.046 ± 0.027	0.038
2,3-Dimethylpentane	0.013 ± 0.017	0.010	0.016 ± 0.010	0.013
3-Methylhexane	0.041 ± 0.018	0.037	0.054 ± 0.027	0.047
2,2,4-Trimethylpentane	0.021 ± 0.026	0.014	0.030 ± 0.018	0.026
n-Heptane	0.041 ± 0.022	0.038	0.076 ± 0.065	0.050
Methylcyclohexane	0.054 ± 0.044	0.039	0.081 ± 0.065	0.058
2,3,4-Trimethylpentane	0.012 ± 0.018	0.010	0.015 ± 0.006	0.015
2-Methylheptane	0.008 ± 0.009	0.005	0.011 ± 0.007	0.008
3-Methylheptane	0.007 ± 0.005	0.006	0.017 ± 0.007	0.014

n-Octane	0.013 ± 0.012	0.011	0.016 ± 0.012	0.011
n-Nonane	0.039 ± 0.020	0.034	0.052 ± 0.032	0.039
Alkenes				
Ethylene	0.652 ± 0.466	0.573	1.443 ± 1.780	0.799
Propylene	0.185 ± 0.189	0.141	0.183 ± 0.216	0.103
1-Butene	0.013 ± 0.016	0.007	0.017 ± 0.021	0.012
Butadiene	0.011 ± 0.015	0.005	0.009 ± 0.012	0.005
trans-2-Butene	0.013 ± 0.020	0.009	0.027 ± 0.030	0.019
cis-2-Butene	0.012 ± 0.019	0.006	0.013 ± 0.014	0.008
3-Methyl-1-Butene	0.008 ± 0.011	0.003	0.010 ± 0.007	0.009
1-Pentene	0.010 ± 0.013	0.006	0.018 ± 0.023	0.012
trans-2-Pentene	0.007 ± 0.013	0.000	0.011 ± 0.016	0.006
cis-2-Pentene	0.004 ± 0.008	0.000	0.008 ± 0.009	0.004
Alkynes				
Acetylene	0.596 ± 0.278	0.553	0.846 ± 0.513	0.658
Aromatics				
Benzene[a]	0.180 ± 0.083	0.167	0.256 ± 0.199	0.204
Toluene[a]	1.135 ± 0.642	0.966	1.154 ± 0.964	0.804
Ethylbenzene	0.293 ± 0.262	0.195	0.322 ± 0.243	0.277
p,m-Xylene	0.223 ± 0.191	0.167	0.201 ± 0.145	0.138
Styrene	0.024 ± 0.038	0.011	0.015 ± 0.014	0.012
o-Xylene	0.093 ± 0.062	0.076	0.018 ± 0.050	0.113
Iso-Propylbenzene	0.007 ± 0.008	0.005	0.016 ± 0.022	0.006
n-Propylbenzene	0.020 ± 0.015	0.015	0.027 ± 0.016	0.022
1,3,5-Trimethylbenzene	0.030 ± 0.025	0.021	0.024 ± 0.018	0.018
1,2,4-Trimethylbenzne	0.118 ± 0.081	0.088	0.097 ± 0.067	0.076
m-Ethyl methyl benzene			0.053 ± 0.035	0.042
p-Ethyl methyl benzene			0.028 ± 0.018	0.022
o-Ethyl methyl benzene			0.032 ± 0.017	0.027
1,2,3-Trimethylbenzene			0.024 ± 0.015	0.019
p-Diethyl benzene			0.013 ± 0.009	0.010
m-Diethyl benzene			0.006 ± 0.005	0.004
Inorganics*				

NO	0.468 ± 2.642	0.169	1.284 ± 2.288	0.291
NO_2	6.520 ± 3.290	5.934	6.602 ± 3.783	5.744
O_3	22.322 ± 11.612	20.805	24.715 ± 19.325	21.574
CO	212.799 ± 59.132	201.227	177.492 ± 164.423	140.183
SO_2	0.199 ± 0.379	0.087		
Biogenics*				
Isoprene	0.469 ± 0.511	0.245	0.989 ± 1.010	0.547
α– Pinene	0.026 ± 0.030	0.016	0.061 ± 0.082	0.031
Camphene	0.008 ± 0.008	0.006	0.022 ± 0.027	0.012
β–Pinene	0.028 ± 0.019	0.024	0.023 ± 0.037	0.011
Myrcene	0.011 ± 0.009	0.009	0.007 ± 0.011	0.003
Δ–3–Carene	0.016 ± 0.017	0.011	0.007 ± 0.003	0.006
α– Terpinene	0.009 ± 0.010	0.006		
Limonene	0.015 ± 0.010	0.014	0.014 ± 0.021	0.008
ρ– Cymene			0.007 ± 0.009	0.005
γ– Terpinene	0.009 ± 0.013	0.004		
Linalool	0.012 ± 0.008	0.011		
Oxygenated VOCs(PTR-MS)*				
Methanol	4.038 ± 2.089	3.602	2.072 ± 1.001	1.819
Acetonitrile	0.195 ± 0.053	0.192		
Acetaldehyde	1.043 ± 0.869	0.855	1.008 ± 0.730	0.775
Acetone	2.076 ± 0.886	1.933	2.061 ± 1.003	1.835
Acetic acid			0.418 ± 0.317	0.331
Methyl vinyl ketone + Methacrolein	0.181 ± 0.123	0.150	0.201 ± 0.155	0.145
Methyl ethyl ketone	0.557 ± 0.401	0.496	0.462 ± 0.370	0.363

4.1.4. NO_X, O_3 and CO measurement

Together with OH reactivity measurements trace species present in the ambient air and meteorological conditions were measured. NO_X, O_3, CO and were measured by O_3 chemiluminescence (Model 42i-TL, Thermo Electron), UV absorption (Model 49C,

Thermo Electron) and non-dispersive infrared spectroscopy (Model 48C, Thermo Electron) respectively.

4.2. Results and discussion

4.2.1. Overview of VOCs and inorganic pollutants

The average mixing ratio of VOCs and inorganic species measured during autumn–2012 and summer–2013 is shown in Table 4-1. Anthropogenic VOCs measured in FM TAMA are compared with those of from long-term measurement 2002–2008 (Tajima et al., 2010) in a nearest (5.4 km) suburban site located at Tokyo Metropolitan University (TMU) to interpret the characteristics of the emission sources. Fig.4-2 shows log scale of the mixing ratio of VOCs measured at FM TAMA and TMU.

Fig. 4-2. Comparison of mixing ratio of VOCs measured at FM TAMA and TMU.

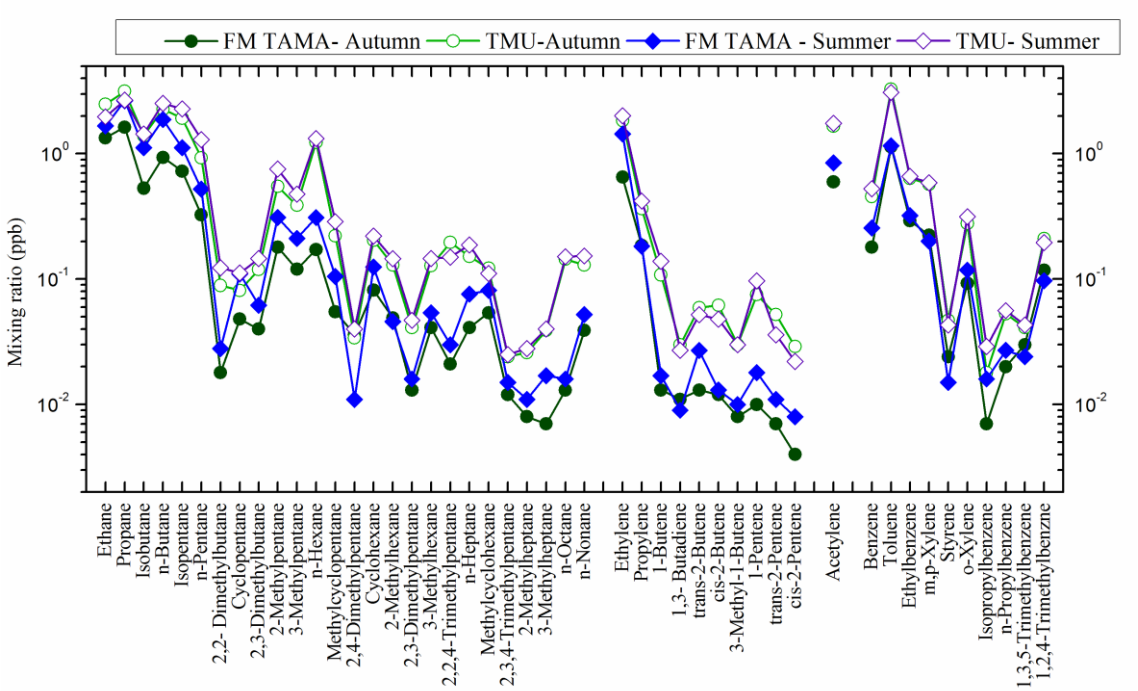

Same trend in VOCs measured in both sites in different season indicates that the common anthropogenic sources. Vehicle exhaust, stationary evaporative sources such as solvents (painting, printing, cleaning, etc.), fuelling, chemical plants, etc. were reported as major sources of VOCs in Tokyo area (Tokyo Metropolitan Government, 2013, Shirai et al., 2007). However, absolute mixing ratios of most of the anthropogenic VOCs in TMU are 2-3 times higher than those of FM TAMA. Mixing ratio of less

reactive species such as ethane, propane, n-butane and iso-butane measured in FM TAMA are comparable to that of TMU. Moreover, mixing ratios of ethane and propane were only slightly less than that observed in Tokyo metropolitan area (TMA) (Yoshino et al., 2012). The mixing ratio of reactive alkenes such as butenes and pentenes are multifold lower compared to TMU and TMA. This indicates that that photochemical removal during urban air transport. During Summer-2013, alkanes showed a strong correlation (r^2 = 0.50– 0.96) and alike trend between themselves and also with benzene and acetylene indicates that common anthropogenic sources such as vehicle exhaust and evaporative emission.

Fig. 4-3. Time series of mixing ratio of CO, O_3, NO and NO_2 during autumn and summer season.

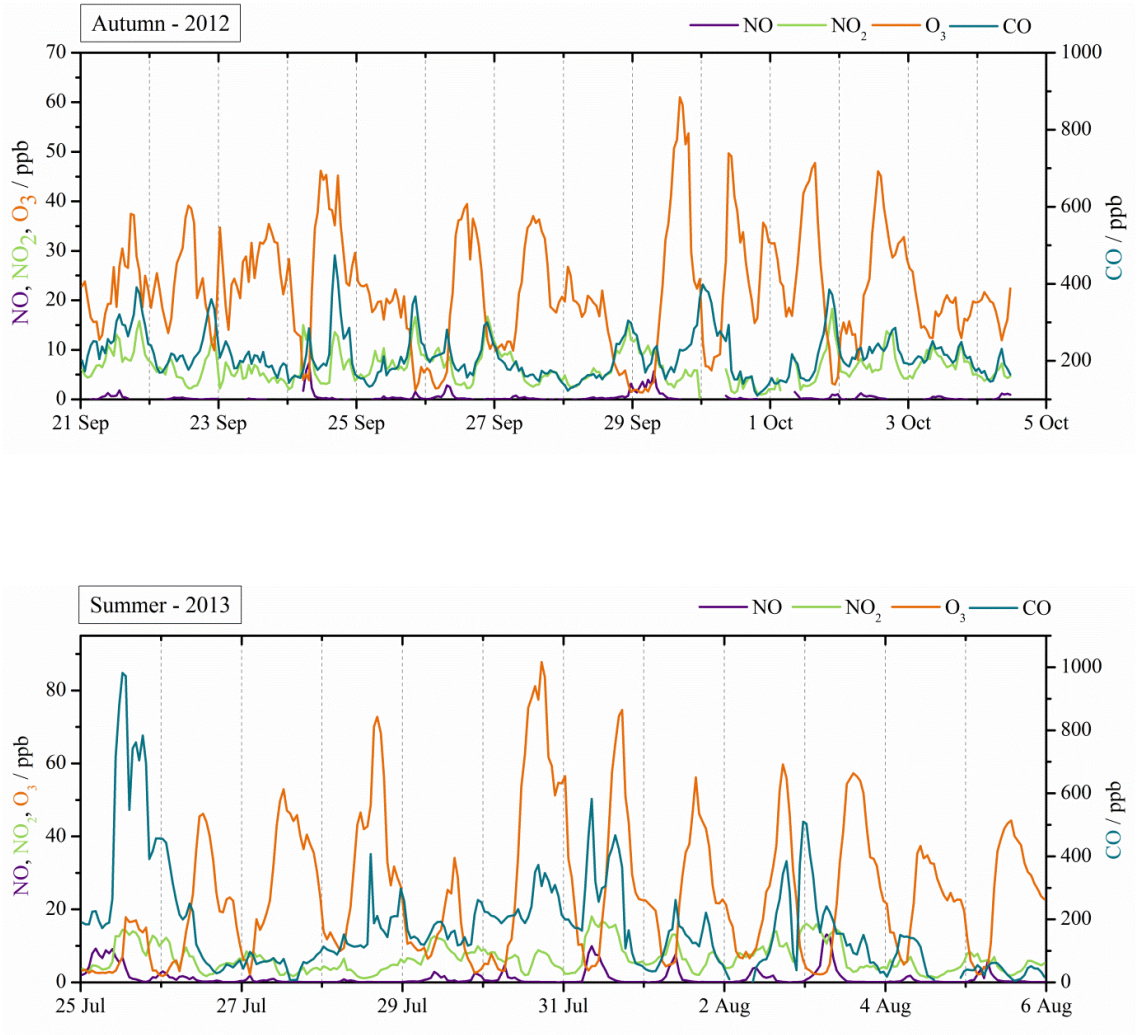

However iso-butane and n-butane have shown only moderate correlation with other species but good correlation with propane and specifically in the autumn season,

these three species have demonstrated a strong correlation (r^2 = 0.84 – 0.96) indicates that different sources. Propane and butanes are well-known species from LPG gas. Extensive usage of LPG gas from residential area seems to be the substantial sources for propane, n-butane, and iso-butane. Daytime (9:00-18:00) average mixing ratio of NO and NO_2 respectively 5.2, 4.6 lower than that of observed in TMA during summer.

NO is anti-correlated with O_3, especially in night time more close to zero due to the titration effect (O_3 + NO = NO_2) and the relatively higher mixing ratio was observed during morning rush hours due to lower OH and O_3 abundance (Fig. 4-4). Isoprene was the dominant biogenic specie and most abundant reactive VOC observed in this site. Isoprene is also can come from automobiles (Sharma et al., 2000; Nakashima et al., 2010) but much higher mixing ratio in the daytime of summer (1.70 ppb) compared to that of nearby suburban TMU (0.61 ppb) depicts that isoprene emitted from biogenic sources.

Fig. 4-4. Regression analysis of NO (ppb) vs. O_3 (ppb).

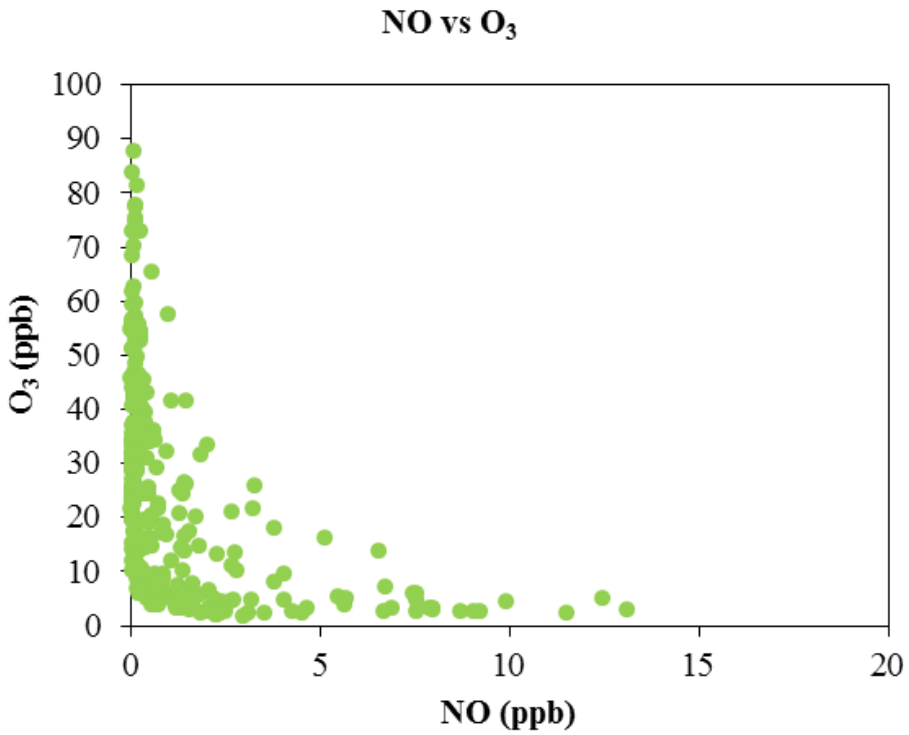

4.2.2. Total OH reactivity

The OH reactivity for inorganic species and VOCs is calculated by multiplying their OH reactive rate constants ($k_{\mathrm{OH+N}_i}$) with their respective mixing ratio [N_i] as Eq. (3). The reaction rate constants were taken from literature (Atkinson, 1994; 1997; 2003; Atkinson et al., 1995; 1997; Calvert et al., 2000; Sander et al., 2002).

$$k_{\mathrm{calc}} = \sum_i k_{\mathrm{OH+N}_i}[\mathrm{N}_i] \qquad (1-17)$$

Fig. 4-5. Measured OH reactivity during the autumn – 2012, AQUAS-TAMA campaign.

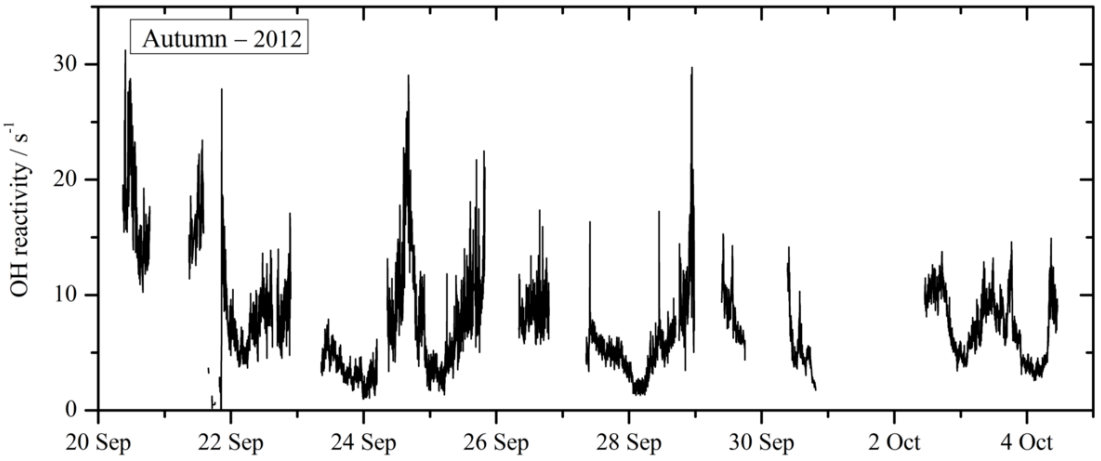

Fig. 4-6. Measured OH reactivity during the summer – 2013, AQUAS-TAMA campaign.

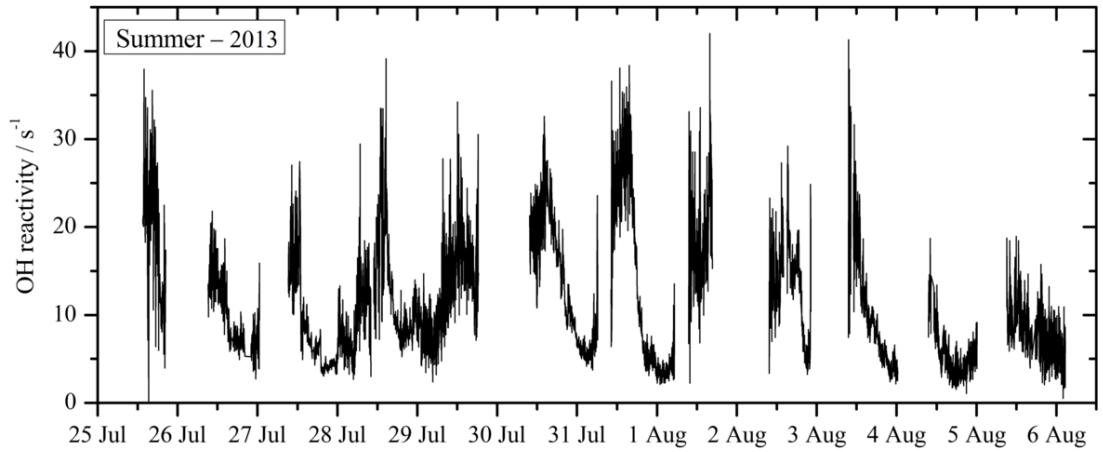

Time series of measured OH reactivity during the autumn and the summer season is shown in Fig. 4-5 and 4-6. Measured OH reactivity ranged 2 – 28 s^{-1} in the autumn – 2012 and 2 – 38 s^{-1} in the summer – 2013 and demonstrated diurnal variation. Average measured OH reactivity was 7.4 s^{-1} in the autumn and 11.4 s^{-1} in the summer. Average measured OH reactivity is much lower than that of the nearby suburban site at TMU (27.7 s^{-1}, Yoshino et al., 2006) and urban central Tokyo (33.4 s^{-1} Yoshino et al., 2012).

4.2.3. Contribution to the OH reactivity

The contribution of calculated OH reactivity of trace species to the measured OH reactivity is shown in Figure 4-7. The contribution of calculated OH reactivity is calculated for the time periods when all the species available (9:30, 12:30, 15:30, 18:30). So it represents the day time contribution and average measured OH reactivity corresponding to this time was 14.4 s^{-1} and 8.9 s^{-1} for summer and autumn respectively.

Fig. 4-7. The average contribution of trace species to the total OH reactivity during autumn and summer campaign.

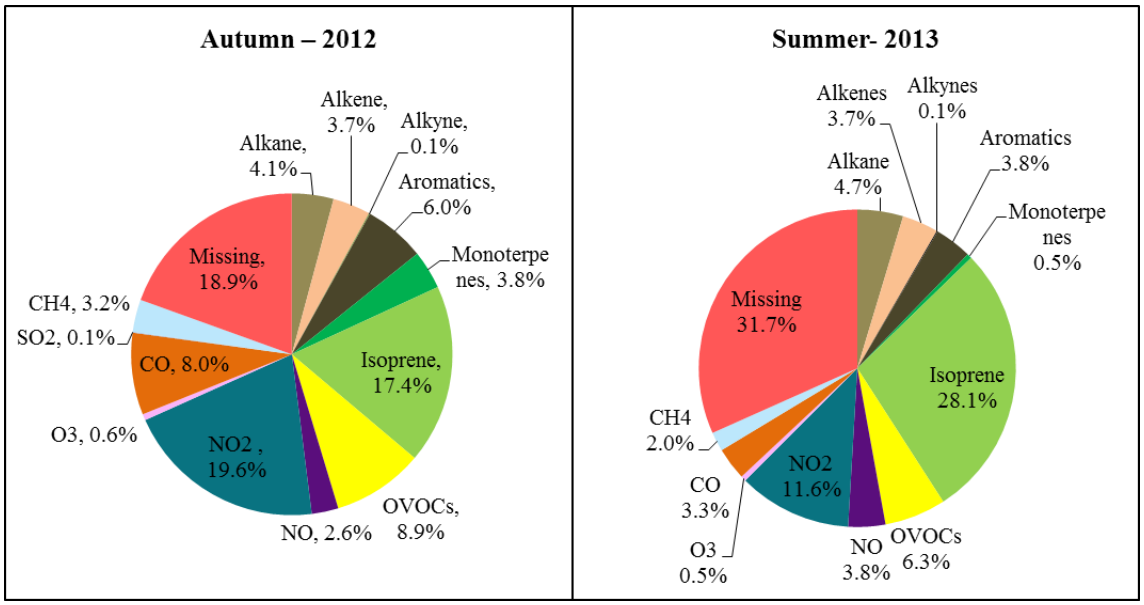

Summertime average measured OH reactivity is much lower than that of the nearby suburban site at TMU (27.7 s^{-1}, Yoshino et al., 2006) and urban central Tokyo (33.4 s^{-1} Yoshino et al., 2012). Although NO_2 was the dominant species accounting for 19.6 % in the autumn season, its contribution in the summer period is only 11.6 % as a result of the efficient photochemical removal. Even though isoprene is highly reactive

than NO_2, it contributed much higher to OH reactivity in the summer because of strong light dependent emission and closer vicinity to the emission source. Alkanes and aromatics contribution to the OH reactivity in FM TAMA is only slightly less compared to TMA. AVOCs were substantially abundant (sum 15.4 ppb) in FM TAMA compared to remote forest WFRS and they account for considerable fraction to the measured OH reactivity. However, BVOCs contributed twice higher (28.6 %) to the measured OH reactivity due to their higher reactivity even though sum of BVOCs mixing ratio 1.13 ppb. Although OH reactivity at FM TAMA was lower than that at Tokyo mixing ratio of O_3 in the summer time was comparable to both sites.

Fig. 4-8. The average contribution of trace species to the measured OH reactivity during the morning (09:30), noon (12:30), afternoon (15:30) and evening (18:30).

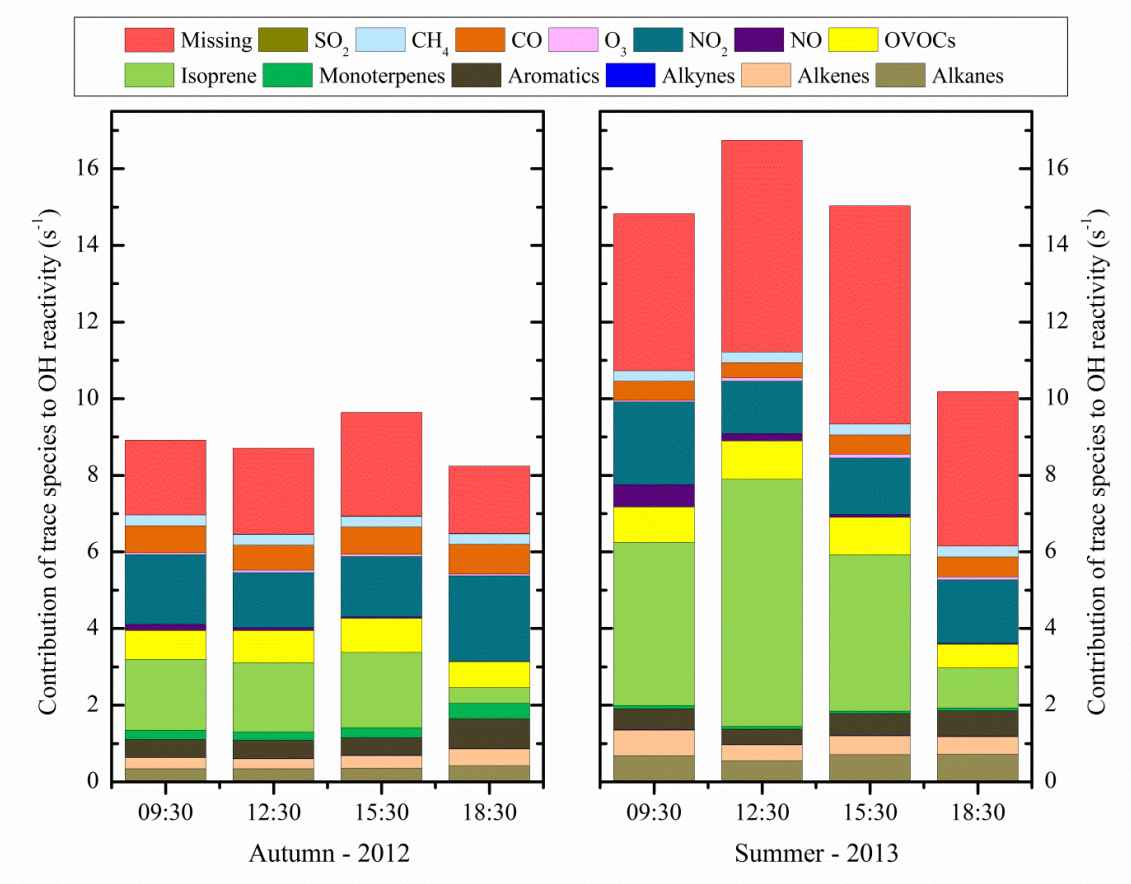

The relatively lower concentration of NO_X compared to that of urban area Tokyo may also have favoured for photochemical O_3 production by effective HO_X recycling rather than chain termination by OH loss by acid formation. Moreover, most of the days in summertime, maximum O_3 mixing ratio observed above 50 ppb whereas in the autumn it was around 40 ppb mostly that indicates enhanced isoprene photochemistry

might be a significant factor. The contribution of trace species OH reactivity to the measured OH reactivity during the morning (09:30), noon (12:30), afternoon (15:30) and evening (18:30) is shown in Fig. 4-8 and 4-9.

Fig. 4-9. The average fraction of trace species to the measured OH reactivity during the morning (09:30), noon (12:30), afternoon (15:30) and evening (18:30).

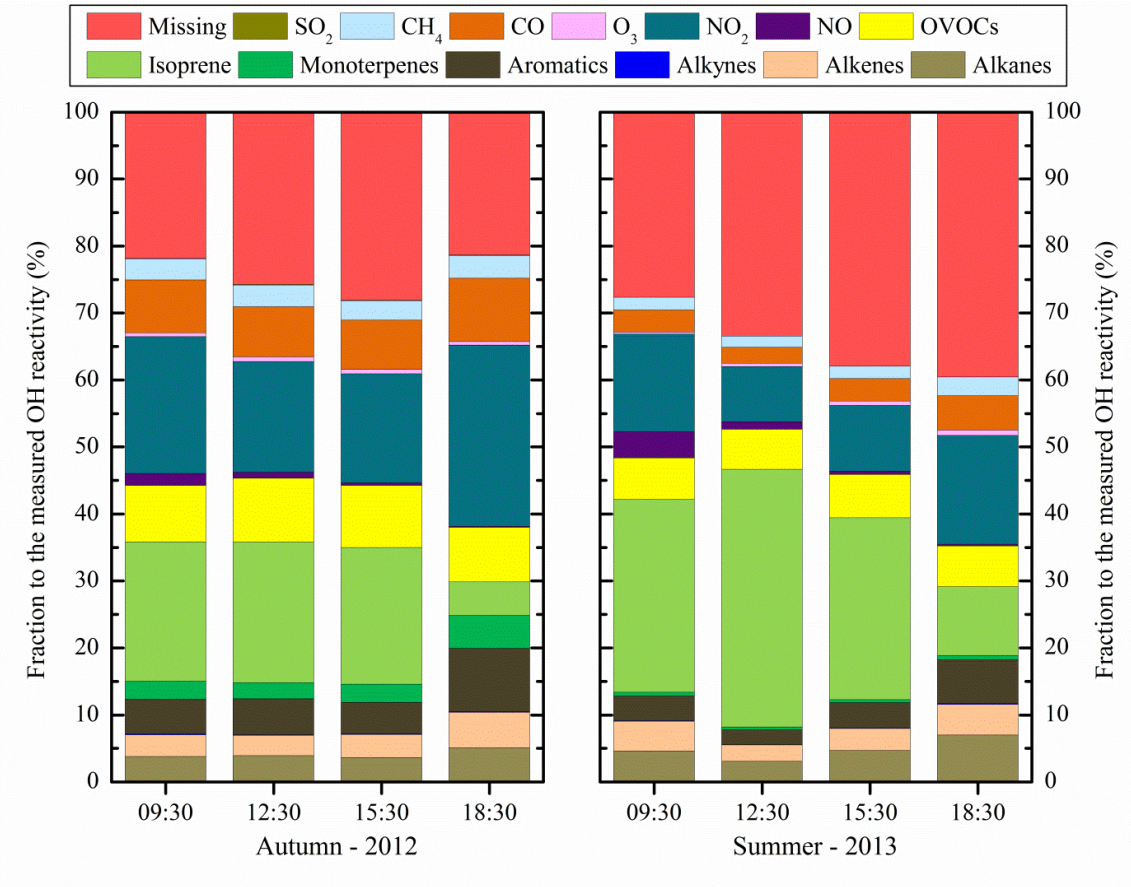

In summer season lowest missing OH reactivity (28 %) was observed during morning time. Higher contribution from VOCs (53 %, mainly isoprene 38 %) compared to NO_X (9%) favours to the shifting towards NO_X limited condition and enhanced the *in situ* photochemical production of O_3. In addition to this, when polluted urban air passing to this site some amount of relatively long living secondary product O_3 also can reach this place. Maximum O_3 mixing ratio was observed at 14:00 (Yoshino et al., 2012) but in this site most of the days it was around 17:00-18:00. Average missing OH reactivity in the evening time during the autumn season was lowest (21.3 %), but in summer it was highest (39.6 %). Here daylight hours play a major role to this different behaviour

that is long daytime (~ 04:45 – ~18:45) in summer (July-August) and short daytime (~ 05:35 – ~17:25) in early autumn. In the autumn due to early sunset primary source emissions, monoterpenes and anthropogenic species sharply increased as combined effect of boundary layer shrank and evening rush hour emission.

Thus due to less photochemical process, the relatively higher agreement between measured and calculated OH reactivity resulted during the autumn evening. Most of the oxygenated VOCs and anthropogenic VOCs showed relatively stronger correlation with missing OH reactivity (Table. 4-2) in summer compared to the autumn season. Strong light dependent biogenic emission of isoprene, strong evaporative emission of anthropogenic VOCs and higher photochemical activity in summer season may have led to several OVOCs production that were not measured by chemical analysis. This may have caused the significant discrepancy between measured and calculated OH reactivity.

Table 4-2. Linear regression analysis coefficient (r^2) for missing OH reactivity vs. trace species.

Species	**Autumn – 2012**	**Summer – 2013**
Alkanes		
Ethane	0.294	0.598
Propane	0.281	0.511
Isobutane	0.272	0.391
n-Butane	0.292	0.321
Isopentane	0.216	0.424
n-Pentane	0.186	0.388
2,2- Dimethylbutane	0.005	0.171
Cyclopentane	0.198	0.052
2,3-Dimethylbutane	0.242	0.377
2-Methylpentane	0.170	0.364
3-Methylpentane	0.123	0.339
n-Hexane	0.000	0.258
Methylcyclopentane	0.202	0.329
2,4-Dimethylpentane	0.159	0.228

Cyclohexane	0.085	0.183
2-Methylhexane	0.067	0.275
2,3-Dimethylpentane	0.012	0.202
3-Methylhexane	0.005	0.309
2,2,4-Trimethylpentane	0.000	0.346
n-Heptane	0.199	0.054
Methylcyclohexane	0.155	0.249
2,3,4-Trimethylpentane	0.143	0.158
2-Methylheptane	0.008	0.305
3-Methylheptane	0.037	0.389
n-Octane	0.011	0.169
n-Nonane	0.046	0.273
n-Decane		0.264
n-Undecane		0.228
Alkenes		
Ethylene	0.124	0.175
Propylene	0.013	0.044
1-Butene	0.067	0.095
Butadiene	0.074	0.001
trans-2-Butene	0.001	0.069
cis-2-Butene	0.000	0.004
3-Methyl-1-Butene	0.036	0.116
1-Pentene	0.056	0.016
trans-2-Pentene	0.003	0.026
cis-2-Pentene	0.082	0.001
Alkynes		
Acetylene	0.068	0.504
Aromatics		
Ethylbenzene	0.040	0.290
p,m-Xylene	0.004	0.145
Styrene	0.019	0.001
o-Xylene	0.016	0.311
Iso-propylbenzene	0.016	0.163
n-Propylbenzene	0.031	0.387
1,3,5-Trimethylbenzene	0.005	0.083
1,2,4-Trimethylbenzne	0.015	0.119

m-Ethylmethylbenzene		0.120
p-Ethylmethylbenzene		0.217
o-Ethylmethylbenzene		0.235
1,2,3-Trimethylbenzene		0.043
p-Diethylbenzene		0.090
m-Diethylbenzene		0.130
Inorganics		
NO	0.064	0.0004
NO_2	0.039	0.153
O_3	0.054	0.242
CO	0.211	0.499
SO_2	0.042	
Aromatics		
Benzene	0.259	0.472
Toluene	0.084	0.335
Biogenics		
Isoprene	0.238	0.118
α– Pinene	0.021	0.023
Camphene	0.0004	0.030
β–Pinene	0.005	0.060
Myrcene	0.0003	0.000
Δ–3–Carene	0.003	0.218
α– Terpinene	0.003	
Limonene	0.004	0.080
ρ– Cymene		0.003
γ– Terpinene	0.003	
Linalool	0.028	
Oxygenated VOCs		
Methanol	0.105	0.342
Acetonitrile	0.042	
Acetaldehyde	0.293	0.523
Acetone	0.229	0.614
Acetic acid		0.381
Methyl vinyl ketone + Methacrolein	0.207	0.279
Methyl ethyl ketone	0.092	0.325

4.2.4. O_3 formation potential calculation

O_3 formation potential is expressed in terms of overall accumulation of peroxy radicals (RO_2 and HO_2) per each OH radicals primarily formed (Sadanaga et al., 2005). Due to the fact that NO mixing ratio is considerable in this campaign, the peroxy radicals produced are assumed to react with NO and not with peroxides and O_3. Then, resulting NO_2 in this reaction is converted to O_3 through photolysis. Therefore, production rate of peroxy radicals ($P_{RO_2HO_2}$) can be used to estimate O_3 formation potential. O_3 production efficiency depends on the chain reactions between OH, VOCs, NO and peroxy radicals before chain termination by OH + NO_2 reaction (Fig. 4-10). Detailed description of box model to calculate O_3 formation potential is given elsewhere (Sadanaga et al., 2005).

Fig. 4-10. Atmospheric photochemical reactions and O_3 formation.

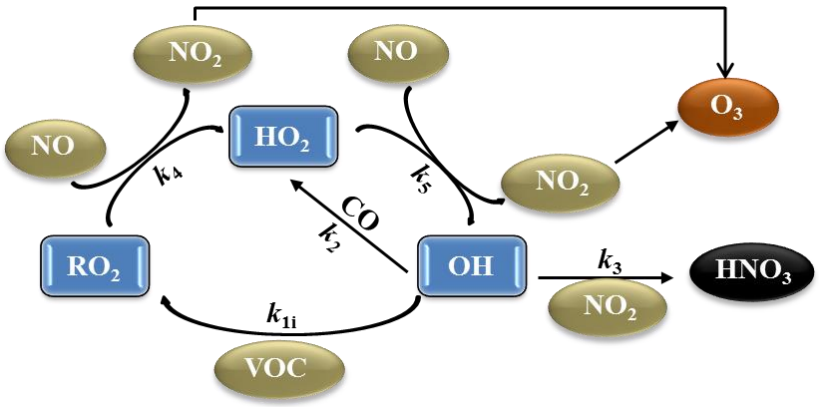

The production rate of peroxy radicals ($P_{RO_2HO_2}$) is calculated using the following equation.

$$P_{RO_2HO_2} = k_2\,[CO]\,[OH] + 2\,\Sigma k_{1i}[VOC_i]\,[OH] \quad (4\text{-}1)$$

O_3 formation potential is calcualted from dividing the overall accumulated peroxy radicals by initial OH concnetration as follows,

$$O_3 \text{ formation potential } (\phi) = \frac{\int_0^{\infty} P_{RO_2HO_2}\,dt}{[OH]_0} \quad (4\text{-}2)$$

Initial concnetration of OH was assigned as 10^6 molec cm^{-3}. $\Sigma k_{1i}[VOC_i]$ [OH] is the sum of the multiplication of [VOCi] with their respective OH reaction rate constant and [OH]. In order to understand the effect of missing OH reactivity on O_3 formation potential it is considered to come from unmeasured VOCs. Therefore, O_3 formation potenital model calculation estimated in two ways. In one way, only calculated VOC OH reactivity used along with other OH chemical partners and that is referred as (ϕ_{calc}).

Fig. 4-11. O_3 formation potential from measured and calculated OH reacctivity.

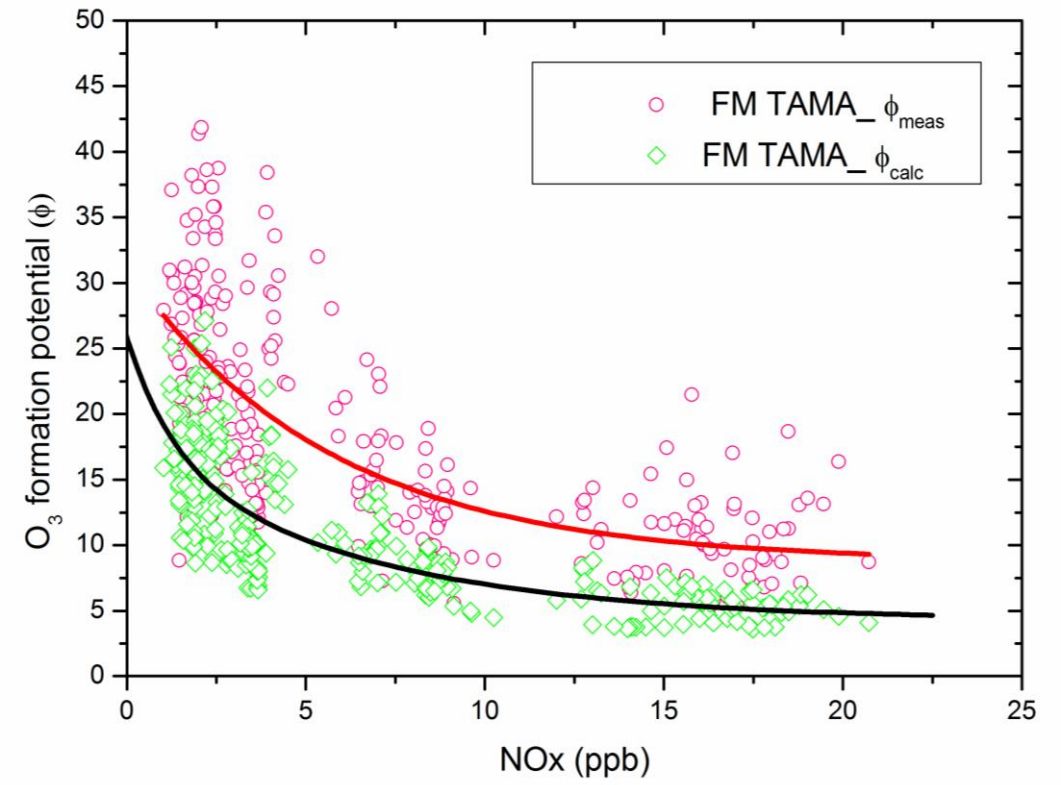

In another way, along with above parameters missing OH reactivity (90 % of measured OH reactivity-calculated OH reactivity) also included as VOC OH reactivity and that is referred as (ϕ_{meas}). 90 % measured OH reactivity is used because HO_X yield calculation showed that only 90 % measured OH reactivity chemical partnes involved in HO_X cycling. O_3 formation potential estimated from measured and calculated OH reactivity for AQUAS-TAMA summer campaign is shown in Fig. 4-11. Average O_3 formation poetial from measured OH reactivity was 1.66 times higher than that from calculated OH reactivity. Therefore, it seems missing OH sinks were effectively involved in O_3 formation. O_3 formation potential estimated in this campaign is comapred with that of

Tokyo Metropolitan Area (TMA) . Interestingly, O_3 formation potenital of FM TAMA expontially fit with TMA. Due to the lower but substantial NO_X level in FM TAMA, O_3 formation potential is effective. This could be one of the reasons for comparable O_3 level in FM TAMA to urban areas even though much smallar OH reactivity.

Fig. 4-12. O_3 formation potential obtained for FM TAMA and Tokyo Metropolitan Area (TMA). (O_3 for TMA is adopted from Yoshino et al., 2012).

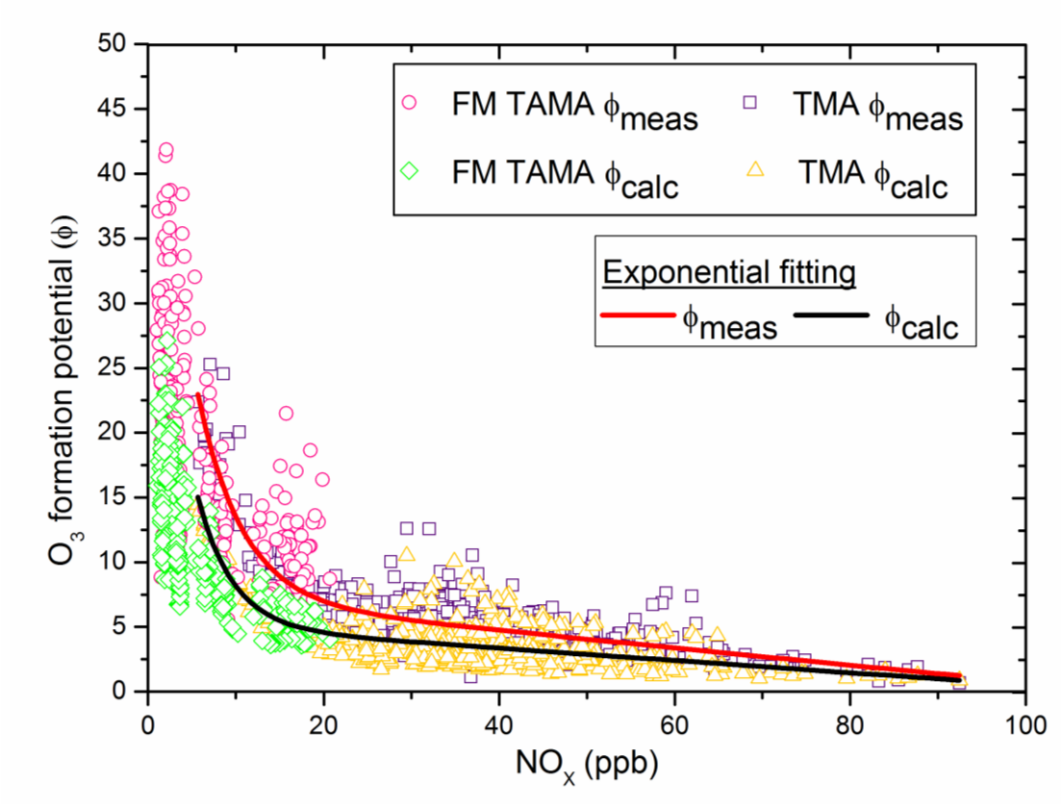

4.3. Summary

Total OH reactivity measurement was conducted in a small suburban forest located ~30 km from Tokyo during AQUAS-TAMA campaign in early autumn–2012 and summer–2013. This forest site receives both biogenic and anthropogenic emission sources because of closer vicinity trees and surrounding residential area and major roads. The average measured OH reactivity during the autumn and summer was respectively 7.4 s^{-1} and 11.4 s^{-1}. In the summer isoprene was the major contributor accounting for 28.2 % to the total OH reactivity as a result of enhanced light dependent biogenic emission while NO_2 was the largest contributor accounting for 19.6 % in autumn due to less photochemical activity. Higher missing OH reactivity was observed in the summer (34.1 %) because of strong biogenic emission and enhanced evaporative anthropogenic emission and subsequent higher unmeasured photochemical secondary production.

5. Conclusion

Intensive measurement campaigns of trace species and OH reactivity were conducted in a remote forest (Wakayama forest research station-WFRS) and a suburban forest (Air QUAlity Study at Field Museum TAMA-AQUAS TAMA) to understand the composition and distribution of trace gases, sources, secondary products and meteorological influences and to address the challenges such as photochemical oxidants increasing problem and larger uncertainty in BVOCs distribution. WFRS is far away from the direct anthropogenic influences and it receives VOCs from trees. Monoterpenes abundance was significant in both day-time and night-time, because of temperature of dependent emission of coniferous trees Japanese cedar (*Cryptomeria japonica*) and Japanese cypress (*Chamaecyparis obutsa*) and additionally shorter boundary layer in night-time. The average measured OH reactivity was (7 s^{-1}) and comparable with that made in similar environments (e.g. boreal forest 9 s^{-1} and coniferous pine forest 10 s^{-1}). Most of the reactive species present in the forest were quantified (missing sinks only 11 %) in cleaner period. Although reactive VOCs were emitted significantly, they didn't produce much O_3 because of the absence of anthropogenic interaction. In another work (Chapter 4), trace gas and OH reactivity measured during autumn and summer season in suburban forest was compared. In contrast to Wakayama forest, sub urban forest site FM TAMA received both biogenic sources from trees and anthropogenic sources from human activities. Although OH reactivity was much lower compare to nearby suburban and urban area photochemical ozone production was comparable due to the interaction of anthropogenic trace pollutants especially NO_X with potentially reactive biogenic VOCs which causes enhanced atmospheric oxidation process and subsequent higher O_3 production in summer time. From the larger fraction of isoprene (28.2 %) to overall reactivity in summer time, it is clear that biogenic VOCs potentially involved in O_3 production. Answers to the research questions are given as follows.

- Although precursors in decreasing trend, O_3 is continuously increasing?

VOCs trend shown in Chapter 1 (Fig. 1-2) includes both highly reactive species and less reactive species. Even though biogenic VOCs contribution is less for the overall mixing ratio, due to their higher reactivity they contribute much to O_3 formation.

For example, as discussed in Chapter 4, section 4.2.3, in suburban forest (AQUA-TAMA) measurement, the sum of BVOCs mixing ratio was (1.13 ppb) much lower than that of AVOCs (15.40 ppb). However, for OH reactivity AVOCs contributed only 12.3 %, whereas BVOCs contributed 28.6 %. Additionally remote forest (WFRS) measurement showed that several potentially reactive terpenoid species supplied to the atmosphere. Moreover, suburban forest measurement showed that NO_X mixing ratio is 5 times lower than that of Tokyo Metropolitan Area but still substantial. Therefore, it seems that BVOCs emission and anthropogenic interaction is one of the candidate for increasing of O_3. However, estimation shows that presence of unknown sinks significantly contributed to O_3 formation (Chapter 4, section 4.2.4). Further development in quantification technique especially for secondary products is needed.

- Substantial uncertainty in BVOCs distribution due to limited measurements and quantification techniques

With recently developed improved BVOC detection technique several BVOCs were quantified in remote forest as shown in Chapter 2, section 2.2.2. Additionally, BVOCs in remote forest showed similar nature with boreal forest (Chapter 2, section 2.2.5). This kind of comparison and further measurements will improve modeling construction and can help to reduce uncertainty in BVOCs distributution.

- Suitable combination of instrument to describe well the distribution of trace gases and photochemical oxidation?

Along with well established total OH reactivity system recently added BVOC detection technique povided absolute mixing ratio of several trace gases from biogenic and anthropogenic origin and additionally relative fraction of each trace gases to the overall reactivity also determined in remote and suburban forest. During clean period of remote forest measurement most of the abundant species were quantified which left only 11 % OH missing sinks (Chapter 3, section 3.3.4). For the other periods of remote forest campaign and suburban forest campaign possible origins of missing OH reactivity sources and the effect of missing sinks on O_3 formation potential were discussed (Chapter 3, section 3.3.4 and Chapter 4, section 4.2.4). This indicates that combination of instruments used in the campaigns worked out well.

- Which place will give a clear picture and serve as a representative place is also subject to question?

Measurement in remote and suburban forest gave a good snapshot of reactive biogenic and anthropogenic species distribution and sources. Homogeneous nature of remote forest since the forest occupied more than half by coniferous trees *Cryptomeria japonica* and *Chamaecyparis obutsa* (Chapter 2, section 2.2.1) which are also major trees in Japan and additionally similar behaviour of most of monoterpenes measured in this forest with boreal forest (Chapter 2, section 2.2.5) indicates that this place can be considered as representative place.

6. Acknowledgement

First of all, I would like to express my sincere gratefulness to my supervisor Professor Yoshizumi Kajii, for accepting me as his student and for his motivation, kindness, and enormous knowledge. His guidance, insightful and interactive research discussions helped me throughout my Ph.D.

I am sincerely appreciate Associate Prof. Shuhei Tanaka (Kyoto University) and Associate Prof. Hitoshi Shinjo (Kyoto University) for accepting as jury members and giving valuable comments and advices.

I would like to extend my gratitude to Asst. Prof. Yosuke Sakamoto and past lab research associates Dr. Akira Ida, Dr. Charlotte Jones, Dr. Hiroshi Tsurumaru for their great help, thoughtful comments, and suggestions. I also thank Dr. Shungo Kato, Dr. Yoshihiro Nakashima and Dr. Yasuhiro Sadanaga for their support.

I genuinely thank all of my present and past lab mates for their timely help, support, and discussions. I would also like to express my appreciation to our lab secretary Mrs. Rumi Ishida and secretaries in Graduate School of Global Environmental Studies for their help.

I am sincerely grateful to all the participants in WFRS campaign and AQUAS TAMA campaign.

I would like to thank Ministry of Education, Culture, Sports, Science and Technology (MEXT) Scholarship for financial support.

Now, I take the chance to express my gratitude to Prof. R. Ramaraj who developed my initial research career, introduced Prof. Yoshizumi Kajii to me and encouraged me to apply Ph.D. position at Kyoto University.

Finally, I thank my parents, sister and all friends for their support, love, encouragement and during the study.

7. References

Aaltonen, H., Pumpanen, J., Pihlatie, M., Hakola, H., Hellén, H., Kulmala, L., Vesala, T., and Bäck, J., 2011. Boreal pine forest floor biogenic volatile organic compound emissions peak in early summer and autumn. Agricultural and Forest Meteorology, 151(6), 682-691. doi: 10.1016/j.agrformet.2010.12.010.

Akimoto, H., Mori, Y., Sasaki, K., Nakanishi, H., Ohizumi, T., Itano, Y., 2015. Analysis of monitoring data of ground-level ozone in Japan for long-term trend during 1990–2010: causes of temporal and spatial variation. Atmos. Environ. 102, 302–310. doi: 10.1016/j.atmosenv.2014.12.001.

Andreae, M.O., and Rosenfeld, D., 2008. Aerosol–cloud–precipitation interactions. Part 1. The nature and sources of cloud-active aerosols. Earth-Sci. Rev., 89, 13–41. doi: 10.1016/j.earscirev.2008.03.001.

Atkinson, R.,1994. Gas-phase tropospheric chemistry of organic compounds. J. Phys. Chem. Ref. Data Monogr. 2, 1-216. http://www.nist.gov/data/PDFfiles/jpcrdM2.pdf.

Atkinson, R., Arey, J., Aschmann, S. M., Corchnoy, S. B., and Shu, Y., 1995. Rate Constants for the Gas-Phase Reactions of cis-3- Hexen-1-ol, is-3-Hexenylacetate, trans-2-Hexenal, and Linalool with OH and NO_3 Radicals and O_3 at 296 ± 2 K, and OH Radical Formation Yields from the O_3 Reactions, Int. J. Chem. Kinet., 27, 941–955. doi: 10.1002/kin.550271002.

Atkinson, R., 1997. Gas-phase tropospheric chemistry of volatile organic compounds: 1. alkanes and alkenes. J. Phys. Chem. Ref. Data 26, 215-290. doi: 10.1063/1.556012.

Atkinson, R., Baulch, D.L., Cox, R.A., Hampson Jr., R.F., Kerr, J.A., Rossi, M.J., and Troe, T., 1997. Evaluated kinetic and photochemical data for atmospheric chemistry: Supplement VI. J. Phys. Chem. Ref. Data 26, 1329-1449. doi: 10.1063/1.556010.

Atkinson, R., 2003. Kinetics of the gas-phase reactions of OH radicals with alkanes and cycloalkanes. Atmos. Chem. Phys., 3, 2233-2307. doi: 10.5194/acp-3-2233-2003.

Atkinson, R., and Arey, J., 2003. Gas-phase tropospheric chemistry of biogenic volatile organic compounds: a review. Atmos. Environ., 2, S197–S219. doi: 10.1016/S1352-2310(03)00391-1.

Bao, H., Kondo, A., Kaga, A., Tada, M., Sakaguti, K., Inoue, Y., Shimoda, Y., Narumi, D., and Machimura, T., 2008. Biogenic volatile organic compound emission potential of forests and paddy fields in the Kinki region of Japan. Environmental Research 106, 156 – 169. doi: 10.1016/j.envres.2007.09.009

Bourtsoukidis, E., Bonn, B., Dittmann, A., Hakola, H., Hellén, H., and Jacobi, S., 2012. Ozone stress as a driving force of sesquiterpene emissions: a suggested parameterisation. Biogeosciences, 9(11), 4337-4352.

Booker, F., Muntifering, R., McGrath, M., Burkey, K., Decoteau, D., Fiscus, E., Manning, W., Krupa, S., Chappelka, and A., Grantz, D., 2009. The ozone component of global change: potential effects on agricultural and horticultural plant yield, product quality and interactions with invasive species. J. Integr. Plant Biol., 51, 337. doi: 10.1111/j.1744-7909.2008.00805.x.

Calvert, J.G., Atkinson, R., Kerr, J.A., Madronich, S., Moortgat, G.K., Wallington, T.J., and Yarwood, G., 2000. Reaction of alkenes with OH radical. In: The Mechanisms of Atmospheric Oxidation of the Alkenes. Oxford Univ. Press, New York.

Chang, C. C., Wang, J. L., Leung, S.-C. C., Chang, C. Y., Lee, P.- J., Chew, C., Liao, W.-N., and Ou-Yang, C.-F., 2014. Seasonal characteristics of biogenic and anthropogenic isoprene in tropical subtropical urban environments, Atmos. Environ., 99, 298–308. doi: 10.1016/j.atmosenv.2014.09.019.

Constable, J. V. H., Litvak, M. E., Greenberg, J. P., and Monson, R. K., 1999. Monoterpene emission from coniferous trees in response to elevated CO_2 concentration and climate warming. Glob. Change Biol., 5, 252–267. doi: 10.1046/j.1365-2486.1999.00212.x.

Copolovici, L., Kaennaste, A., Remmel, T., Vislap, V., and Niinemets, U., 2011. Volatile Emissions from Alnus glutionosa Induced by Herbivory are Quantitatively Related to the Extent of Damage. J. Chem. Ecol., 37, 18–28. doi: 10.1007/s10886-010-9897-9.

Carlo, D.P., Brune, W. H., Martinez, M., Harder, H., Lesher, R., Ren, X. R., Thornberry, T., Carroll, M. A., Young, V., Shepson, P. B., Riemer, D., Apel, E., and Campbell, C., 2004. Missing OH reactivity in a forest: Evidence for unknown

reactive biogenic VOCs. Science, 304 (5671), 722–725. doi: 10.1126/science.1094392.

Draxler, R. R., and Rolph, G. D., 2014. HYSPLIT (HYbrid Single-Particle Lagrangian Integrated Trajectory), Model access via NOAA ARL READY Website http://ready.arl.noaa.gov/HYSPLIT.php, NOAA Air Resources Laboratory, Silver Spring, MD, USA.

Eisele, F. L., G. H. Mount, F. C. Fehsenfeld, J. Harder, E. Marovich, D. D. Parrish, J. Roberts, M. Trainer and D. Tanner, 1994. Intercomparison of tropospheric OH and ancillary trace gas measurements at Fritz Peak Observatory, Colorado. J. Geo. Res. 99 18605–18626. doi: 10.1029/91JD00198.

Edwards, P.M., Evans, M.J., Furneaux, K.L., Hopkins, J., Ingham, T., Jones, C., Lee, J.D., Lewis, A.C., Moller, S.J., Stone, D., Whalley, L.K., and Heard, D.E., 2013. OH reactivity in a South East Asian tropical rainforest during the Oxidant and Particle Photochemical Processes (OP3) project. Atmos. Chem. Phys., 13, 9497-9514. doi: 10.5194/acp-13-9497-2013.

Fuchs, H., Hofzumahaus, A., Rohrer, F., Bohn, B., Brauers, T., Dorn, H.P., Häseler, R., Holland, F., Kaminski, M., Li, X. and Lu, K., 2013. Experimental evidence for efficient hydroxyl radical regeneration in isoprene oxidation. Nature Geoscience, 6(12),1023-1026. doi:10.1038/ngeo1964.

Fuhrer, J., Skarby, L., and Ashmore, M. R., 1997. Critical levels for ozone effects on vegetation in Europe. Environ. Pollut., 97, 91. doi: 10.1016/S0269-7491(97)00067-5

Godish, T., 2004. Air Quality, 4th ed.; CRC Press LLC: Boca Raton, FL.

Goldstein, A. H., and Galbally, I. E., 2007. Known and Unexplored Organic Constituents in the Earth's Atmosphere, Environ. Sci. Tech., 41, 15141521, doi: 10.1021/ es072476p.

Guenther, A., Geron, C., Pierce, T., Lamb, B., Harley, P., and Fall, R., 2000. Natural emissions of non-methane volatile organic compounds, carbon monoxide, and oxides of nitrogen from North America, Atmos. Environ., 34, 2205–2230. doi: 10.1016/S1352-2310(99)00465-3.

Guenther, A. B., Jiang, X., Heald, C. L., Sakulyanontvittaya, T., Duhl, T., Emmons, L. K., and Wang, X., 2012. The Model of Emissions of Gases and Aerosols from Nature version 2.1 (MEGAN2.1): an extended and updated framework for modeling biogenic emissions, Geosci. Model Dev., 5, 1471–1492. doi: 10.5194/gmdd-5-1-2012.

Guo, P., Yokoyama, K., Suenaga, M., & Kida, H. 2008. Mortality and life expectancy of Yokkaichi Asthma patients, Japan: Late effects of air pollution in 1960–70s. Environmental Health, 7(1), 1. doi: 10.1186/1476-069X-7-8

Haagen-Smit, A.J., 1952. Chemistry and physiology of Los Angeles smog. Ind. Eng.Chem. Res. 4 4, 1342-1346. doi: 10.1021/ie50510a045

Hakola, H., Tarvainen, V., Laurila, T., Hiltunen, V., Hellén, H. and Keronen, P., 2003. Seasonal variation of VOC concentrations above a boreal coniferous forest. Atmos. Environ., 37(12), pp.1623-1634. doi: 10.1016/S1352-2310(03)00014-1

Hakola, H., Hellén, H., Hemmilä, M., Rinne, J., and Kulmala, M., 2012. In situ measurements of volatile organic compounds in a boreal forest, Atmos. Chem. Phys., 12, 11665-11678. doi: 10.5194/acp-12-11665-2012.

Hansen, R. F., Griffith, S. M., Dusanter, S., Rickly, P. S., Stevens, P. S., Bertman, S. B., Carroll, M. A., Erickson, M. H., Flynn, J. H., Grossberg, N., Jobson, B. T., Lefer, B. L., and Wallace, H. W., 2014. Measurements of total hydroxyl radical reactivity during CABINEX 2009 – Part 1: 15 field measurements, Atmos. Chem. Phys., 14, 2923–2937. doi: 10.5194/acp-14-2923-2014.

Heiden, A. C., Hoffmann, T., Kahl, J., Kley, D., Klockow, D., Langebartels, C., Mehlhorn, H., Sandermann Jr, H., Schraudner, M., Schuh, and G., Wildt, J., 1999. Emission of volatile organic compounds from ozone-exposed plants, Ecol. Appl., 9, 1160–1167. doi: 10.2307/2641386.

Holzke, C., Dindorf, T., Kesselmeier, J., Kuhn, U., & Koppmann, R., 2006. Terpene emissions from European beech (shape Fagus sylvatica~ L.): Pattern and Emission Behaviour Over two Vegetation Periods. J. Atmos. Chem., 55(1), 81-102. doi:10.1007/s10874-006-9027-9,2006.

Ingham, T., Goddard, A., Whalley, L. K., Furneaux, K. L., Edwards, P. M., Seal, C. P., Self, D. E., Johnson, G. P., Read, K. A., Lee, J. D., and Heard, D. E, 2009. A flow-tube based laser-induced fluorescence instrument to measure OH reactivity in the troposphere, Atmos. Meas. Tech., 2, 465–477. doi: 10.5194/amt-2-465-2009.

Jones, C, E., Kato, S., Nakashima, Y., and Kajii, Y., 2014. A novel fast gas chromatography method for higher time resolution measurements of speciated monoterpenes in air. Atmos. Meas. Tech., 7, 1259–1275 doi: 10.5194/amt-7-1259-2014.

Kajii, Y., Yoshino, A., Watanabe, K., Sadanaga, Y., Matsumoto, J., Nishida, S., Kato, S., 2006. Evaluation of oxidant potential in the semi-urban atmosphere. Journal of Japan Society of Atmospheric Environment 41, 259 –267 (in Japanese). doi: 10.11298/taiki1995.41.5_259.

Karl, M., Guenther, A., Koble, R., Leip, A., and Seuferet, G., al, 2009. A new European plant-specific emission inventory of biogenic volatile organic compounds for use in atmospheric transport models, Biogeosciences, 6, 1059–1087. doi: 10.5194/bg-6-1059-2009.

Kato, S., Pochanart, P., and Kajii, Y., 2001. Measurements of ozone and nonmethane hydrocarbons at Chichi-jima island, a remote island in western Pacific: long-range transport of polluted air from the Pacific rim region. Atmos. Environ., 35, 6021 - 6029 doi: 10.1016/S1352-2310(01)00453-8.

Kato, S., Miyakawa, Y., Kaneko, T., and Kajii, Y., 2004. Urban air measurements using PTRMS in Tokyo area and comparison with GC-FID measurement. International Journal of Mass Spectrometry 253, 103 -110 doi: 10.1016/j.ijms.2004.03.013.

Kesselmeier, J., and Staudt, M., 1999. Biogenic volatile organic compounds (VOC): An overview on emission, physiology, and ecology. J. Atmos. Chem., 33(1), 23–88. doi: 10.1023/A:1006127516791.

Kim, S. Y., Jiang, X. Y., Lee, M., Turnipseed, A., Guenther, A., Kim, J. C., Lee, S. J., and Kim, S., 2013. Impact of biogenic volatile organic compounds on ozone production at the Taehwa Research Forest near Seoul, South Korea, Atmos. Environ., 70, 447–453, doi: 10.1016/J.Atmosenv.2012.11.005.

Kim, S., Lee, M., Kim, S., Choi, S., Seok, S., and Kim, S.,2013a. Photochemical characteristics of high and low ozone episodes observed in the Taehwa Forest Observatory (TFO) in June 2011 near Seoul South Korea, Asia-Pac. J. Atmos. Sci., 49, 325–331, doi: 10.1007/S13143-013-0031-0.

Kim, S., Wolfe, G.M., Mauldin, L., Cantrell, C., Guenther, A., Karl, T., Turnipseed, A., Greenberg, J., Hall, S.R., Ullmann, K. and Apel, E., 2013. Evaluation of HOx sources and cycling using measurement-constrained model calculations in a 2-methyl-3-butene-2-ol (MBO) and monoterpene (MT) dominated ecosystem. Atmospheric Chemistry and Physics, 13(4), 2031-2044. doi:10.5194/acp-13-2031-2013.

Kitagawa, T., 1984. Cause analysis of the Yokkaichi asthma episode in Japan. Journal of the Air Pollution Control Association, 34(7),743-746. doi: 10.1080/00022470.1984.10465807.

Kovacs, T. A., and Brune, W. H., 2001. Total OH Loss Rate Measurement, J. Atmos. Chem., 39, 105- 122, doi: 10.1023/A:1010614113786.

Kumagai, K., Iijima, A., Shimoda, M., Saitoh, Y., Kozawa, K., Hagino, H., and Sakamoto, K., 2010. Determination of dicarboxylic acids and levoglucosan in fine particles in the Kanto Plain, Japan, for source apportionment of organic aerosols. Aerosol Air Qual. Res, 10, 282-291. doi: 10.4209/aaqr.2009.11.0075.

Laothawornkitkul, J., Taylor J.E., Paul N.D., and Hewitt C.N., 2009. Biogenic volatile organic compounds in the Earth system. New Phytol., 183(1), 27–51. doi: 10.1111/j.1469-8137.2009.02859.x.

Lee, J. D., Young, J. C., Read, K. A., Hamilton, J. F., Hopkins, J. R., Lewis, A. C., Bandy, B. J., Davey, J., Edwards, P., Ingham, T., Self, D. E., Smith, S. C., Pilling, M. J., and Heard, D. E., 2009. Measurement and calculation of OH reactivity at a United Kingdom coastal site, J. Atmos. Chem., 64, 53–76. doi: 10.1007/s10874-010-9171-0.

Lelieveld, J., Butler, T.M., Crowley, J.N., Dillon, T.J., Fischer, H., Ganzeveld, L., Harder, H., Lawrence, M.G., Martinez, M., Taraborrelli, D. and Williams, J., 2008. Atmospheric oxidation capacity sustained by a tropical forest. Nature, 452(7188), 737-740. doi:10.1038/nature06870.

Loreto, F., Nascetti, P., Graverini, A., and Mannozzi, M., 2000. Emission and content of monoterpenes in intact and wounded needles of the Mediterranean pine, Pinus pinea, Funct. Ecol., 14, 589–595. doi: 10.1046/j.1365-2435.2000.t01-1-00457.x.

Loreto, F. and Schnitzler, J., 2010. Abiotic stresses and induced BVOCs, Trends Plant Sci., 15, 154–166. doi: 10.1016/j.tplants.2009.12.006.

Mao, J., Ren, X., Brune, W.H., Olson, J.R., Crawford, J.H., Fried, A., Huey, L.G., Cohen, R.C., Heikes, B., Singh, H.B., Blake, D.R., Sachse, G.W., Diskin, G.S., Hall, S.R., and Shetter, R.E., 2009. Airborne measurement of OH reactivity during INTEX-B, Atmos. Chem. Phys., 9, 163–173, doi: 10.5194/acp-9-163-2009.

Matsunaga et al. 2010. Evaluation of non-meth ane hydrocarbon (NMHC) emissions based on an ambient air measurement in Tokyo area, Japan, Atmospheric Environment 44, 4982-4993, doi: 10.1016/j.atmosenv.2010.08.002.

Matsunaga, S., Mochizuki, T., Ohno, T., Endo, Y., Kusumoto, D., and Tani, A., 2011. Monoterpene and sesquiterpene emissions from Sugi (Cryptomeria japonica) based on a branch enclosure measurements, Atmospheric Pollution Research, 2, 16-23. doi: 10.5094/APR.2011.003.

Mochizuki, T., Endo, Y., Matsunaga, S., Chang, J., Ge, Y., Huang, C., and Tani, A., 2011. Factors affecting monoterpene emission from Chamaecyparis obtusa, Geochemical Journal, 45(3), e15- e22. doi: 10.2343/geochemj.1.0130.

Monks, P.S., 2005. Gas-phase radical chemistry in the troposphere. Chem. Soc. Rev. 34, 376–395. doi: 10.1039/b307982c.

Nakashima, Y., Kamei, N., Kobayashi, S., Kajii, Y., 2010. Total OH reactivity and VOC analyses for gasoline vehicular exhaust with a chassis dynamometer. Atmospheric Environment 44, 468 –475. doi: 10.1016/j.atmosenv.2009.11.006

Nakashima, Y., Kato, S., Greenberg, J., Harley, P., Karl, T., Turnipseed, T., Apel, E., Guenther, A., Smith, J., and Kajii, Y., 2014. Total OH reactivity measurements in ambient air in a southern Rocky Mountain ponderosa pine forest during BEACHON-SRM08 summer campaign, Atmos. Environ., 85, 1- 8. doi: 10.1016/j.atmosenv.2013.11.042.

Nölscher, A. C., Williams, J., Sinha, V., Custer, T., Song, W., Johnson, A. M., Axinte, R., Bozem, H., Fischer, H., Pouvesle, N., Phillips, G., Crowley, J. N., Rantala, P., Rinne, J., Kulmala, M., Gonzales, D., Valverde-Canossa, J., Vogel, A., Hoffmann, T., Ouwersloot, H. G., Vilà-Guerau de Arellano, J., and Lelieveld, J., 2012. Summertime total OH reactivity measurements from boreal forest during HUMPPA-COPEC 2010, Atmos. Chem. Phys., 12, 8257–8270. doi: 10.5194/acp-12-8257-2012.

Niinemets, U., Loreto, F., and Reichstein, M., 2004. Physiological and physicochemical controls on foliar volatile organic compound emissions, Trends Plant Sci., 9, 180–186. doi: 10.1016/j.tplants.2004.02.006.

Niinemets, U., 2010. Mild versus severe stress and BVOCs: thresholds, priming, and consequences. Trends Plant Sci., 15, 145–153. doi: 10.1016/j.tplants.2009.11.008.

Patokoski, J., Ruuskanen, T.M., Kajos, M.K., Taipale, R., Rantala, P., Aalto, J., Ryyppö, T., Nieminen, T., Hakola, H., and Rinne, J., 2015. Sources of long-lived atmospheric VOCs at the rural boreal forest site, SMEAR II. Atmos. Chem. Phys., 15(23), 13413-13432. doi: 10.1016/10.5194/acp-15-13413-2015.

Patz, J.A., Campbell-Lendrum, D., Holloway, T., Foley, J.A., 2005. Impact of regional climate change on human health. Nature 438, 310–317. doi: 10.1038/nature04188.

Ran, L., Zhao, C. S., Xu, W. Y., Lu, X. Q., Han, M., Lin, W. L., Yan, P., Xu, X. B., Deng, Z. Z., Ma, N., Liu, P. F., Yu, J., Liang, W. D., and Chen, L. L., 2011. VOC reactivity and its effect on ozone production during the HaChi summer campaign, Atmos. Chem. Phys., 11, 4657–4667, doi: 10.5194/acp-11-4657-2011.

Rinne, J., Back, J., and Hakola, H., 2009. Biogenic volatile organic compound emissions from the Eurasian taiga: current knowledge and future directions, Boreal Environ. Res., 14, 807–826.

Rottenberger, S., Kuhn, U., Wolf, A., Schebeske, G., Oliva, S. T., Tavares, T. M., and Kesselmeier, J. 2004. Exchange of short-chain aldehydes between Amazonian vegetation and the atmosphere. Ecol. Appl., 14(sp4), 247-262. doi: 10.1890/01-6027.

Sadanaga, Y., Yoshino, A., Watanabe, K., Yoshioka, A., Wakazono, Y., Kanaya, Y., and Kajii, Y., 2004. Development of a measurement system of OH reactivity in the

atmosphere by using a laser-induced pump and probe technique. Rev. Sci. Instrum., 75, 2648-2655. doi: 10.1063/1.1775311.

Sadanaga, Y., Yoshino, A., Kato, S., and Kajii, Y., 2005. Measurements of OH reactivity and photochemical ozone production in the urban atmosphere. Environ. Sci. Technol., 39, 8847-8852. doi: 10.1021/es049457p.

Sander, S.P., Friedl, R.R., DeMore, W.B., Golden, D.M., Kurlyo, M.J., Huie, R.E., Orkin, V.L., Moortgat, G.K., Ravishankara, A.R., Kolb, C.E., Molina, M.J., and Finlayson-Pitts, B.J., 2002. Chemical Kinetics and Photochemical Data for Use in Atmospheric Studies. Evaluation Number 14. JPL Publication, pp. 2-25. http://jpldataeval.jpl.nasa.gov/pdf/JPL_02-25_rev02.pdf.

Sharma, U.K., Kajii, Y., Akimoto, H., 2000. Characterization of NMHCs in downtown urban center Kathmandu and rural site Nagarkot in Nepal. Atmos. Environ. 34 (20), 3297– 3307. doi: 10.1016/S1352-2310(99)00485-9.

Shirai, T., Yokouchi, Y., Blake, D.R., Kita, K., Izumi, K., Koike, M., Komazaki, Y., Miyazaki, Y., Fukuda, M., Kondo, Y., 2007. Seasonal variations of atmospheric C2–C7 nonmethane hydrocarbons in Tokyo. J. Geophys. Res. 112, D24305. doi: 10.1029/2006JD008163

Sindelarova, K., Granier, C., Bouarar, I., Guenther, A., Tilmes, S., Stavrakou, T., Müller, J.F., Kuhn, U., Stefani, P., and Knorr, W., 2014. Global data set of biogenic VOC emissions calculated by the MEGAN model over the last 30 years. Atmos. Chem. Phys., 14(17), 9317-9341. doi:10.5194/acp-14-9317-2014.

Sinha, V., Williams, J., Crowley, J.N., and Lelieveld, J., 2008. The comparative reactivity method e a new tool to measure total OH reactivity in ambient air. Atmos. Chem. Phys., 8, 2213-2227. doi: 10.5194/acp-8-2213-2008.

Sinha, V., Williams, J., Lelieveld, J., Ruuskanen, T. M., Kajos, M. K., Patokoski, J., Hellen, H., Hakola, H., Mogensen, D., Boy, M., Rinne, J., and Kulmala, M., 2010. OH Reactivity Measurements within a Boreal Forest: Evidence for Unknown Reactive Emissions. Environ. Sci. Technol., 44, 6614–6620. doi: 10.1021/es101780b.

Stevens, P. S., Mather, J. H., and Brune, W. H., 1994. Measurement of tropospheric OH and HO_2 by laser-induced fluorescence at low pressure, J. Geophys. Res., 99, 3543–3557, doi: 10.1029/93JD03342.

Stocker, T. F., Qin, D., Plattner, G.-K., Alexander, L.V., Allen, S. K., Bindoff, N.L., Bréon, F.-M., Church, J.A., Cubasch, U., Emori, S., Forster, P., Friedlingstein, P., Gillett, N., Gregory, J.M., Hartmann, D.L., Jansen, E., Kirtman, B., Knutti, R., Kumar, K.K., Lemke, P., Marotzke, J., Masson-Delmotte, V., Meehl, G.A., Mokhov, I.I., Piao, S., Ramaswamy, V., Randall, D., Rhein, M., Rojas, M., Sabine, C., Shindell, D., Talley, L. D., Vaughan, D.G., Xie, S.-P, 2013. Technical Summary. In Climate Change 2013: The Physical Science Basis. Contribution of Working Group I to the Fifth Assessment Report of the Intergovernmental Panel on Climate Change; Cambridge, UK and New York, NY, USA. http://www.climatechange2013.org/images/report/WG1AR5_TS_FINAL.pdf.

Taipale, R., Kajos, M.K., Patokoski, J., Rantala, P., Ruuskanen, T.M., and Rinne, J., 2011. Role of de novo biosynthesis in ecosystem scale monoterpene emissions from a boreal Scots pine forest. Biogeosciences, 8 (8):2247–55. doi: 10.5194/bg-8-2247-2011.

Tajima, Y., Kato, S., Suthawaree, J., Kajii, Y., 2010. Long-term measurement of various volatile organic compounds and air quality assessment using OH reactivity and ozone formation potential in sub-urban area of Tokyo (In Japanese). Journal of Japan Society for Atmos. Environ. 45, 56–65. doi: 10.11298/taiki.45.56

Tanaka, M., Kamiura, T., Warashina, M., Maeda, Y., Uno, I., Wakamatsu, S., 1995. Vertical distribution of ambient hydrocarbon and carbon monoxide concentrations measured aloft over Kansai area. Environ. Sci. 8, 387–396. doi: 10.11353/sesj1988.8.387

Tang, M.J., Cox, R.A., and Kalberer M., 2014. Compilation and evaluation of gas phase diffusion coefficients of reactive trace gases in the atmosphere: volume 1. Inorganic compounds. Atmos. Chem. Phys., 14, 9233–9247. doi: 10.5194/acp-14-9233-2014.

Wakamatsu, S., Morikawa, T., Ito, A., 2013. Air pollution trends in Japan between 1970 and 2012 and impact of urban air pollution countermeasures. Asian J. Atmos. Environ. 7, 177–190. doi: 10.5572/ajae.2013.7.4.177.

Watanabe, T., Izumi, T., Matsuyama, H., 2016. Accumulated phytotoxic ozone dose estimation for deciduous forest in Kanto, Japan in summer. Atmos. Environ., 129, 176-185. doi: 10.1016/j.atmosenv.2016.01.016

Williams, J., Keßel, S. U., Nölscher, A. C., Yang, Y., Lee, Y., Yáñez-Serrano, A. M., Wolff, S., Kesselmeier, J., Klüpfel, T., Lelieveld, J., and Shao, M. 2015. Opposite OH reactivity and ozone cycles in the Amazon rainforest and megacity Beijing: Subversion of biospheric oxidant control by anthropogenic emissions. Atmos. Environ., 125, 112-118 doi: 10.1016/j.atmosenv.2015.11.007.

Yatagai, M., Ohira, M., Ohira, T., and Nagai, S., 1995. Seasonal variations of terpene emission from trees and influence of temperature, light and contact stimulation on terpene emission. Chemosphere, 30(6), 1137-1149. doi: /10.1016/0045-6535(95)00006-T.

Yassaa, N., Song, W., Lelieveld, J., Vanhatalo, A., Bäck, J., and Williams, J., 2012. Diel cycles of isoprenoids in the emissions of Norway spruce, four Scots pine chemotypes, and in Boreal forest ambient air during HUMPPA-COPEC-2010. Atmos. Chem. Phys., 12(15), 7215-7229. doi: 10.5194/acp-12-11665-2012.

Yoshida, K., Morio, K., & Yokoyama, K. (2007). Epidemiology and environmental pollution: a lesson from Yokkaichi Asthma, Japan. Prog. Environ. Res., 263-278.

Yoshino, A., Sadanaga, Y., Watanabe, K., Kato, S.Y., Miyakawa, Y., Matsumoto, J., Kajii, Y., 2006. Measurements of total OH reactivity by laser-induced pump and probe technique –comprehensive observations in the urban atmosphere of Tokyo. Atmos. Environ. 40, 7869–7881. doi: 10.1016/j.atmosenv.2006.07.023

Yoshino, A., Nakashima Y., Miyazaki K., Kato S., Suthawaree J., Shimo N., Matsunaga S., Chatani S., Apel E., Greenberg J., Guenther A., Ueno H., Sasaki H., Hoshi J.Y., Yokota H., Ishii K., Kajii Y., 2012. Air quality diagnosis from comprehensive observations of total OH reactivity and reactive trace species in urban central Tokyo, Atmos. Environ. 49, 51–59. doi: 10.1016/j.atmosenv.2011.12.029